NASA TECHNICAL NOTE

NASA TN D-8238




# EFFECT OF REYNOLDS NUMBER ON THE SUBSONIC BOATTAIL DRAG OF SEVERAL WING-BODY CONFIGURATIONS

*David E. Reubush*

*Langley Research Center*
*Hampton, Va. 23665*


NATIONAL AERONAUTICS AND SPACE ADMINISTRATION • WASHINGTON, D. C. • JULY 1976

| 1. Report No. | 2. Government Accession No. | 3. Recipient's Catalog No. |
|---|---|---|
| NASA TN D-8238 | | |

| 4. Title and Subtitle | 5. Report Date |
|---|---|
| EFFECT OF REYNOLDS NUMBER ON THE SUBSONIC BOATTAIL DRAG OF SEVERAL WING-BODY CONFIGURATIONS | July 1976 |
| | 6. Performing Organization Code |
| 7. Author(s) | 8. Performing Organization Report No. |
| David E. Reubush | L-10853 |
| | 10. Work Unit No. |
| 9. Performing Organization Name and Address | 505-04-11-01 |
| NASA Langley Research Center<br>Hampton, Va. 23665 | 11. Contract or Grant No. |
| | 13. Type of Report and Period Covered |
| 12. Sponsoring Agency Name and Address | Technical Note |
| National Aeronautics and Space Administration<br>Washington, D.C. 20546 | 14. Sponsoring Agency Code |

15. Supplementary Notes

16. Abstract

An investigation was conducted in the Langley 1/3-meter transonic cryogenic tunnel to determine the effect of varying Reynolds number on the boattail drag of several wing-body configurations. This investigation was made at $0^{o}$ angle of attack at Mach numbers from 0.6 to 0.9 for Reynolds numbers up to $67 \times 10^{6}$ (based on distance from the nose to the start of the boattail). Results indicate that as the Reynolds number was increased the boattail static-pressure coefficients in the expansion region of the boattail became more negative while those in the recompression region became more positive. These two trends were compensating and, as a result, there was only a small (if any) effect of Reynolds number on boattail pressure drag. This result is the same as that previously found for a series of isolated boattails, even though there were large interference effects of the wing on the flow over the boattails in this investigation.

| 17. Key Words (Suggested by Author(s)) | 18. Distribution Statement |
|---|---|
| Boattail drag<br>Reynolds number<br>Cryogenic tunnel | Unclassified – Unlimited<br><br>Subject Category 02 |

| 19. Security Classif. (of this report) | 20. Security Classif. (of this page) | 21. No. of Pages | 22. Price* |
|---|---|---|---|
| Unclassified | Unclassified | 82 | $4.75 |

*For sale by the National Technical Information Service, Springfield, Virginia 22161

# EFFECT OF REYNOLDS NUMBER ON THE SUBSONIC BOATTAIL DRAG OF SEVERAL WING-BODY CONFIGURATIONS

David E. Reubush
Langley Research Center

## SUMMARY

An investigation was conducted in the Langley 1/3-meter transonic cryogenic tunnel to determine the effect of varying Reynolds number on the boattail drag of several wing-body configurations. This investigation was conducted at $0^{o}$ angle of attack at Mach numbers M from 0.6 to 0.9. The Reynolds number was based on the distance from the nose to the start of the boattail and varied from about $2.8 \times 10^{6}$ to $57 \times 10^{6}$ at M = 0.6, from about $3.5 \times 10^{6}$ to $66 \times 10^{6}$ at M = 0.85, and from about $3.6 \times 10^{6}$ to $67 \times 10^{6}$ at M = 0.9. Reynolds number was varied by operating the tunnel at stagnation pressures which ranged from 1.2 atm to 5.0 atm and at stagnation temperatures which ranged from about 98 K to 308 K.

Results from this investigation indicate that as the Reynolds number was increased the boattail static-pressure coefficients in the expansion region of the boattail became more negative while those in the recompression region became more positive. These two trends were compensating, and as a result, there was a small (if any) effect of Reynolds number on boattail pressure drag. Even though there were large interference effects of the wing on the flow over the boattails, the result of this investigation is the same as that found previously for a series of isolated boattails.

## INTRODUCTION

Current prediction methods for full-scale aircraft propulsion system installation drag rely heavily on wind-tunnel simulation of the actual conditions. Wind-tunnel tests are required because the drag-producing components of the propulsion system are usually installed in areas where the flow field is extremely complex; and at present, there are no adequate theoretical techniques with which to predict these complex flows. Especially in the afterbody-nozzle region, high slopes and large boundary-layer runs result in large and unpredictable viscous effects on boattail pressure drag. Attention has recently been focused on scaling effects, particularly the effects of Reynolds number variation on boattail pressure drag. Investigations by the Lewis Research Center (refs. 1 to 5) have identified possible large effects of Reynolds number variation on installed boattail drag.

These flight tests used an F-106B airplane which had two research nacelles mounted under the wings and the boattails to be tested were mounted on these nacelles. The airplane was flown at various altitudes to obtain boattail pressure drag data for a significant range of Reynolds numbers. In addition to the flight tests, two scale models (5 percent and 22 percent) of this airplane were tested in the Lewis 8- by 6-foot supersonic wind tunnel to provide data at Reynolds numbers lower than those achievable in flight and a comparison between flight and wind-tunnel data. Results from these investigations showed large apparent effects of Reynolds number variation on boattail pressure drag and indicated that the wind-tunnel boattail pressure drags could not be extrapolated to flight. These data accentuated the need for further research in this area.

A recent investigation for a series of isolated boattail models (refs. 6 and 7) showed that, for isolated boattails, there were no significant effects of Reynolds number on boattail pressure drag. This discrepancy between the isolated boattail results and the results of references 1 to 5 may be caused by interference effects due to adjacent airframe surfaces.

The purpose of the present investigation is, therefore, to gain some insight as to how the Reynolds number affects interference flows and how these effects impact the flow over nozzle boattails. This investigation utilized two cone-cylinder nacelle models (2.54 cm in diameter) with different boattail geometries, which had provisions for mounting a 10.16-cm-span $60^{\circ}$ delta wing on top of the nacelle in three positions with the wing trailing edge 0.05, 0.55, and 1.55 model diameters forward of the start of the boattail. It is believed that the wing would provide significant interference effects in the flow over the boattail and, then, the resulting interference flow field on the boattail drag could be assessed. The boattail geometries of the two nacelles chosen were the same as those of two boattails used in the isolated boattail investigation. One was a circular-arc—conic with a ratio of length to model maximum diameter $l/d_m$ of 0.96 which had some separated flow at all test conditions and the other was a circular arc with an $l/d_m$ of 1.77 which had all attached flow at all test conditions. The models were tested in the Langley 1/3-meter transonic cryogenic tunnel at the subsonic Mach numbers of 0.6, 0.85, and 0.9 for an angle of attack of $0^{\circ}$. The Reynolds number based on the distance from the nose to the start of the boattail (20.32 cm) varied from about $2.8 \times 10^6$ to $57 \times 10^6$ at $M = 0.6$, from about $3.5 \times 10^6$ to $66 \times 10^6$ at $M = 0.85$, and from about $3.6 \times 10^6$ to $67 \times 10^6$ at $M = 0.9$. Limited portions of these data have been previously published in references 8 and 9.

## SYMBOLS

$A$ cross-sectional area

$A_m$ maximum cross-sectional area of model

$A_\beta$ incremental area assigned to boattail static pressure orifice for drag integration

$C_{D,\beta}$ boattail pressure drag coefficient (see Data Reduction section)

$C_{p,\beta}$ boattail static-pressure coefficient, $\frac{p_\beta - p_\infty}{q}$

$d_m$ maximum diameter of model

$l$ length of boattail

M free-stream Mach number

$p_t$ free-stream total pressure

$p_\infty$ free-stream static pressure

$p_\beta$ boattail static pressure

q free-stream dynamic pressure

R Reynolds number (based on length from nose to start of boattail or 20.32 cm)

$T_t$ free-stream total temperature

x axial distance from start of boattail, positive aft

$\phi$ meridian angle about model axis, clockwise positive facing upstream, $0^\circ$ at top of model

## APPARATUS AND PROCEDURE

### Wind Tunnel

This investigation was conducted in the Langley 1/3-meter transonic cryogenic tunnel, which is a single-return, continuous-flow pressure tunnel. The test section is a regular octagon in cross section (34.29 cm across the flats) with slots at the corners of the octagon and is essentially a model of the Langley 16-foot transonic tunnel test section. This facility has the capability of operating at stagnation pressures from about 1 atm to 5 atm (1 atm = 101 325 Pa) and stagnation temperatures from about 78 K to 350 K over

the tunnel's operating Mach number range of approximately 0.05 to 1.3. Further description of the Langley 1/3-meter transonic cryogenic tunnel can be found in references 10 to 15.

## Models and Support System

A generalized sketch of the boattailed cone-cylinder nacelle models used in this investigation is shown in figure 1. The models were both 2.54 cm in diameter and the resulting tunnel blockage was about 0.52 percent. A photograph of one of the models installed in the tunnel is shown as figure 2. The two models used had a length of 20.32 cm (8 model diameters) from the nose to the start of the boattail (characteristic length used in Reynolds number calculation), but differing boattail geometry. Details of the geometry of the two boattails are shown in figure 3. The boattail geometries were a circular-arc—conic with a ratio of length to maximum diameter $l/d_m$ (fineness ratio) of 0.96 and a circular arc with a fineness ratio of 1.77.

Both models have provision for mounting a 10.16-cm-span $60^\circ$ delta wing (NACA 0003.9-65 airfoil) on top of the nacelles at $0^\circ$ incidence in three positions (fig. 4). The wing was mounted with its trailing edge 0.05, 0.55, and 1.05 model diameters forward of the start of the boattail.

The models were both sting mounted with the sting simulating the geometry of a jet exhaust plume for a nozzle operating at its design point (ref. 16). The ratios of sting diameter to maximum diameter were both 0.50. The length of the constant diameter portion of the sting was such that, based on reference 17, there should be no effect of the tunnel support sting flare on the boattail pressure coefficients. Also, the sum of the boattail and sting lengths (before the flare) was constant which resulted in the noses of both models being at the same tunnel station.

The models were constructed of cast aluminum with stainless-steel pressure tubes and stainless-steel sting cast as integral parts of the models. The pressure tubes and sting were placed in the sand mold in the proper positions, the aluminum poured, and the model machined to the proper contours.

## Instrumentation and Tests

The two boattails were each instrumented with 50 static pressure orifices in 5 rows of 10 orifices each ($\phi$ = $0^\circ$, $45^\circ$, $135^\circ$, $180^\circ$, and $270^\circ$) at the locations given in table I. These orifices were connected to two remotely located pressure scanning valves.

All tests were conducted in the Langley 1/3-meter transonic cryogenic tunnel at Mach numbers from about 0.6 to 0.9 (primarily at M = 0.6 and 0.85) for an angle of attack

of $0^{o}$. The Reynolds number based on the distance from the nose to the beginning of the boattail varied from about $2.8 \times 10^6$ to $57 \times 10^6$ at $M = 0.6$, from about $3.5 \times 10^6$ to $66 \times 10^6$ at $M = 0.85$, and from about $3.6 \times 10^6$ to $67 \times 10^6$ at $M = 0.9$. The Reynolds number was varied by operating the tunnel at stagnation pressures which ranged from approximately 1.2 atm to 5.0 atm and by operating the tunnel at stagnation temperatures which ranged from about 98 K to 308 K (tests primarily conducted at 117 K and 308 K). Tables II presents the approximate test conditions for all three Mach numbers. Boundary-layer transition was natural for all tests.

## DATA REDUCTION

Model and wind-tunnel data were recorded on magnetic tape and a digital computer was used to compute standard force and pressure coefficients. Pressure drag coefficients, based on the maximum cross-sectional area of the model, were computed from the measured pressures on each boattail by assigning an area to each orifice and computing the coefficients from the following equation:

$$C_{D,\beta} = \frac{1}{qA_m} \sum_{i=1}^{50} \left(p_\infty - p_{\beta,i}\right) A_{\beta,i}$$

Accuracy of this step-integration scheme was spot checked by plotting the pressure coefficients as a function of $A/A_m$ and integrating with a planimeter.

## DISCUSSION

### Boattail Pressure Coefficient Distributions

Boattail pressure coefficient distributions for the two models, each with three wing positions, are shown in figures 5 to 10. These basic data are not discussed as such but are summarized and discussed in the following sections. The only point to be made about these figures is that by comparing the pressure distributions of each of the five orifice rows, it becomes readily apparent that the presence of the wing significantly affected the flow over the boattails. The pressures on the circular-arc—conic boattail were more affected by the wing than those on the circular-arc boattail. This effect was probably due to the steeper slopes and high pressure gradients for the circular-arc—conic boattail. In addition, the closer the wing was to either of the boattails, the larger the interference effects.

### Effect of Reynolds Number on Boattail Pressure Coefficient Distributions

Boattail pressure coefficient distributions at $\phi = 0^{o}$ and $\phi = 180^{o}$ for the circular-arc—conic boattail with the wing in the aft position were obtained at three Reynolds numbers which span the range of Reynolds numbers for the test Mach numbers from 0.6 to 0.9. These distributions are shown in figure 11. The presence of the wing significantly affected the flow over the boattail as evidenced by the differences between the pressure coefficients at $\phi = 0^{o}$ (directly behind the wing) and those at $\phi = 180^{o}$ (essentially in undisturbed flow). However, the trends with Reynolds number for both pressure distributions are the same and these trends are also the same as those found for the isolated series of boattails (refs. 6 and 7). That is, as the flow expands around the shoulder of the boattail, the pressure coefficients at the different Reynolds numbers begin to spread apart such that the higher the Reynolds number, the more negative are the pressure coefficients in this expansion region. As the flow begins to recompress over the aft portion of the boattail, the trend is reversed; that is, the higher the Reynolds number, the more positive are the pressure coefficients.

The pressure coefficient distributions for the other boattail-wing combinations (figs. 12 to 16) show the same trends with Reynolds number as previously discussed. As Reynolds number is increased, the expansion pressure coefficients become more negative while the recompression pressure coefficients become more positive.

### Effect of Reynolds Number on Boattail Pressure Drag Coefficients

Boattail pressure drag coefficients as a function of Reynolds number for Mach numbers of 0.6, 0.85, and 0.9 are shown in figures 17 and 18. These figures show that, as for the isolated boattails (refs. 6 and 7), the trends for the boattail pressure coefficients are compensating and, consequently, there is only a small (if any) effect of Reynolds number on boattail pressure drag, even with the interference from the wing. Therefore, it seems that the results obtained in references 1 to 5 are not due to interference effects, such as those of the present investigation, which can be simply produced.

### Effect of Wing Position on Boattail Drag

An interesting observation can be made which is not really a part of the Reynolds number investigation but deserves mention. When the drag levels for the three wing positions of the two boattails are compared, it is found that the closer the wing was to the boattail for each of the boattail configurations, the lower the pressure drag. In other words, the interference effect from the wing was a beneficial one to the flow over these boattails.

## CONCLUDING REMARKS

An investigation to determine the effects of variations in Reynolds number on the boattail pressure drag of several wing-body configurations was conducted in the Langley 1/3-meter transonic cryogenic tunnel at a $0^{o}$ angle of attack at Mach numbers from 0.6 to 0.9 for Reynolds numbers up to $67 \times 10^{6}$. It was found that, as the Reynolds number was increased, the boattail static-pressure coefficients in the expansion region of the boattails became more negative, while those pressure coefficients in the recompression region of the boattails became more positive. These trends were compensating and, thus, there was only a small (if any) effect of Reynolds number on boattail pressure drag. Even though there were large interference effects of the wing on the flow over the boattails, these results are the same as those found for a series of isolated boattails. Apparently, the large effects of Reynolds number on boattail pressure drag in previous flight test work were not due to interference effects, such as those of the present investigation, which can be simply produced.

Langley Research Center
National Aeronautics and Space Administration
Hampton, Va. 23665
May 24, 1976

## REFERENCES


1. Chamberlin, Roger: Flight Investigation of 24° Boattail Nozzle Drag at Varying Subsonic Flight Conditions. NASA TM X-2626, 1972.

2. Chamberlin, Roger; and Blaha, Bernard J.: Flight and Wind Tunnel Investigation of the Effects of Reynolds Number on Installed Boattail Drag at Subsonic Speeds. NASA TM X-68162, [1973].

3. Wilcox, Fred A.: Comparison of Ground and Flight Test Results Using a Modified F-106B Aircraft. AIAA Paper No. 73-3105, Nov. 1973.

4. Chamberlin, Roger: Flight Reynolds Number Effects on a Contoured Boattail Nozzle at Subsonic Speeds. NASA TM X-3053, 1974.

5. Wilcox, Fred A.; and Chamberlin, Roger: Reynolds Number Effects on Boattail Drag of Exhaust Nozzle From Wind Tunnel and Flight Tests. Airframe/Propulsion Interference, AGARD-CP-150, Mar. 1975, pp. 21-1 – 21-15.

6. Reubush, David E.: The Effect of Reynolds Number on Boattail Drag. AIAA Paper 75-63, Jan. 1975.

7. Reubush, David E.; and Putnam, Lawrence E.: An Experimental and Analytical Investigation of the Effect on Isolated Boattail Drag of Varying Reynolds Number Up to $130 \times 10^6$. NASA TN D-8210, 1976.

8. Reubush, David E.: The Effect of Reynolds Number on the Boattail Drag of Two Wing-Body Configurations. AIAA Paper No. 75-1294, Sept.-Oct. 1975.

9. Reubush, David E.: Experimental Investigation To Validate Use of Cryogenic Temperatures To Achieve High Reynolds Numbers in Boattail Pressure Testing. NASA TM X-3396, 1976.

10. Polhamus, E. C.; Kilgore, R. A.; Adcock, J. B.; and Ray, E. J.: The Langley Cryogenic High Reynolds Number Wind-Tunnel Program. Astronaut. & Aeronaut., vol. 12, no. 10, Oct. 1974, pp. 30-40.

11. Kilgore, Robert A.; Goodyer, Michael J.; Adcock, Jerry B.; and Davenport, Edwin E.: The Cryogenic Wind-Tunnel Concept for High Reynolds Number Testing. NASA TN D-7762, 1974.

12. Kilgore, Robert A.; Adcock, Jerry B.; and Ray, Edward J.: Simulation of Flight Test Conditions in the Langley Pilot Transonic Cryogenic Tunnel. NASA TN D-7811, 1974.

13. Ray, Edward J.; Kilgore, Robert A.; Adcock, Jerry B.; and Davenport, Edwin E.: Analysis of Validation Tests of the Langley Pilot Transonic Cryogenic Tunnel. NASA TN D-7828, 1975.

14. Adcock, Jerry B.; Kilgore, Robert A.; and Ray, Edward J.: Cryogenic Nitrogen as a Transonic Wind-Tunnel Test Gas. AIAA Paper 75-143, Jan. 1975.

15. Hall, Robert M.: Preliminary Study of the Minimum Temperatures for Valid Testing in a Cryogenic Wind Tunnel. NASA TM X-72700, 1975.

16. Reubush, David E.: Experimental Study of the Effectiveness of Cylindrical Plume Simulators for Predicting Jet-On Boattail Drag at Mach Numbers up to 1.30. NASA TN D-7795, 1974.

17. Cahn, Maurice S.: An Experimental Investigation of Sting-Support Effects on Drag and a Comparison With Jet Effects at Transonic Speeds. NACA Rep. 1353, 1958. (Supersedes NACA RM L56F18a.)

TABLE I.- BOATTAIL STATIC PRESSURE ORIFICE LOCATIONS

| $x/d_m$ for – | | | | | | | | | |
|---|---|---|---|---|---|---|---|---|---|
| Circular-arc—conic boattail at – | | | | | Circular-arc boattail at – | | | | |
| $\phi = 0^o$ | $\phi = 45^o$ | $\phi = 135^o$ | $\phi = 180^o$ | $\phi = 270^o$ | $\phi = 0^o$ | $\phi = 45^o$ | $\phi = 135^o$ | $\phi = 180^o$ | $\phi = 270^o$ |
| -0.0043 | 0.0092 | 0.0059 | 0.0029 | -0.0016 | -0.0016 | -0.0053 | -0.0009 | 0.0007 | -0.0008 |
| .0940 | .0996 | .1029 | .0982 | .0935 | .3619 | .3569 | .3600 | .3661 | .3641 |
| .1906 | .2104 | .2054 | .1857 | .1963 | .6357 | .6319 | .6362 | .6398 | .6468 |
| .2870 | .2986 | .3066 | .2891 | .2892 | .8260 | .8274 | .8276 | .8311 | .8241 |
| .3887 | .4041 | .4054 | .3963 | .3765 | .9885 | .9867 | .9909 | .9939 | .9849 |
| .4910 | .4968 | .5017 | .4937 | .4964 | 1.1487 | 1.1297 | 1.1419 | 1.1457 | 1.1425 |
| .5899 | .5988 | .5928 | .5905 | .5896 | 1.2865 | 1.2774 | 1.2842 | 1.2897 | 1.2899 |
| .6906 | .7014 | .7037 | .6899 | .6883 | 1.4208 | 1.4050 | 1.4219 | 1.4271 | 1.4150 |
| .7837 | .7984 | .7974 | .7894 | .7893 | 1.5629 | 1.5593 | 1.5597 | 1.5605 | 1.5569 |
| .8887 | .8908 | .8829 | .8866 | .8764 | 1.6874 | 1.6833 | 1.6840 | 1.6943 | 1.6817 |

TABLE II.- APPROXIMATE TEST CONDITIONS

| $T_t$, K | $p_t$, atm | M | R |
|---|---|---|---|
| 98 | 5.0 | 0.6 | $56.5 \times 10^6$ |
| 101 | ↓ | .85 | 67.5 |
| 103 | ↓ | .6 | 52.2 |
| ↓ | ↓ | .85 | 65.3 |
| 117 | ↓ | .9 | 67.1 |
| ↓ | ↓ | .6 | 43.3 |
| ↓ | ↓ | .85 | 54.0 |
| ↓ | ↓ | .9 | 55.2 |
| ↓ | 4.019 | .85 | 43.4 |
| ↓ | 4.0 | .6 | 34.4 |
| ↓ | 4.0 | .9 | 44.3 |
| ↓ | 3.0 | .6 | 25.9 |
| ↓ | 3.0 | .85 | 32.4 |
| ↓ | 2.5 | .6 | 21.7 |
| ↓ | ↓ | .85 | 26.9 |
| ↓ | ↓ | .9 | 27.3 |
| ↓ | 2.0 | .6 | 17.2 |
| ↓ | 2.0 | .85 | 21.6 |
| ↓ | 1.5 | .6 | 12.8 |
| ↓ | 1.5 | .85 | 16.3 |
| ↓ | 1.3 | .6 | 11.4 |
| ↓ | ↓ | .85 | 14.2 |
| ↓ | ↓ | .9 | 14.6 |
| 308 | 5.0 | .6 | 11.2 |
| ↓ | ↓ | .85 | 13.9 |
| ↓ | ↓ | .9 | 14.2 |
| ↓ | 3.8 | .6 | 8.5 |
| ↓ | ↓ | .85 | 10.5 |
| ↓ | ↓ | .9 | 10.9 |
| ↓ | 3.138 | .6 | 7.1 |
| ↓ | 2.56 | .85 | 7.1 |
| ↓ | 2.50 | .6 | 5.7 |
| ↓ | 2.50 | .9 | 7.1 |
| ↓ | 1.25 | .6 | 2.8 |
| ↓ | ↓ | .85 | 3.5 |
| ↓ | ↓ | .9 | 3.6 |

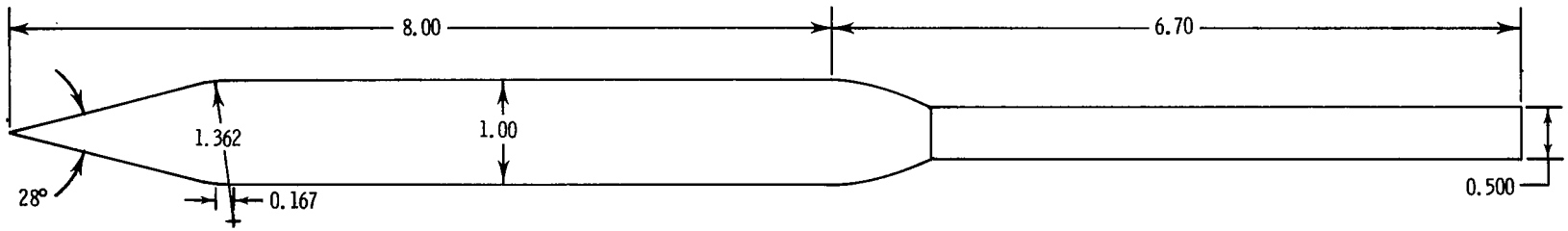


Figure 1.- Boattailed cone-cylinder nacelle model. All dimensions are nondimensionalized by model maximum diameter (2.54 cm).

L-75-2900

Figure 2.- Nacelle model installed in cryogenic tunnel.

CIRCULAR ARC

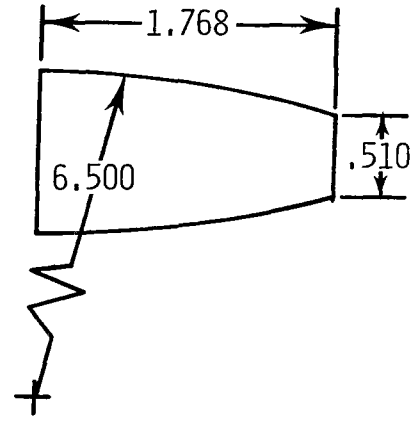


CIRCULAR-ARC—CONIC

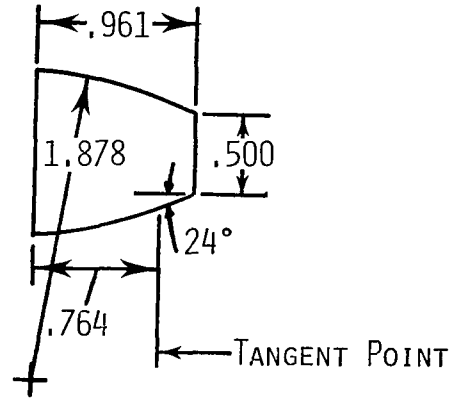


Figure 3.- Details of boattail geometries. All dimensions are nondimensionalized by model maximum diameter (2.54 cm).

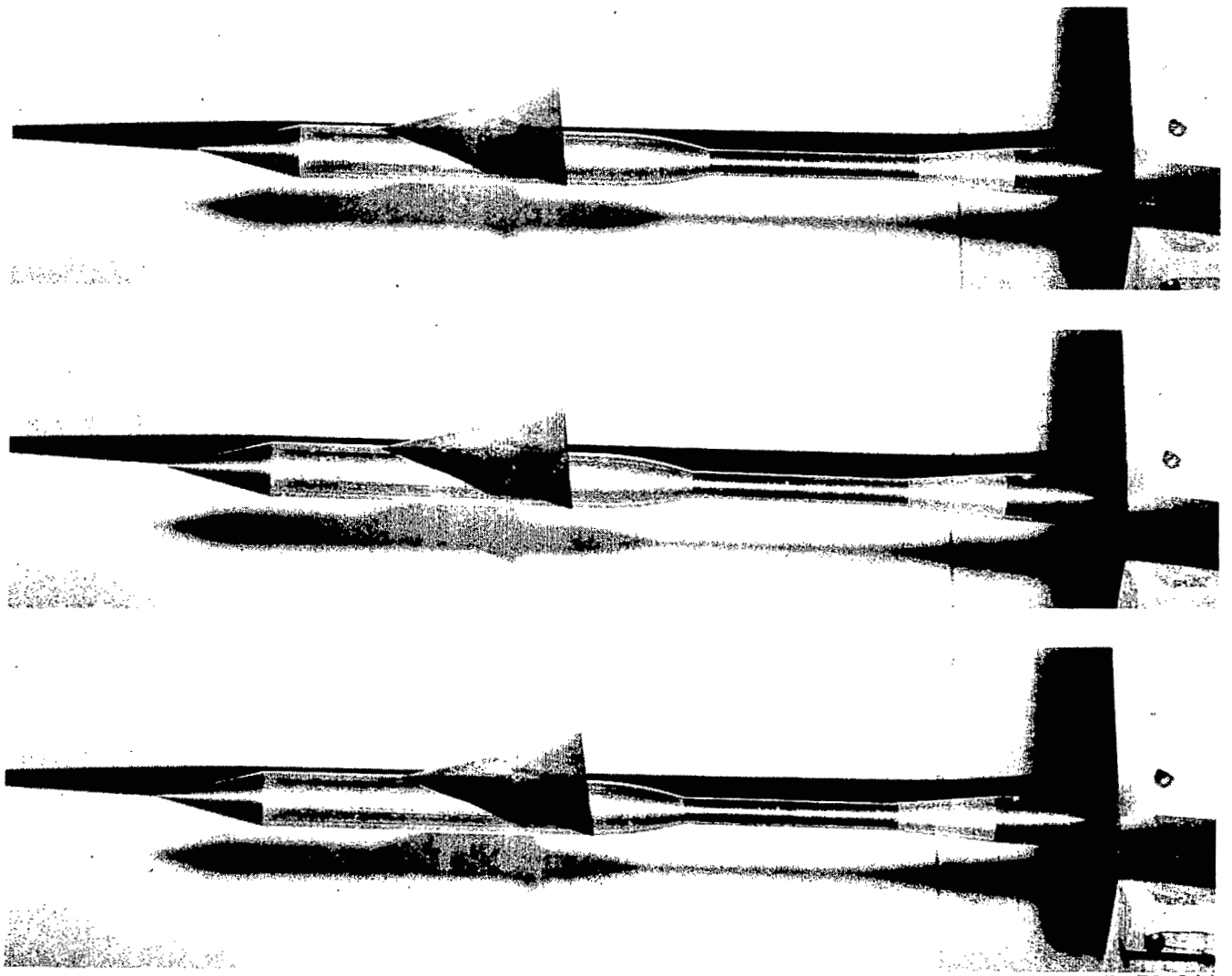

L-76-214

Figure 4.- Nacelle model (circular-arc boattail) with wing installed in the three positions tested.

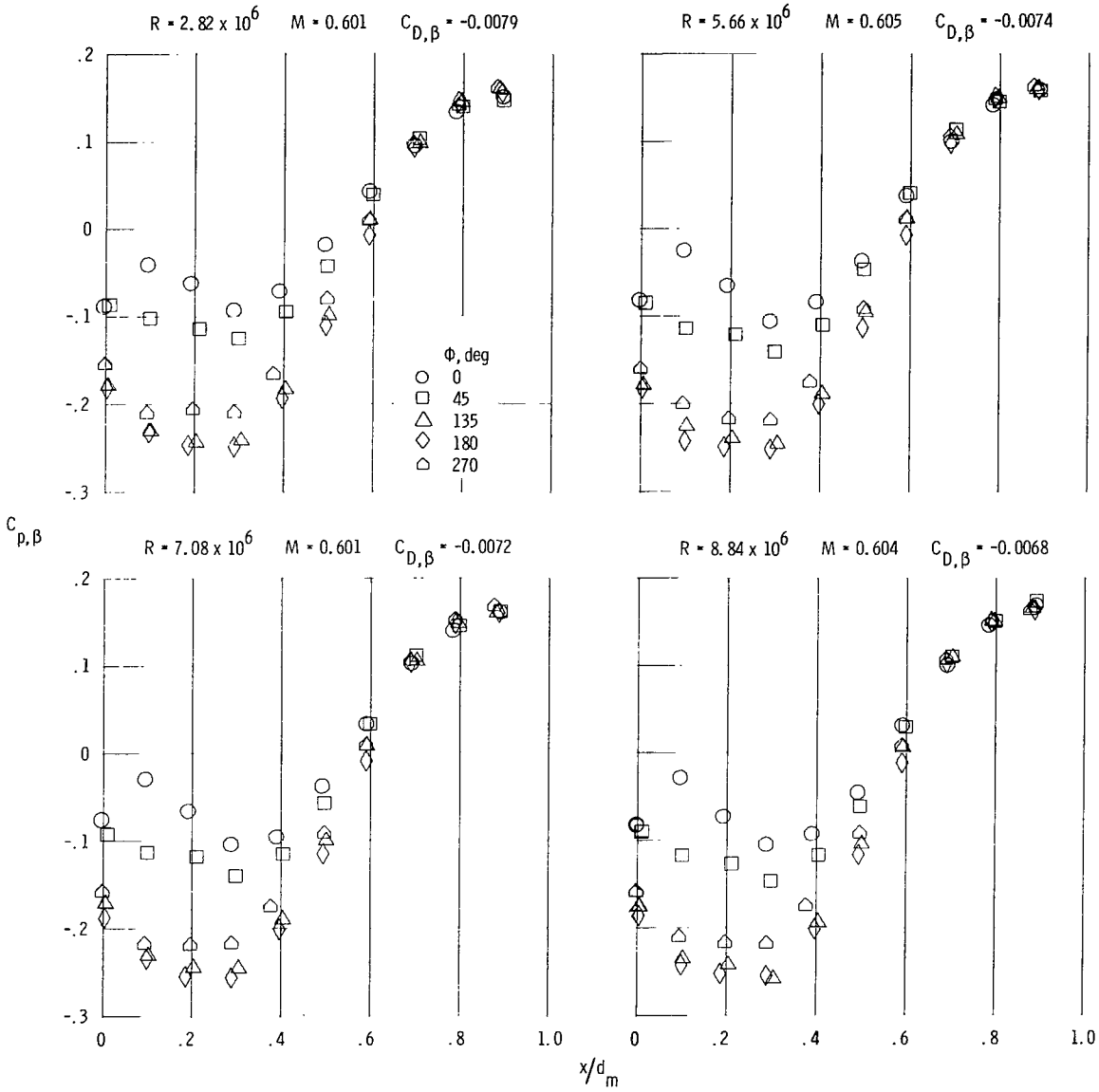


(a) M = 0.6.

Figure 5.- Boattail pressure coefficient distributions at various Reynolds numbers for the circular-arc—conic boattail with wing in aft position.

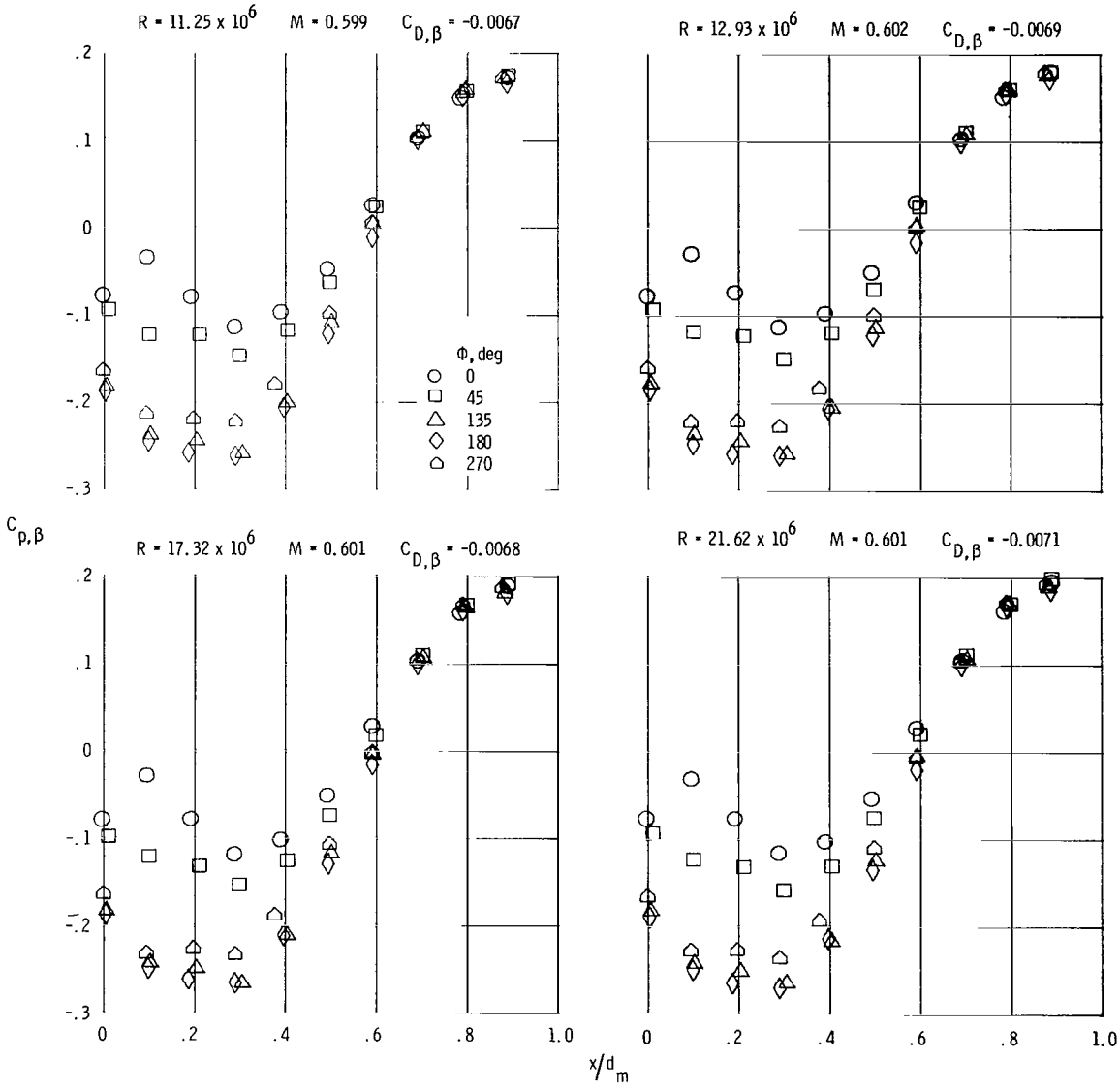


(a) Continued.

Figure 5.- Continued.

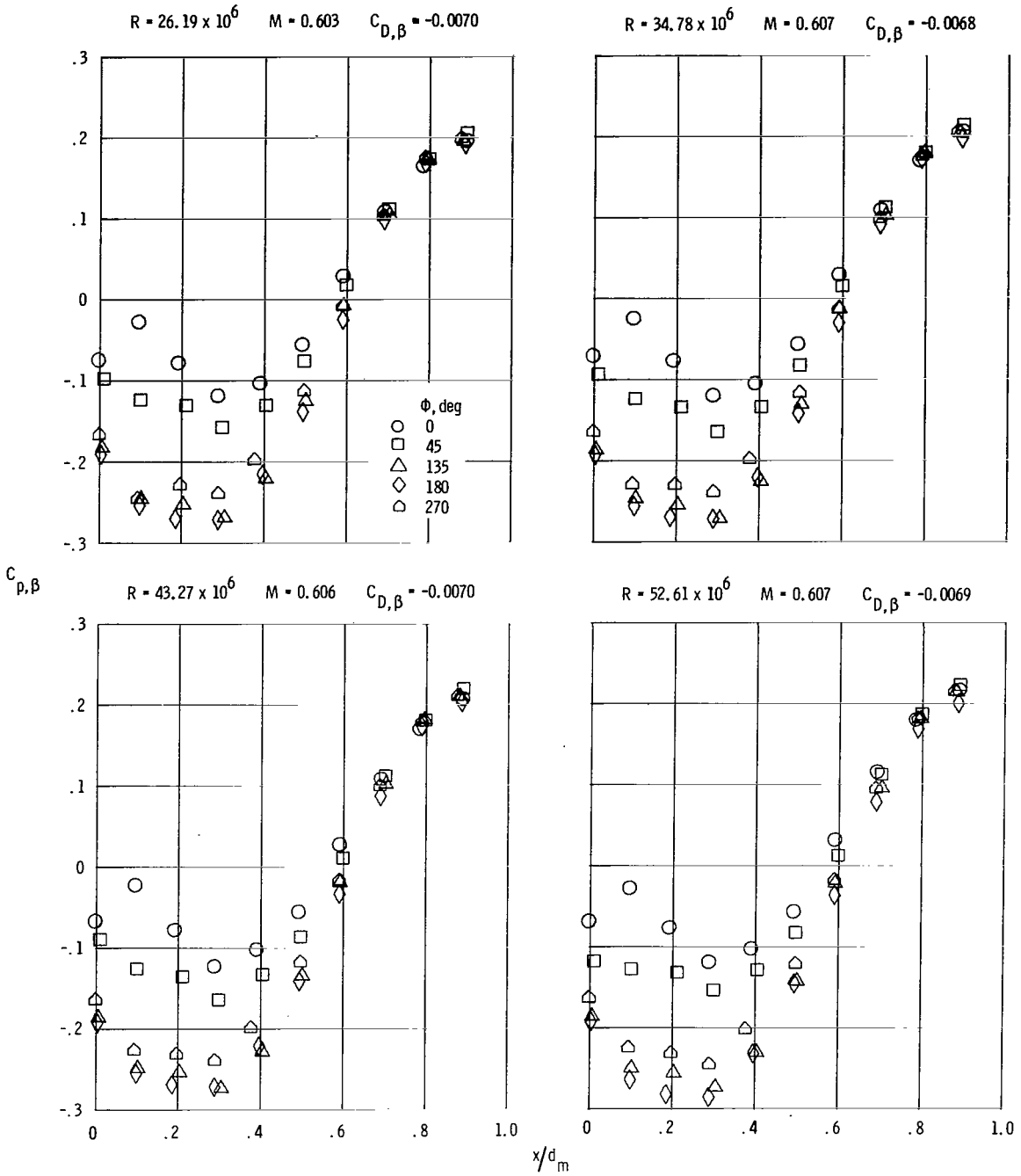


(a) Concluded.

Figure 5.- Continued.

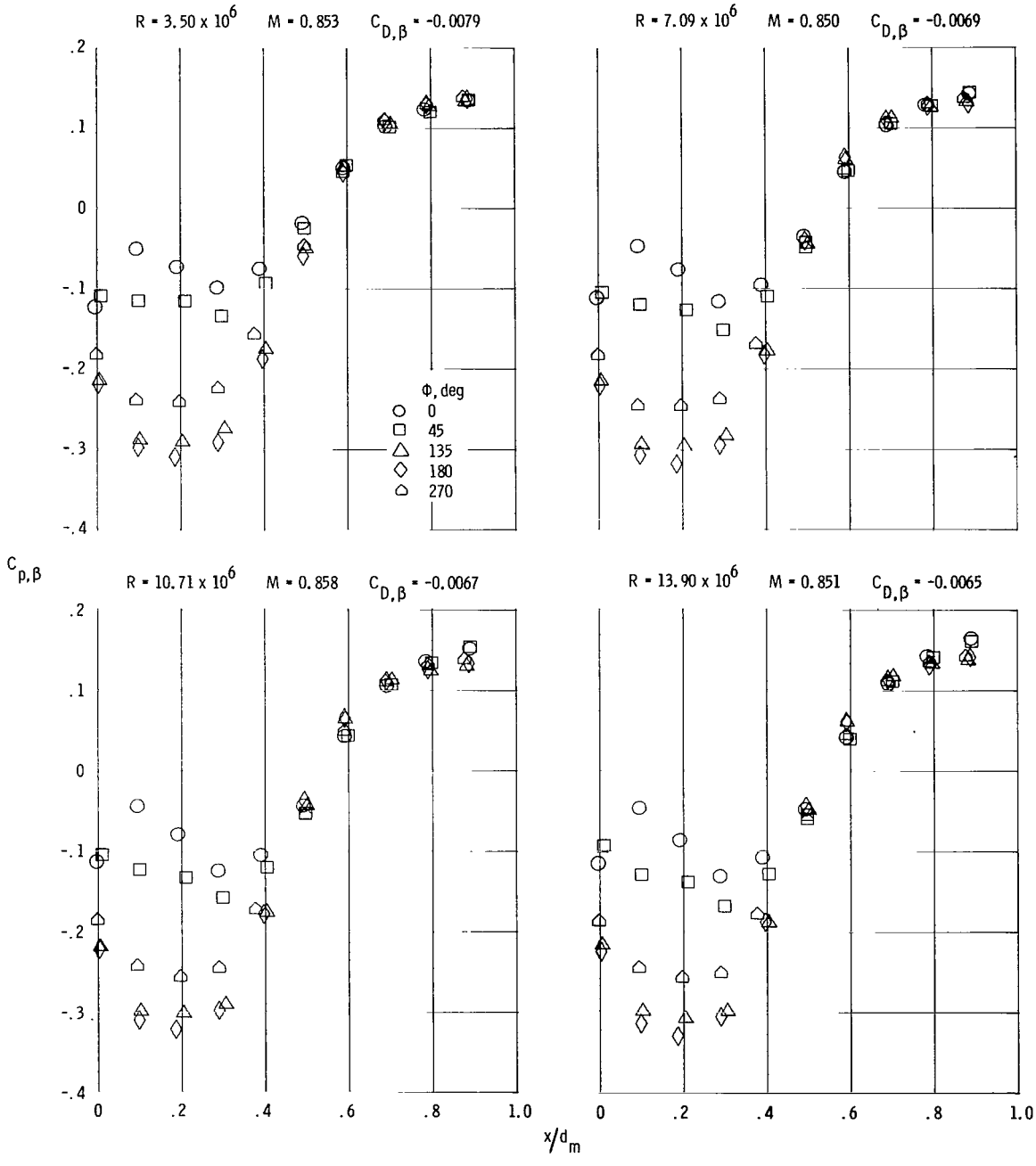


(b) M = 0.85.

Figure 5.- Continued.

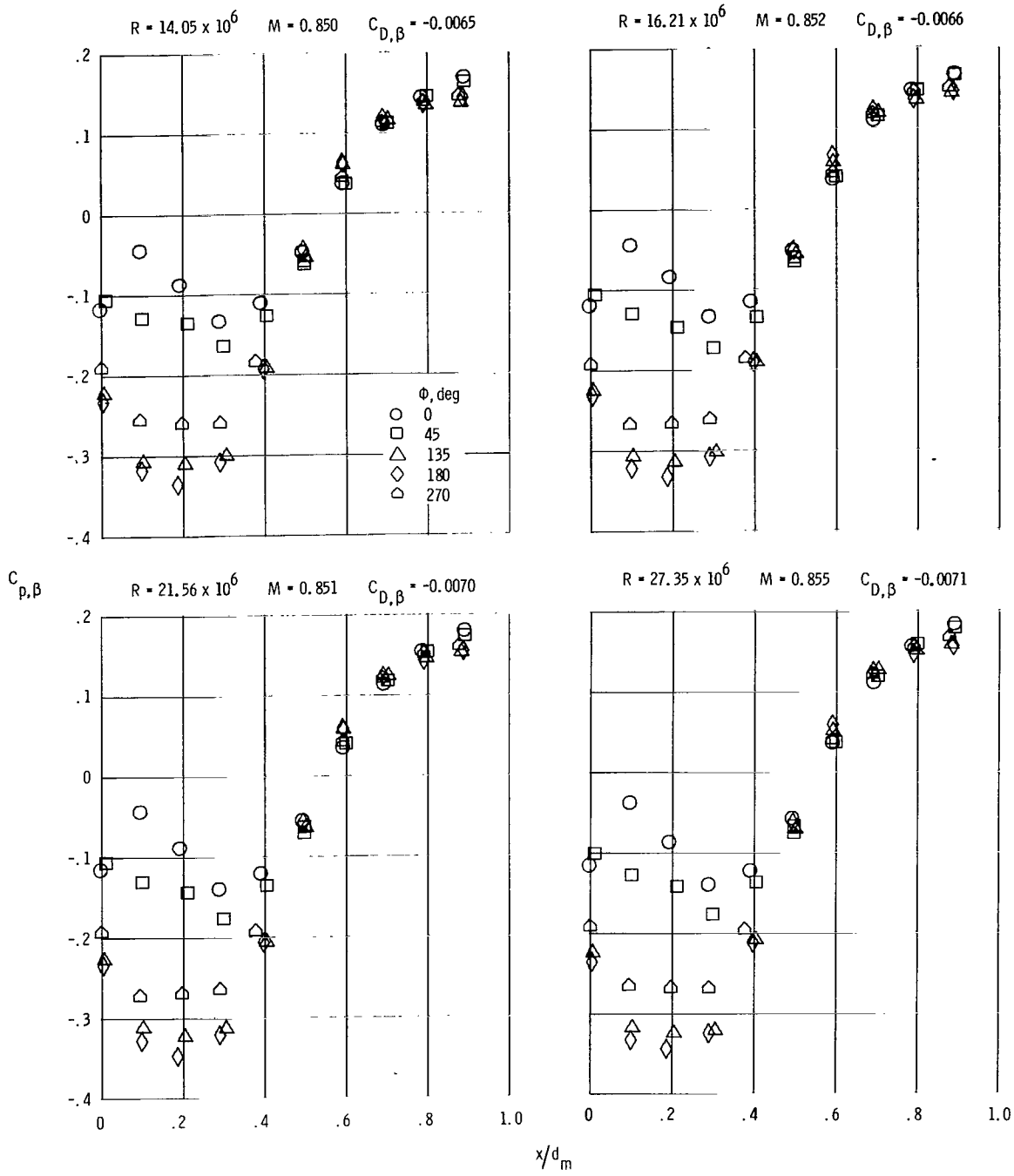


(b) Continued.

Figure 5.- Continued.

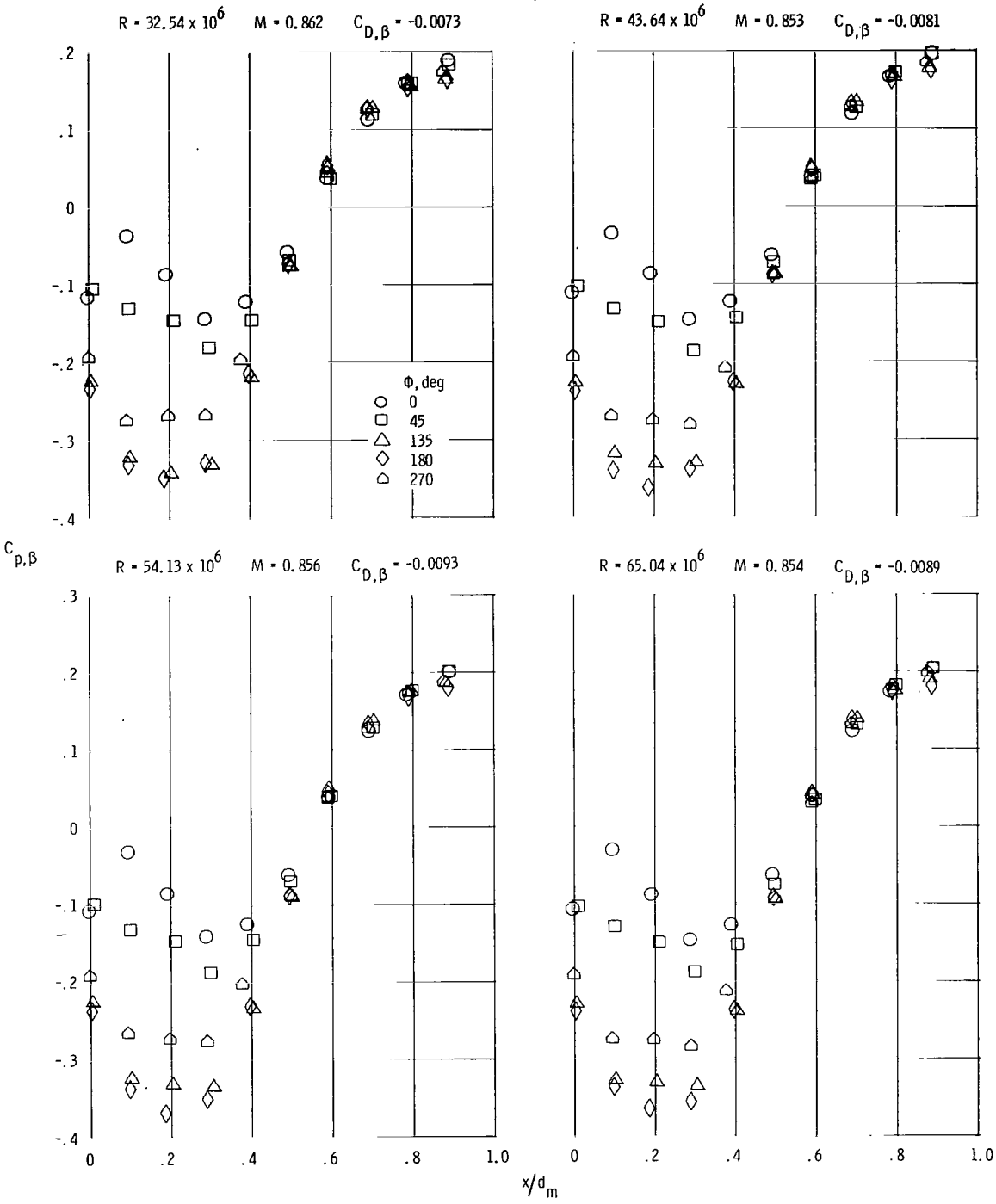


(b) Concluded.

Figure 5.- Continued.

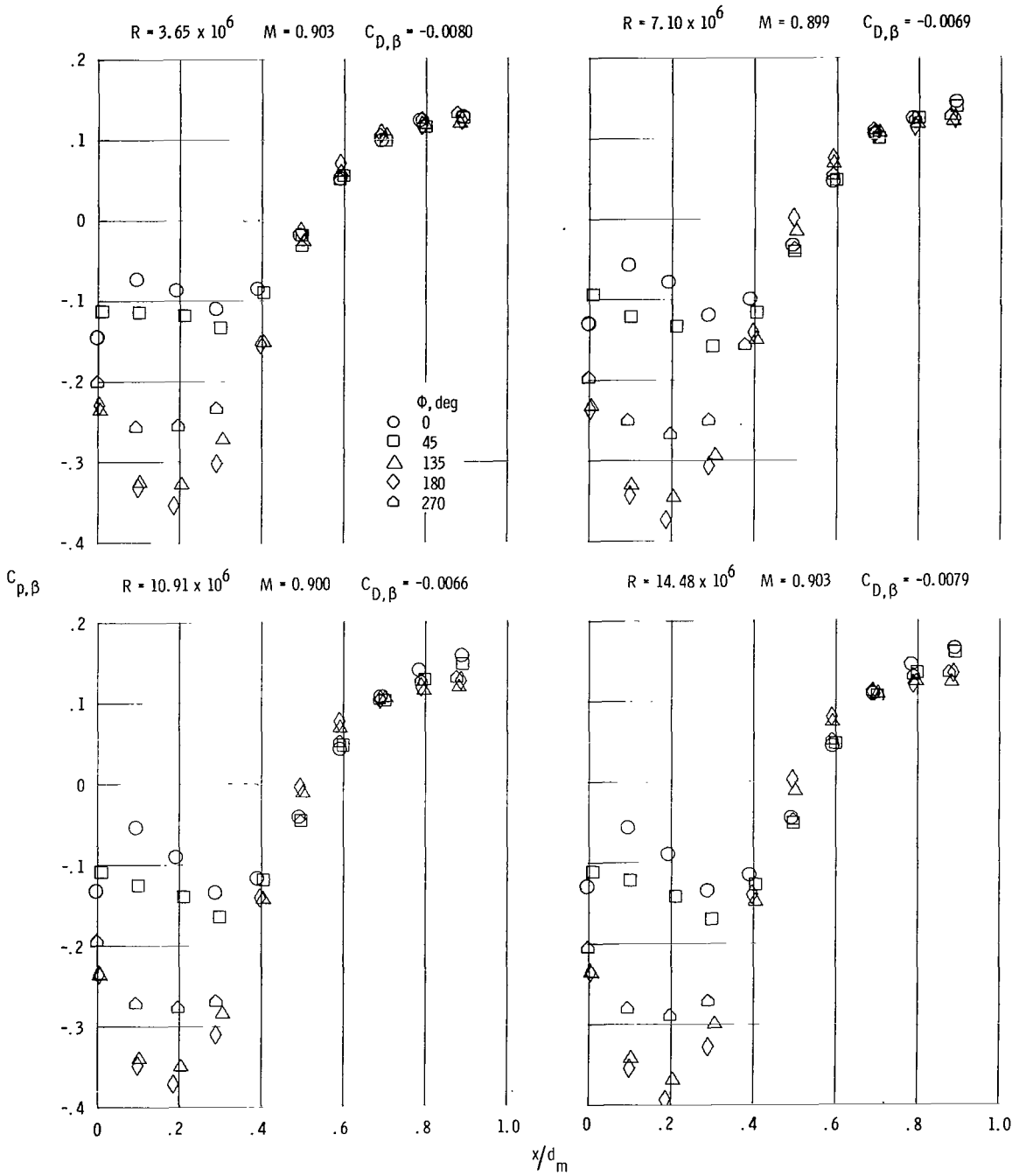


(c) M = 0.9.

Figure 5.- Continued.

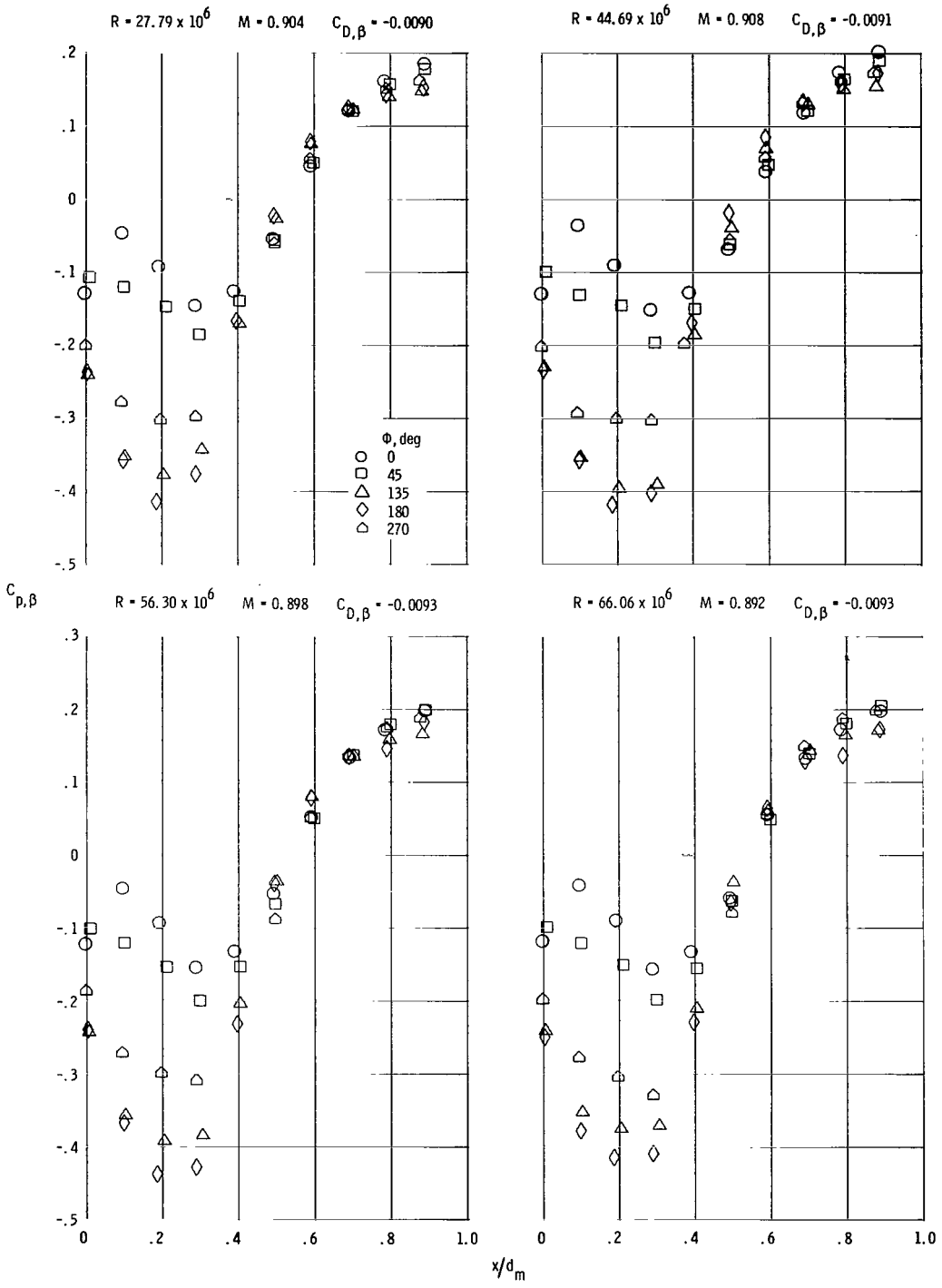


(c) Concluded.

**Figure 5.- Concluded.**

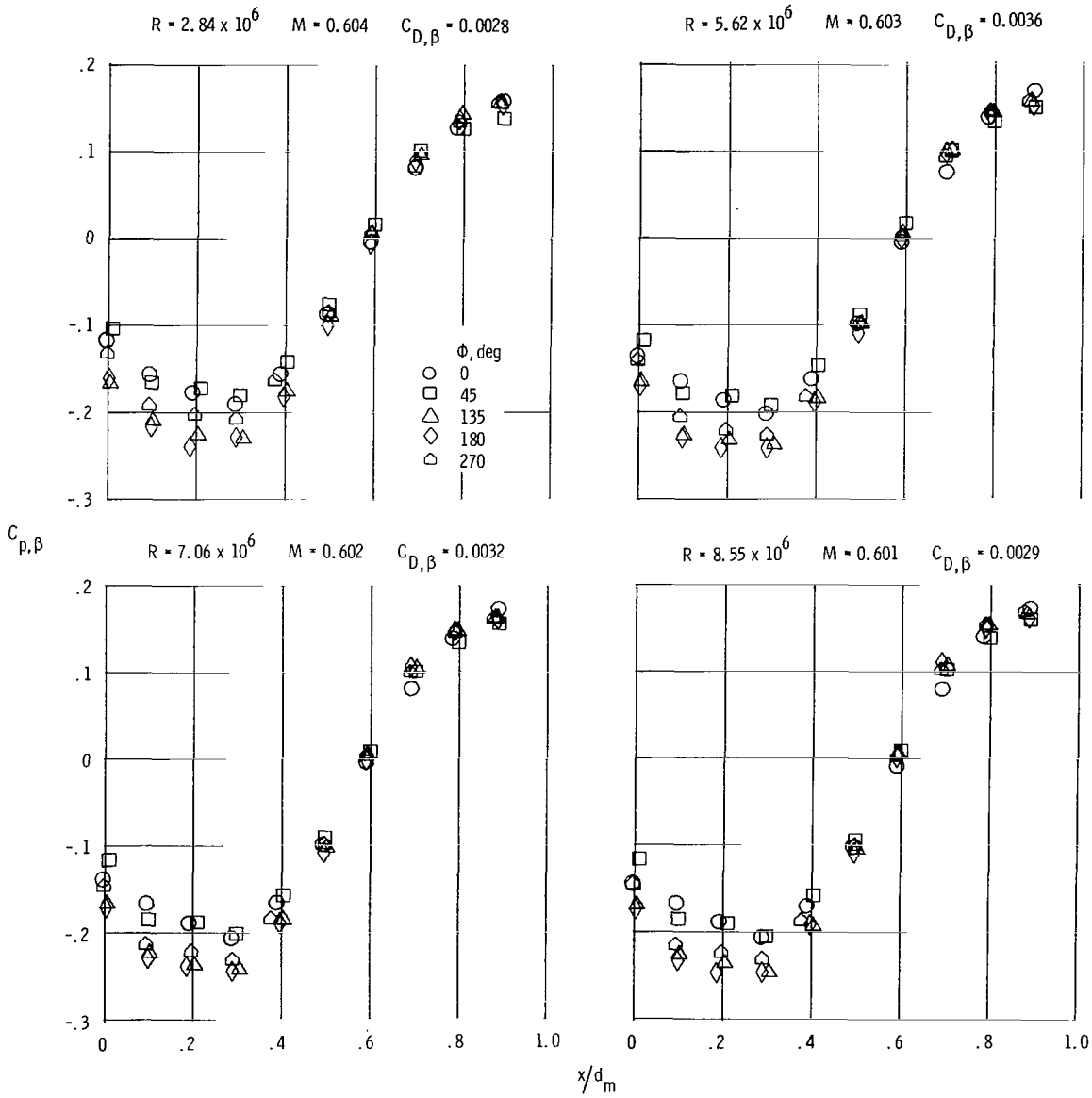


(a) M = 0.6.

Figure 6.- Boattail pressure coefficient distributions at various Reynolds numbers for the circular-arc—conic boattail with wing in middle position.

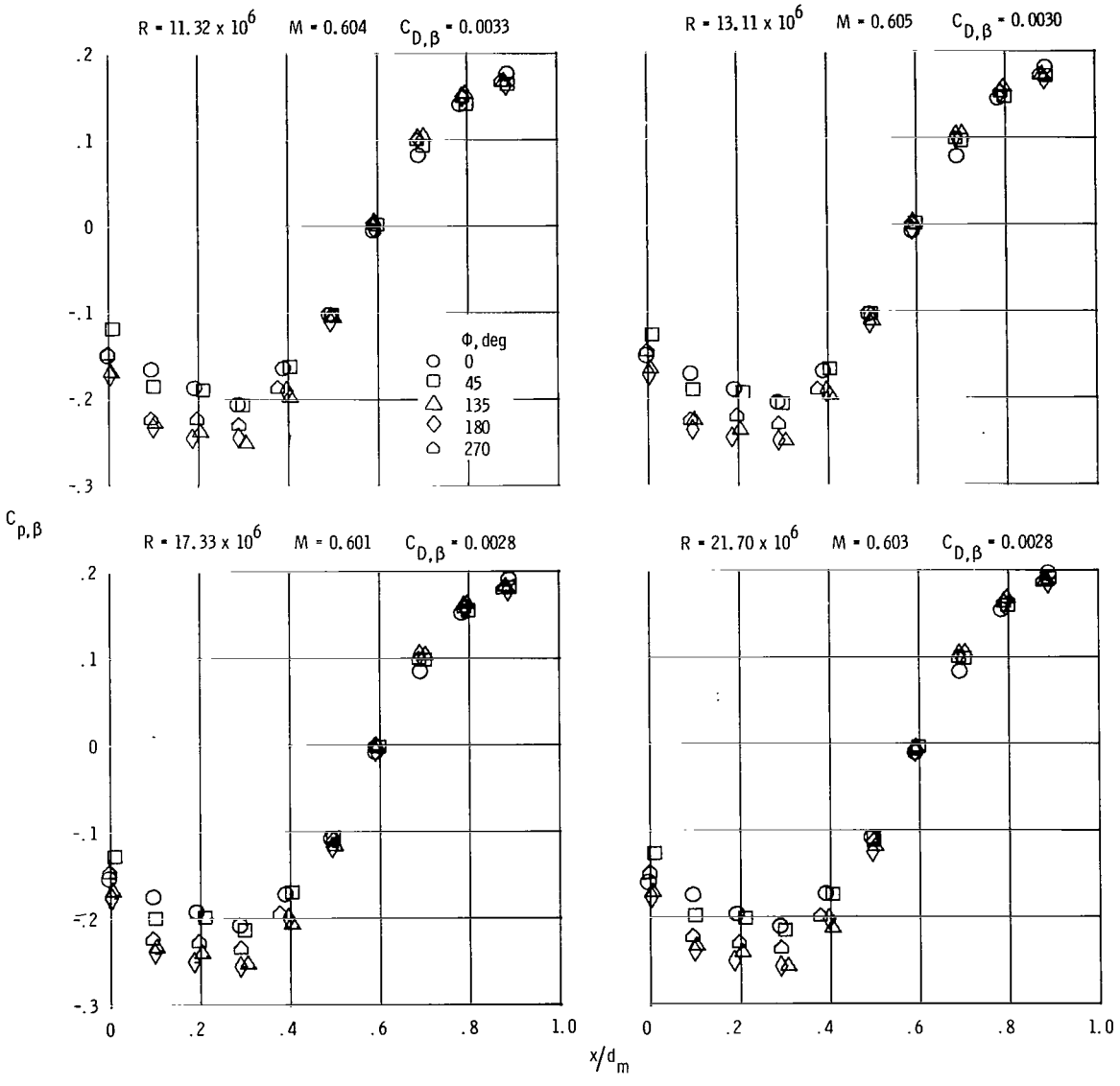


(a) Continued.

Figure 6.- Continued.

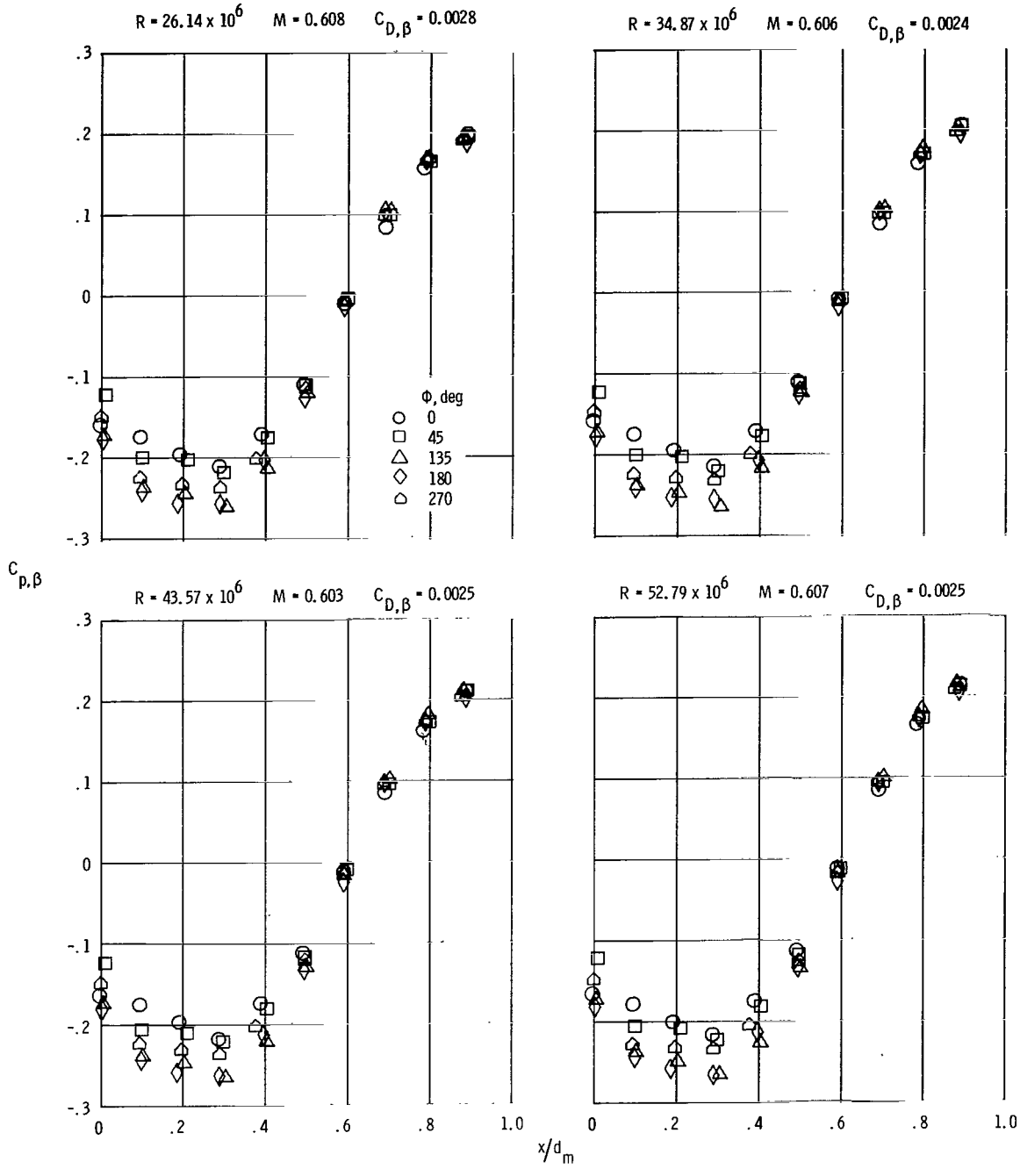


(a) Concluded.

Figure 6.- Continued.

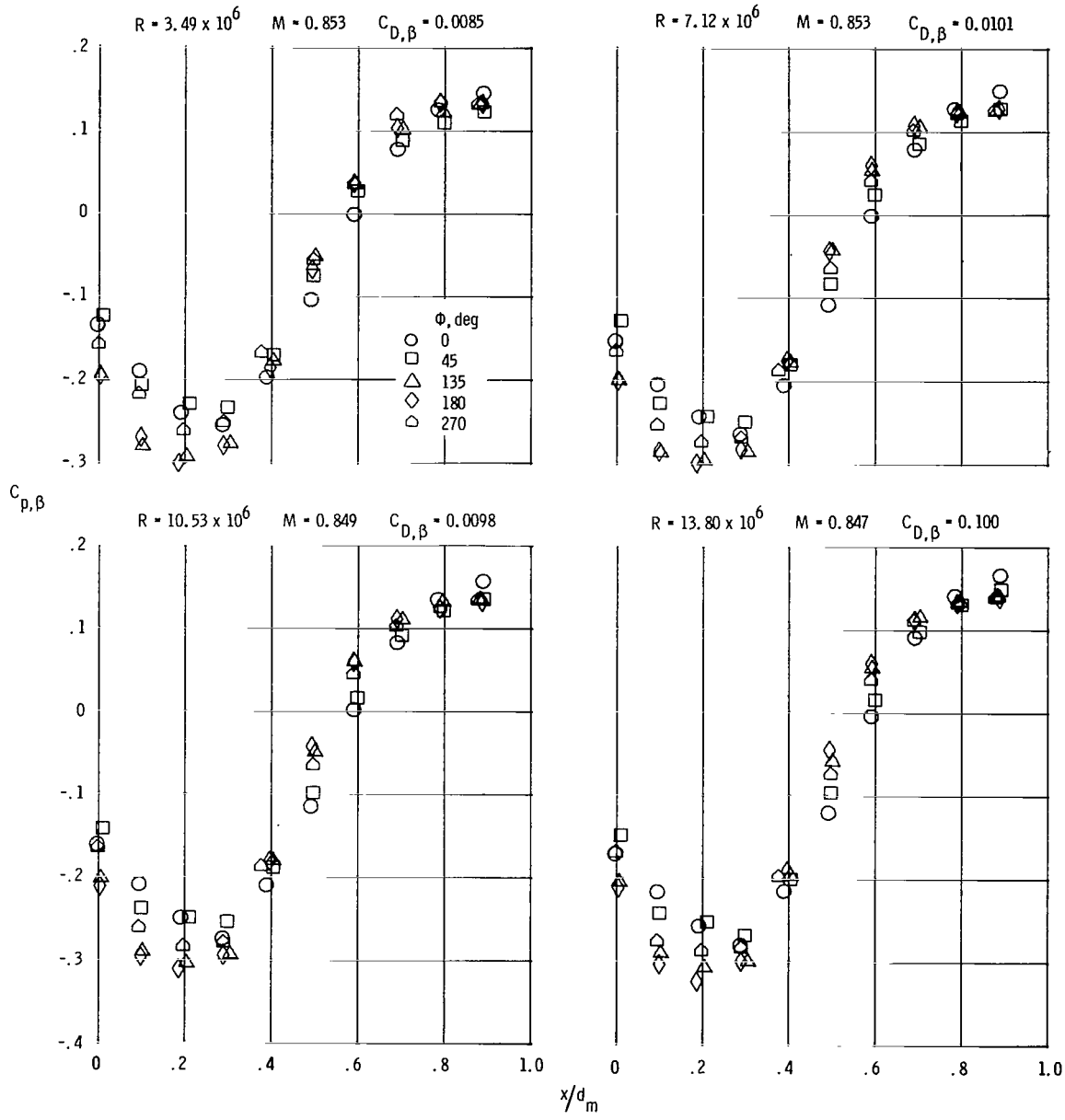


(b) M = 0.85.

Figure 6.- Continued.

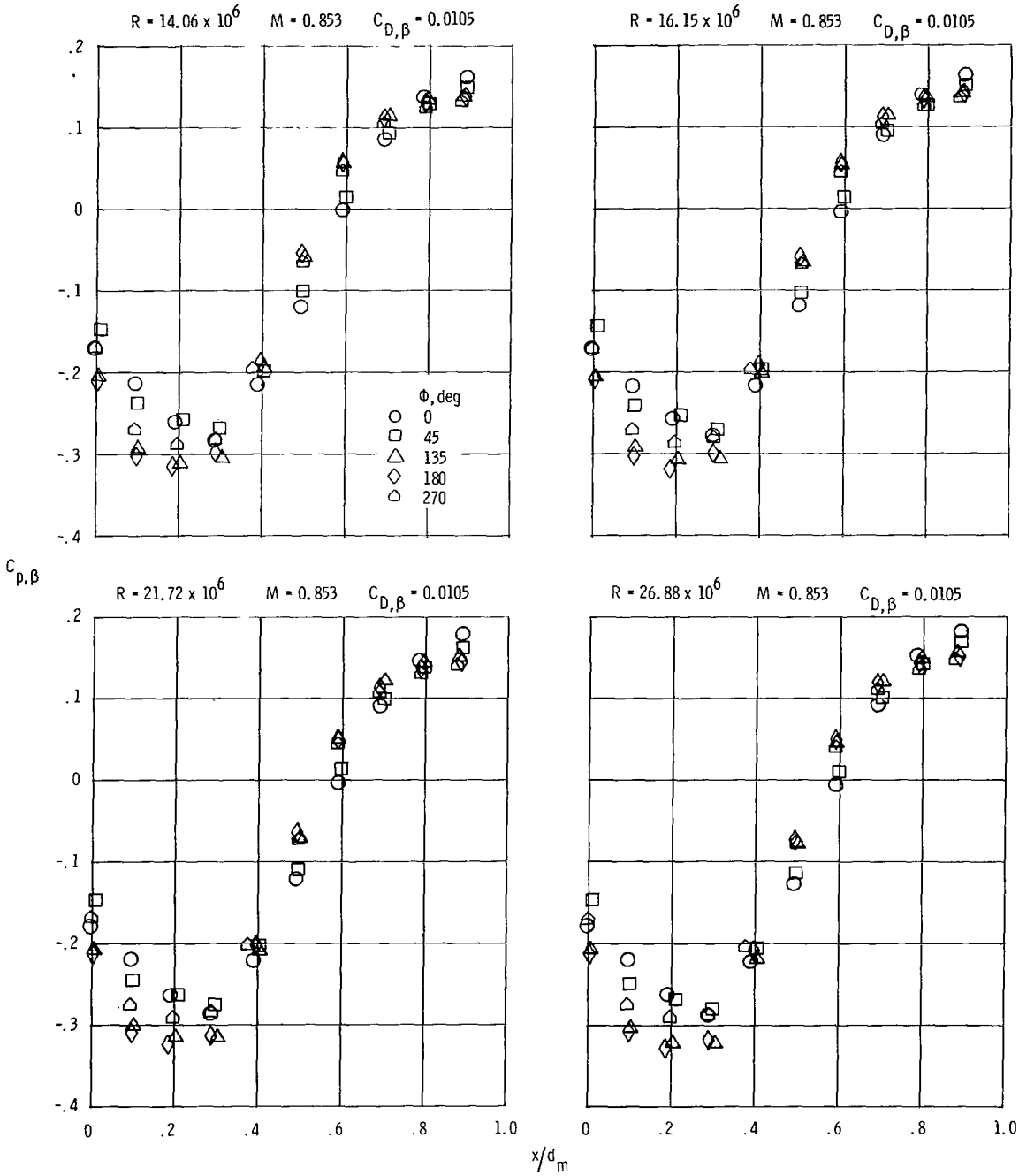


(b) Continued.

Figure 6.- Continued.

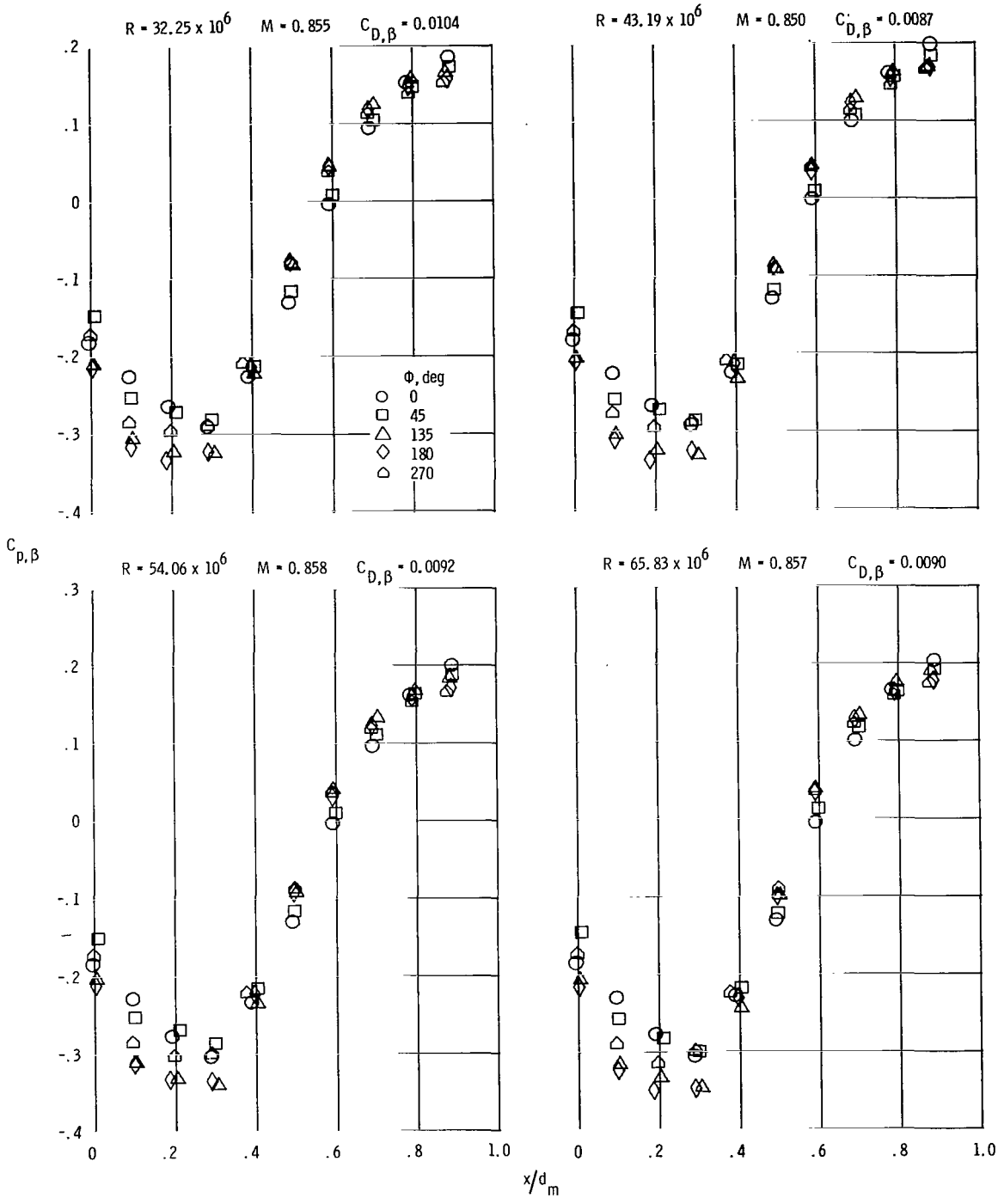


(b) Concluded.

Figure 6.- Concluded.

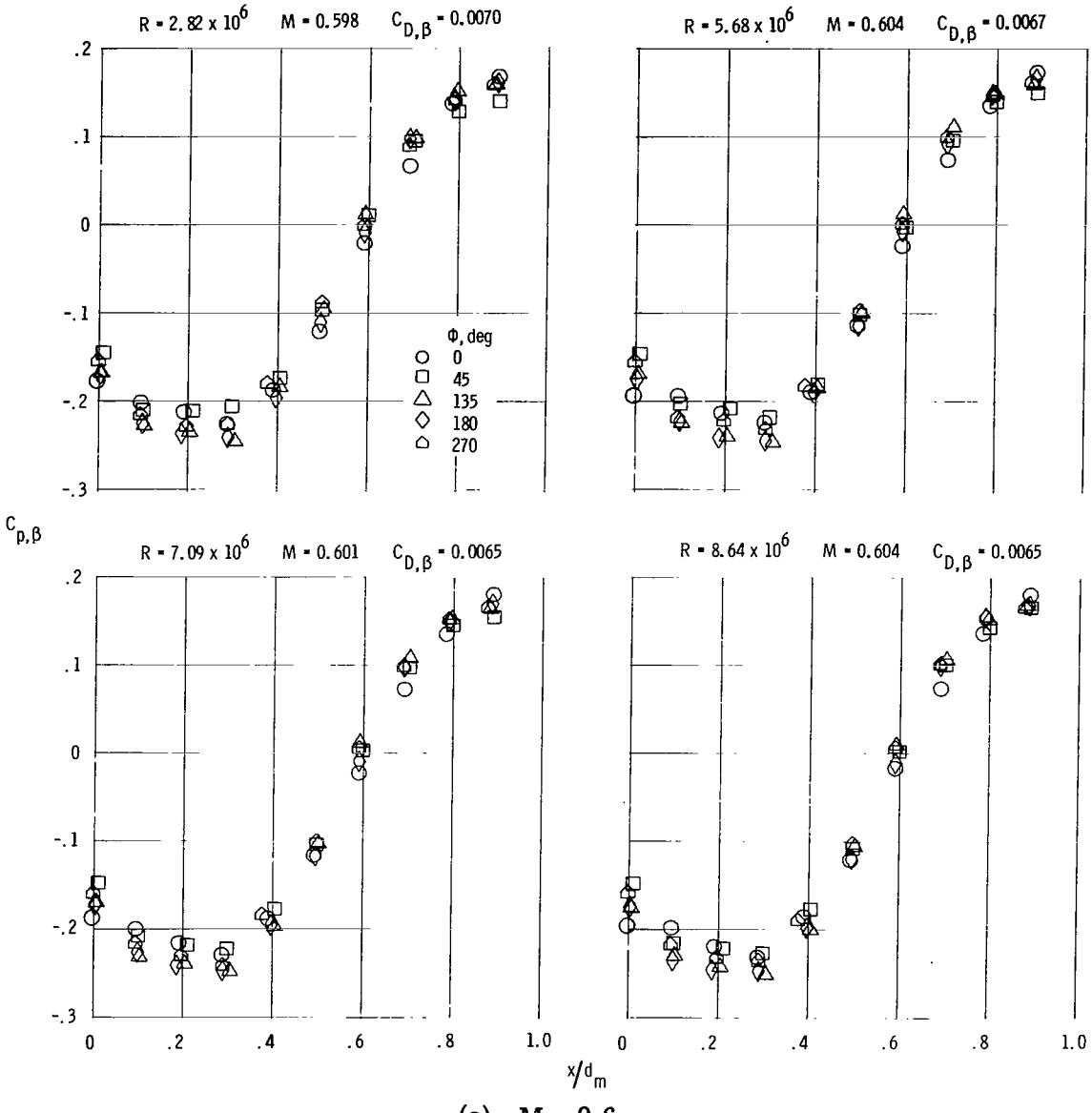


(a) M = 0.6.

Figure 7.- Boattail pressure coefficient distributions at various Reynolds numbers for the circular-arc—conic boattail with wing in forward position.

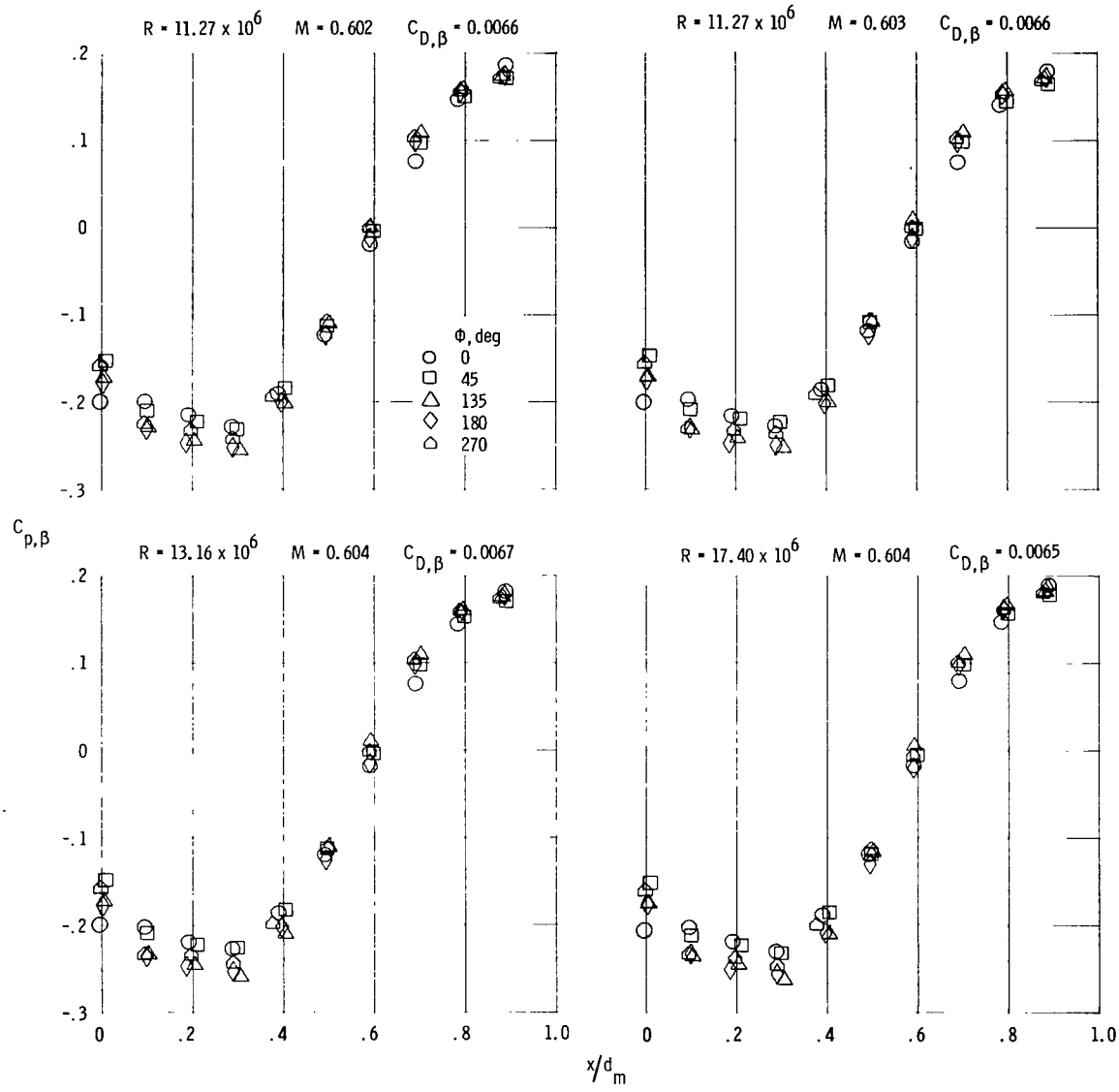


(a) Continued.

Figure 7.- Continued.

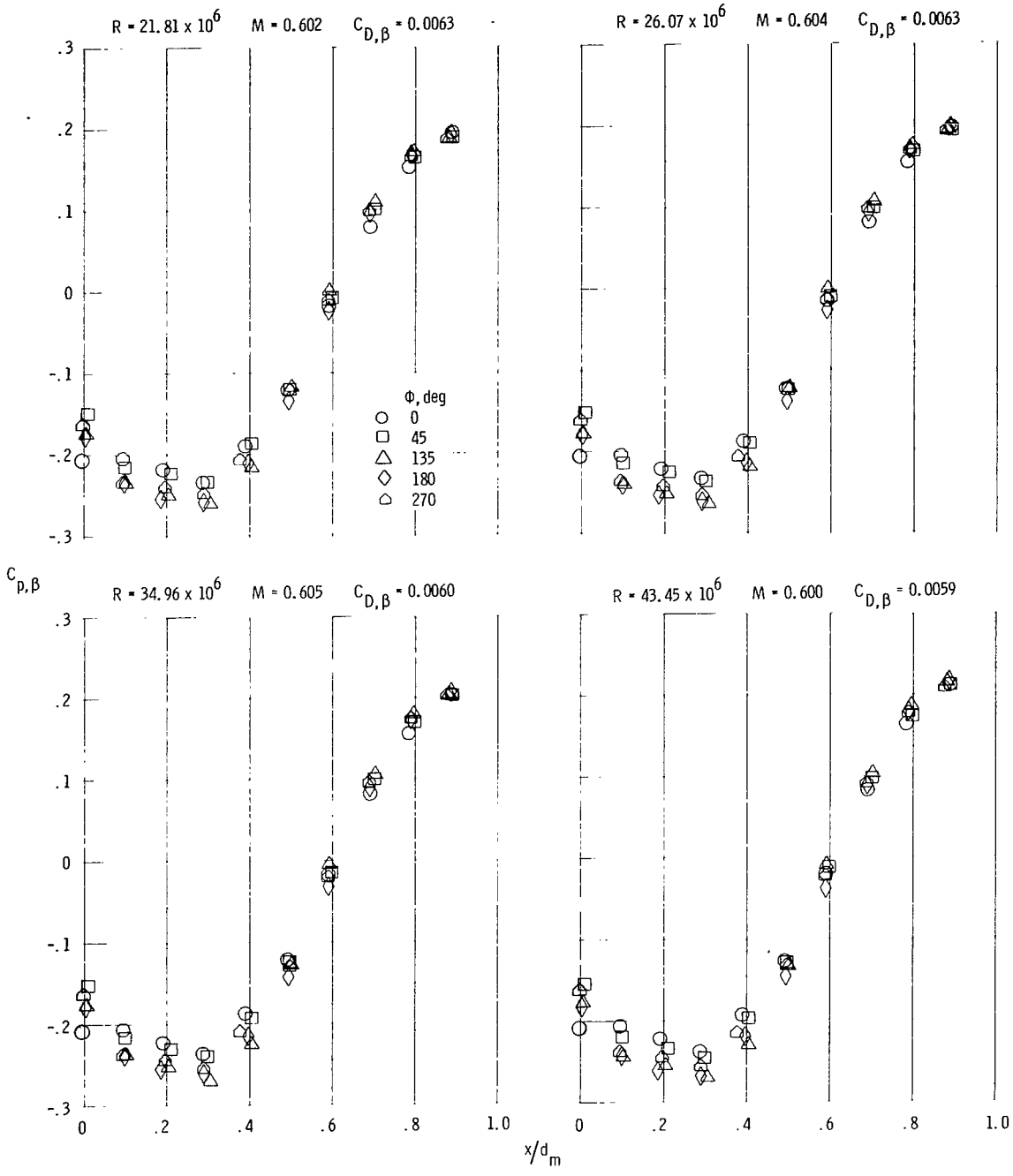


(a) Continued.

Figure 7.- Continued.

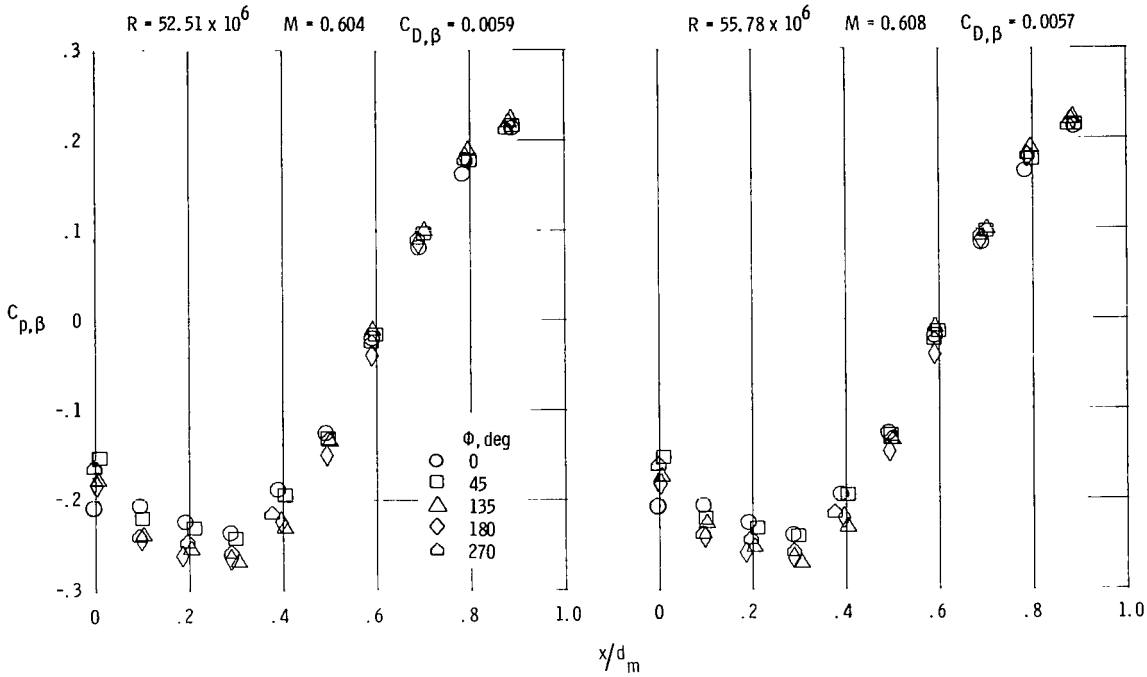


(a) Concluded.

Figure 7.- Continued.

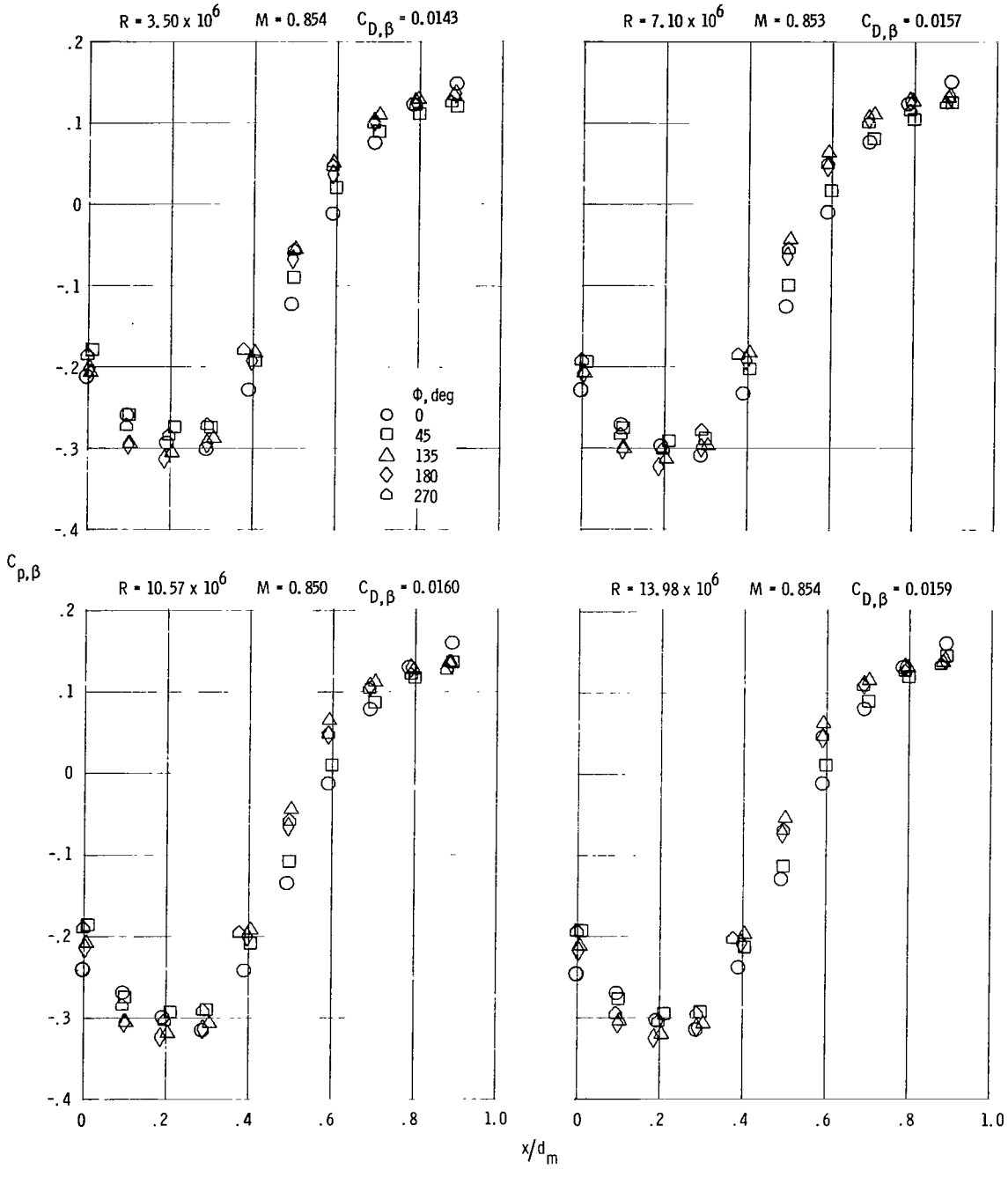


(b) M = 0.85.

Figure 7.- Continued.

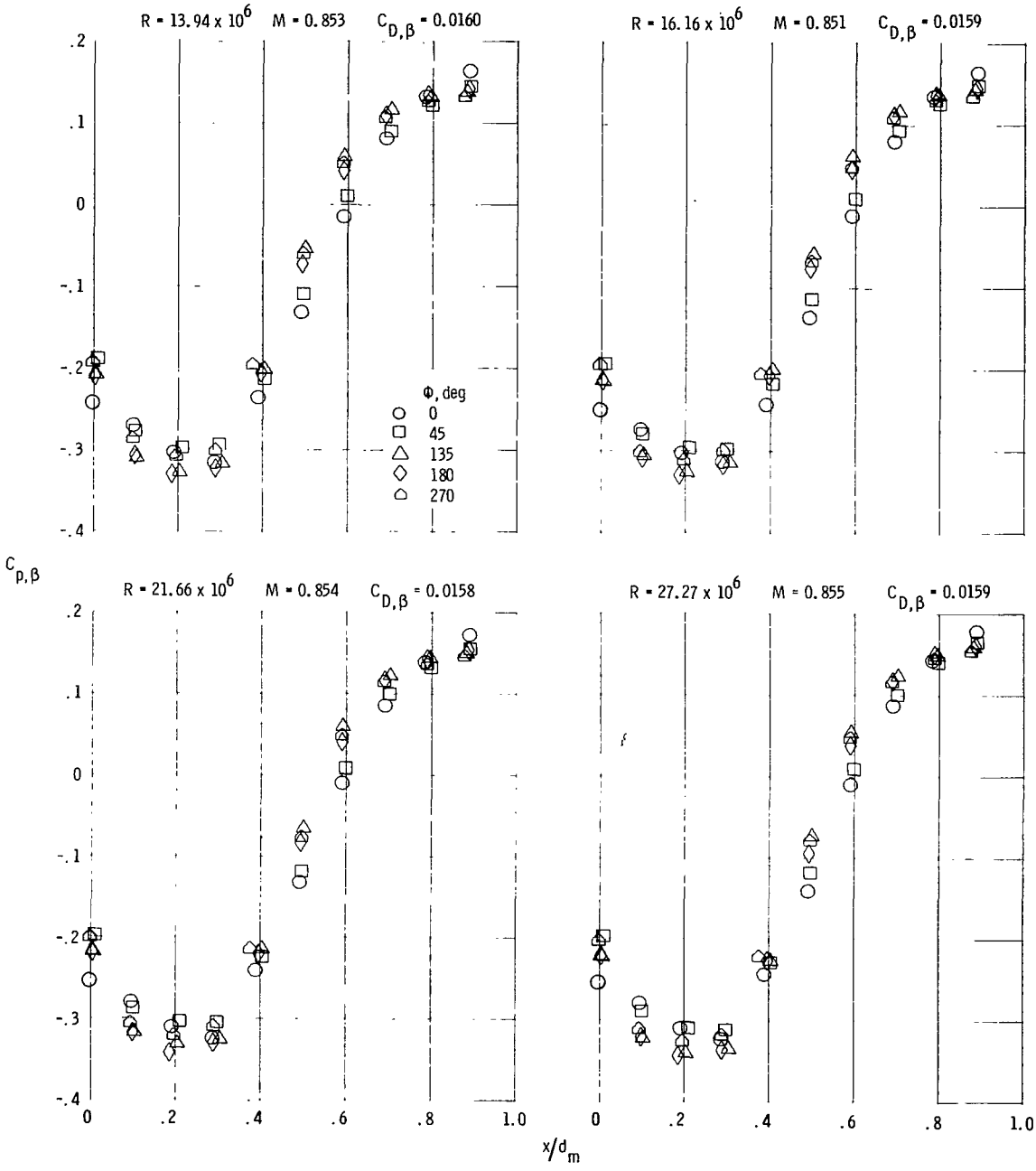


(b) Continued.

**Figure 7.- Continued.**

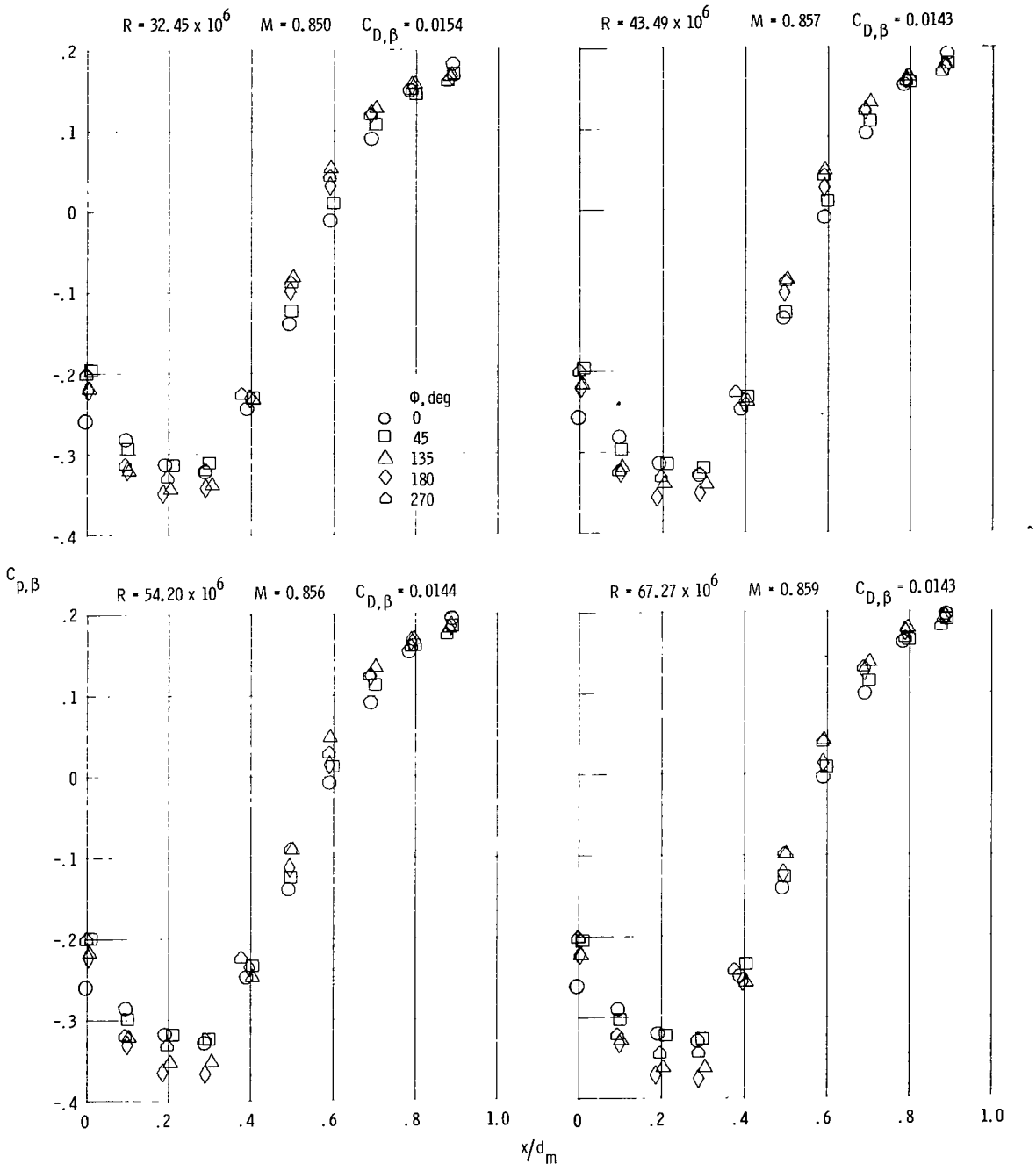


(b) Concluded.

Figure 7.- Concluded.

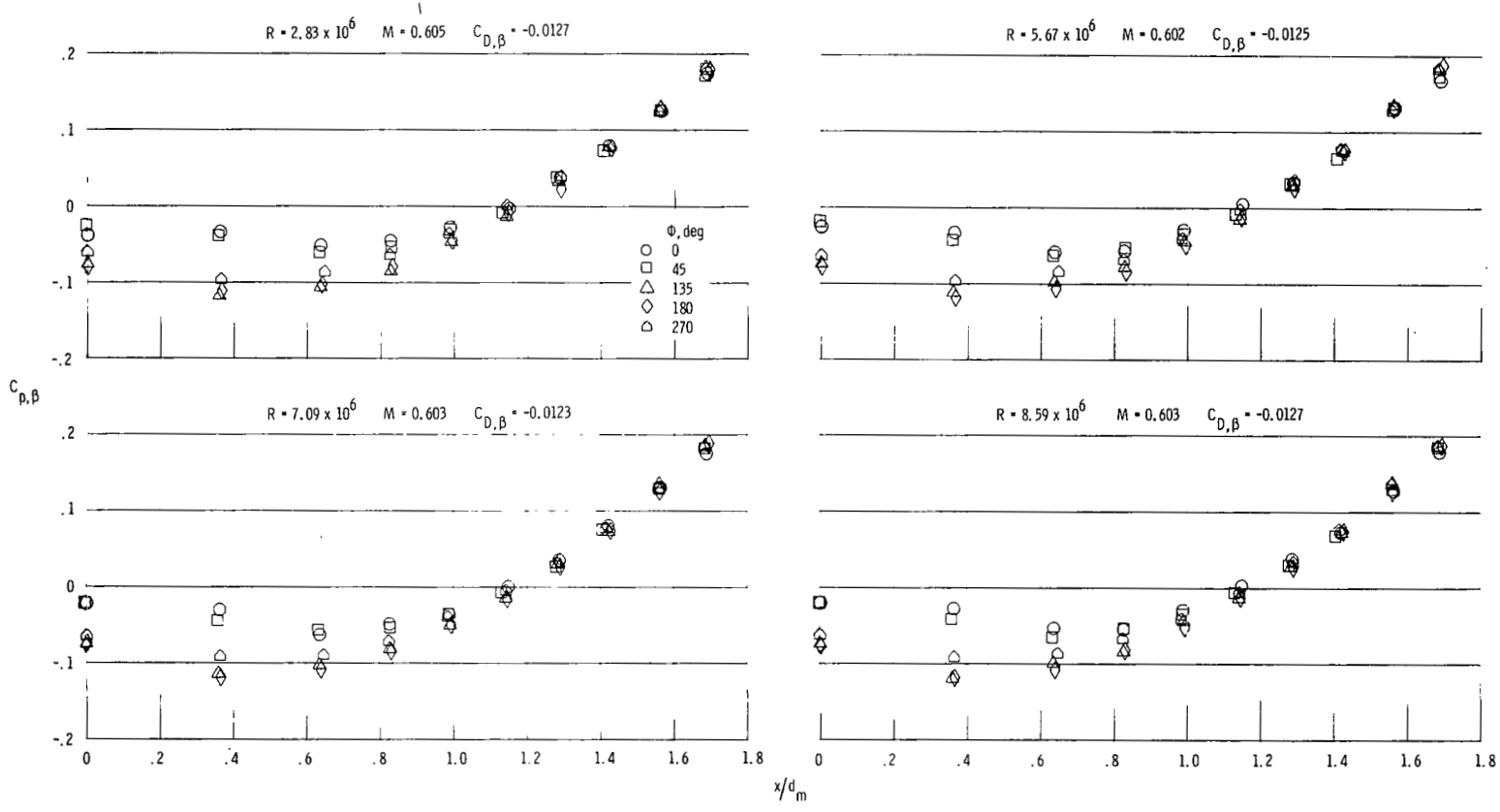


(a) M = 0.6.

Figure 8.- Boattail pressure coefficient distributions at various Reynolds numbers for the circular-arc boattail with wing in aft position.

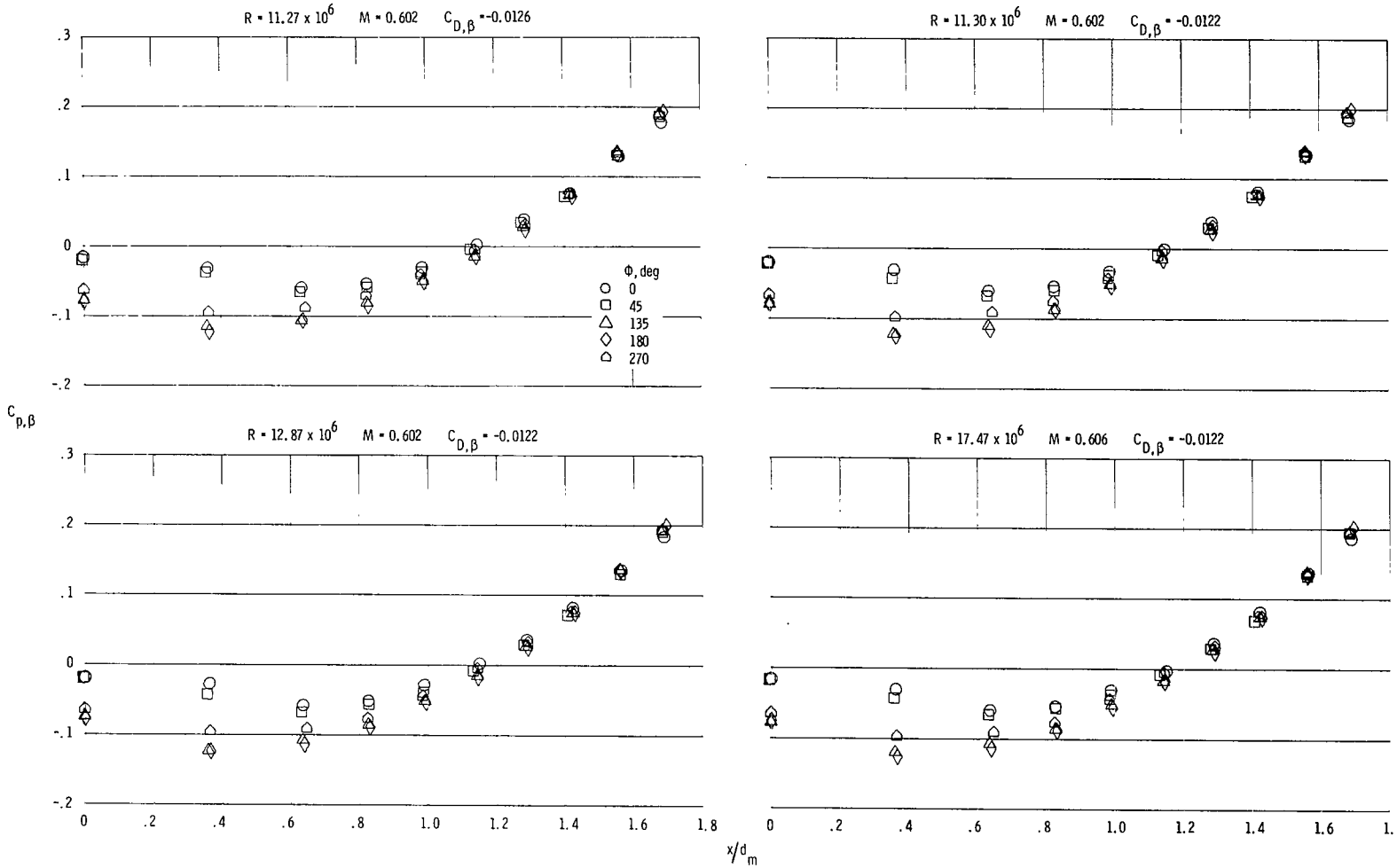


(a) Continued.

Figure 8.- Continued.

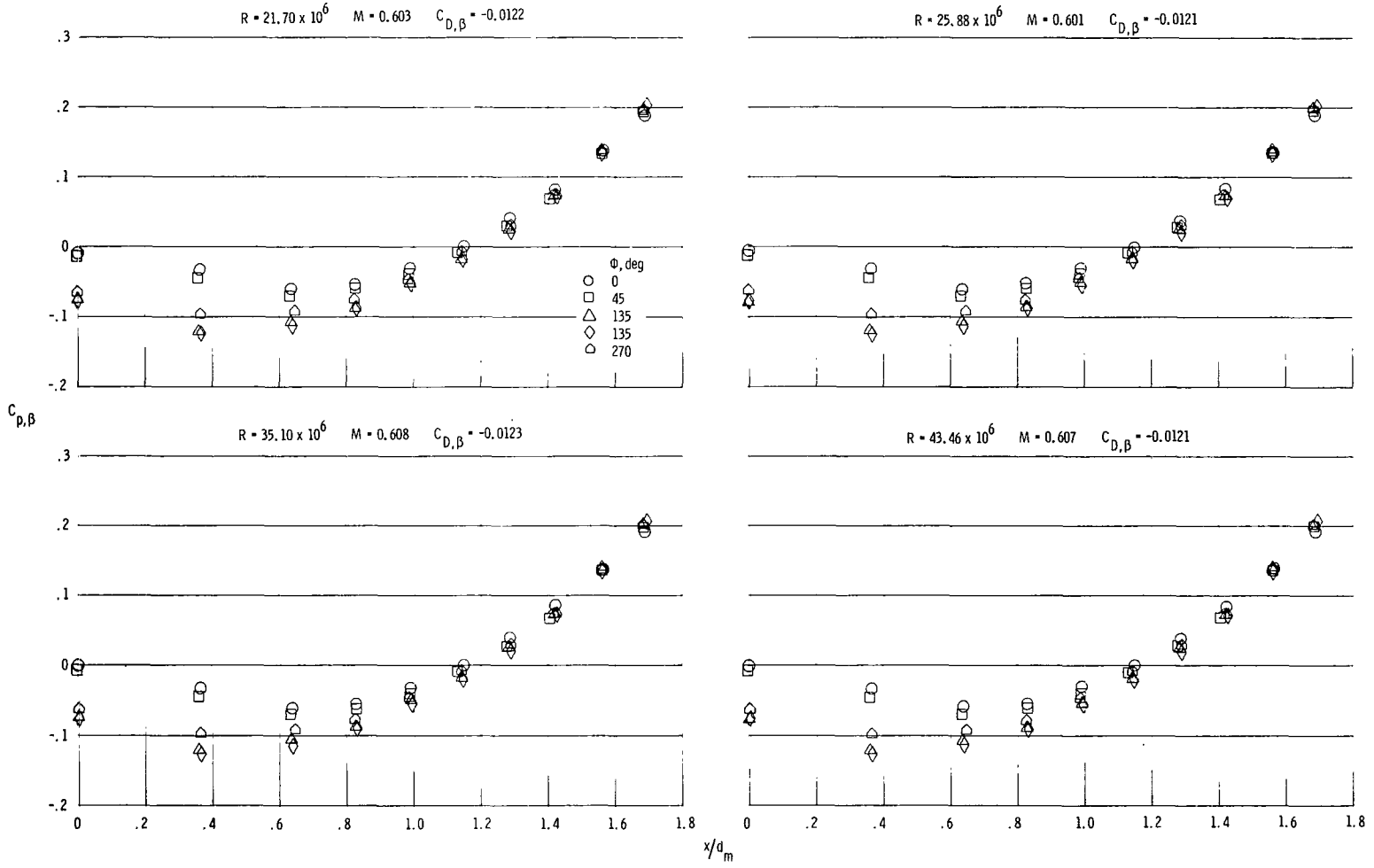


(a) Continued.

Figure 8.- Continued.

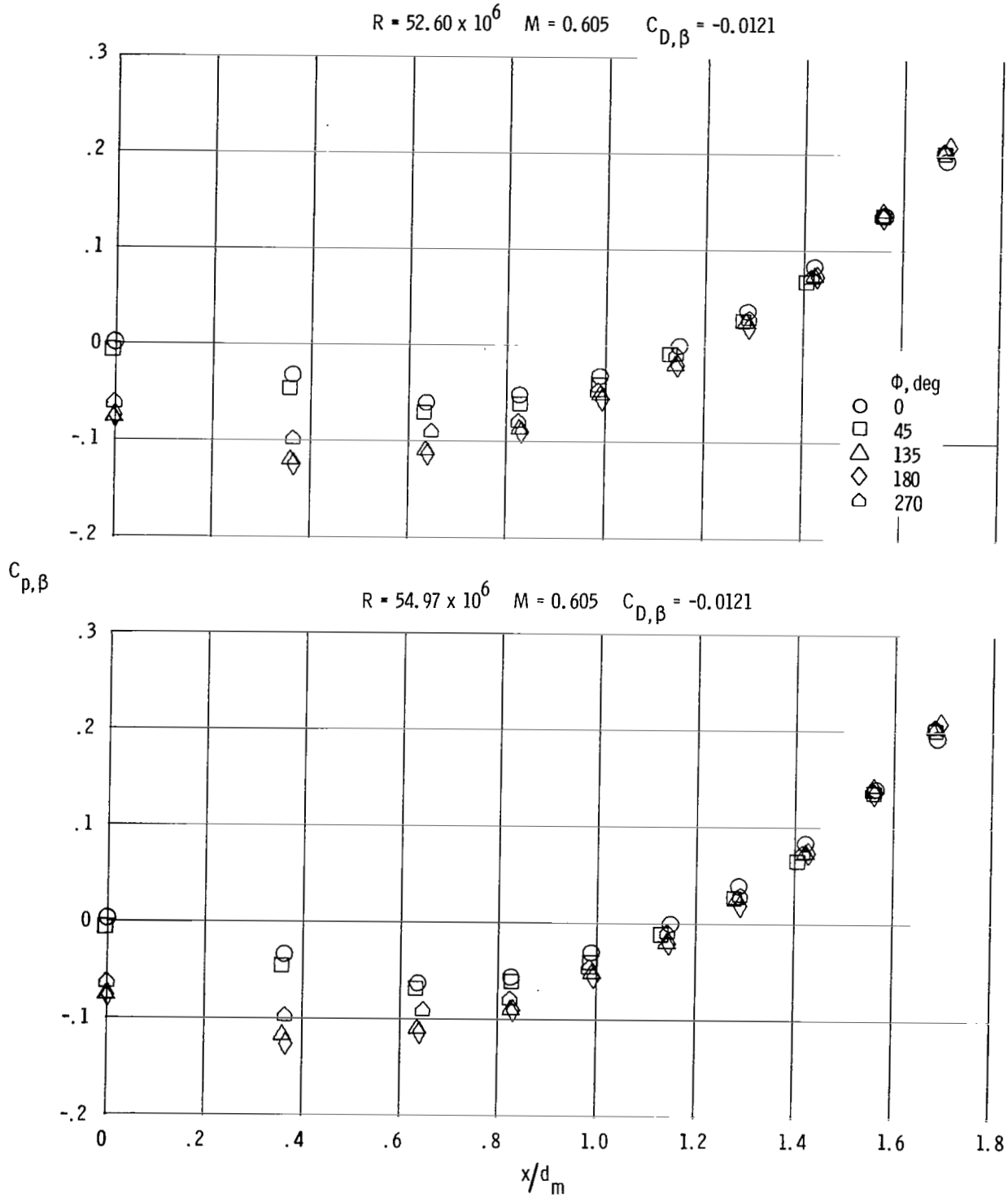


(a) Concluded.

Figure 8.- Continued.

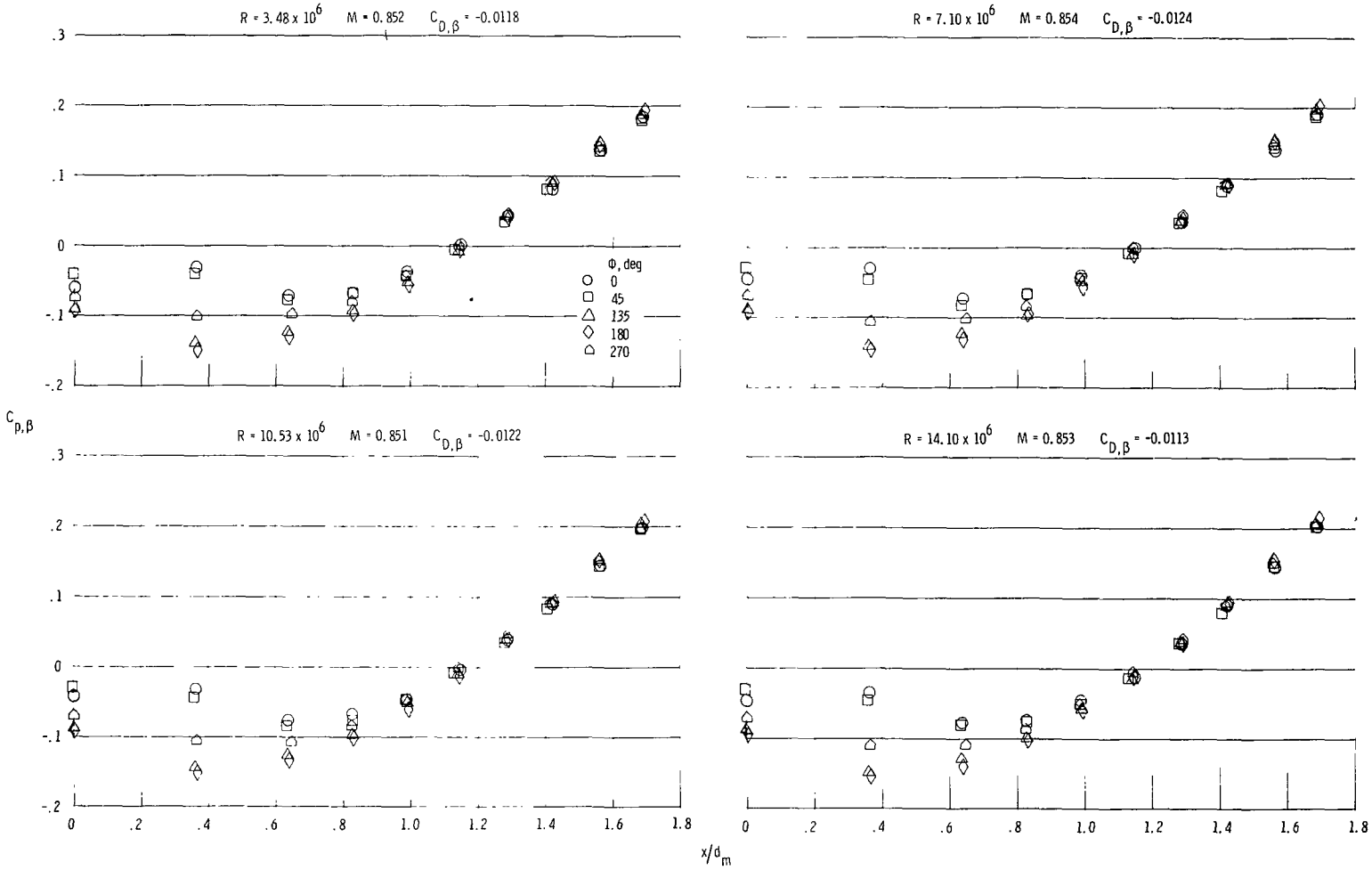


(b) M = 0.85.

Figure 8.- Continued.

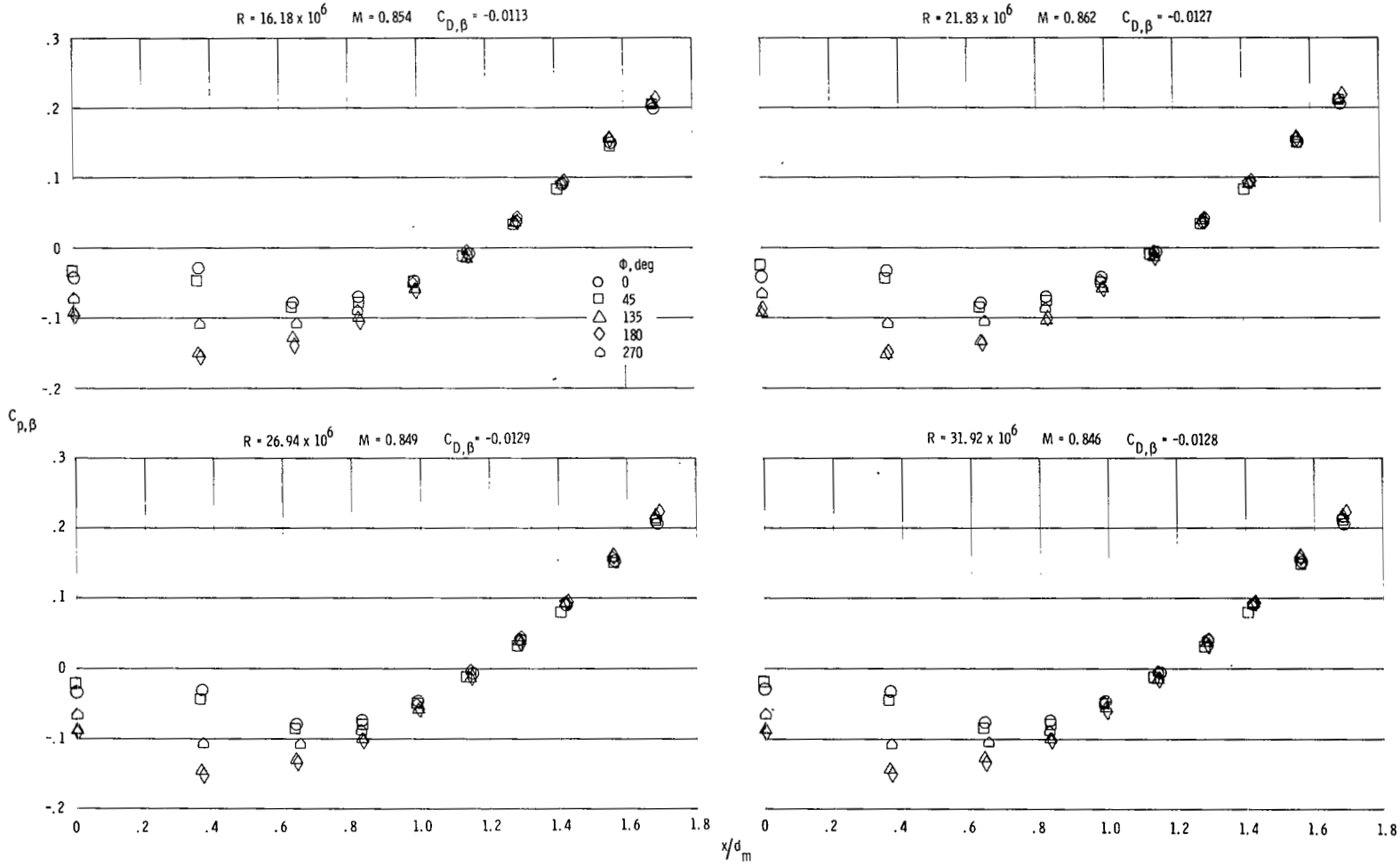


(b) Continued.

Figure 8.- Continued.

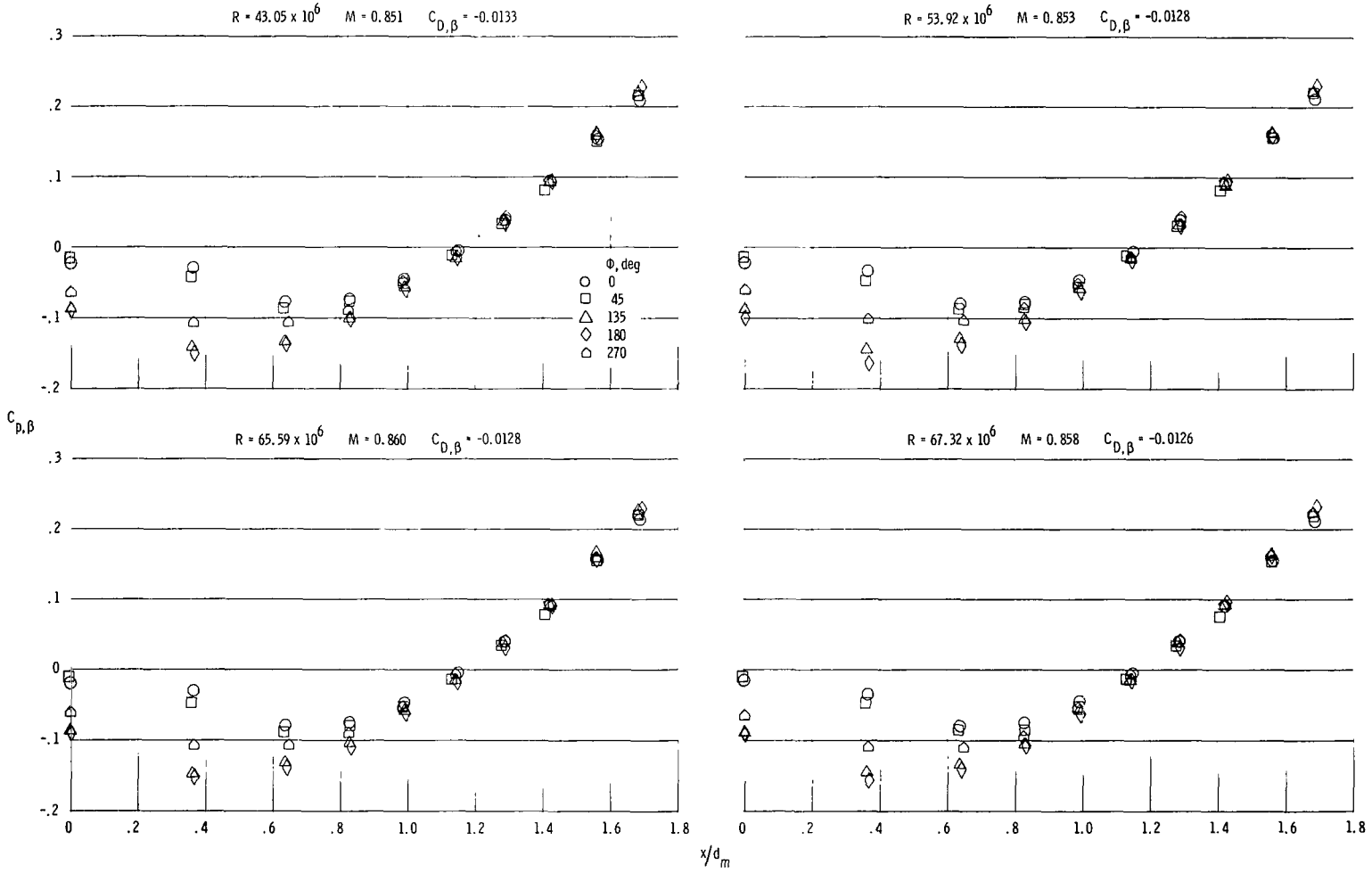


(b) Concluded.

Figure 8.- Continued.

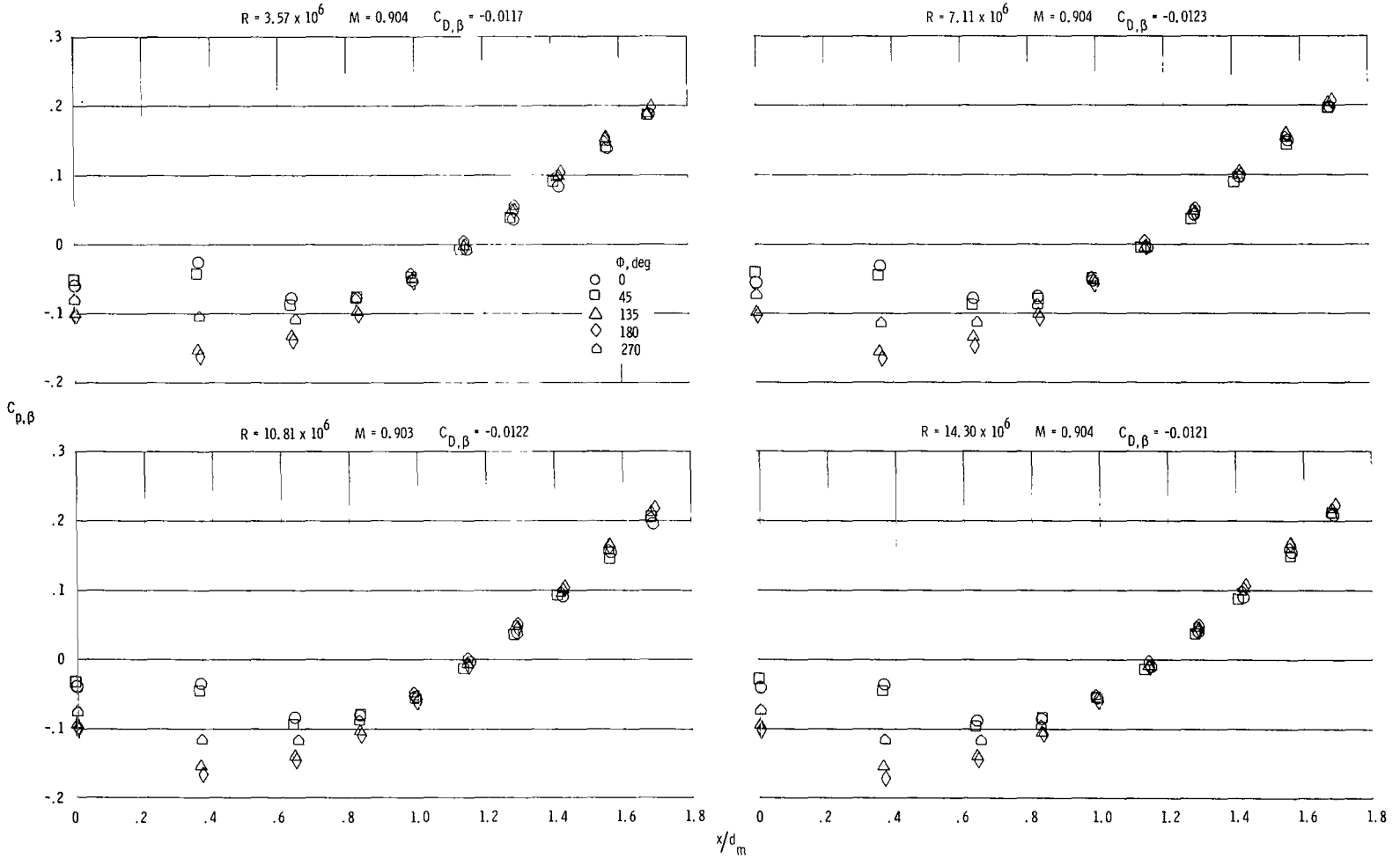


(c) M = 0.9.

Figure 8.- Continued.

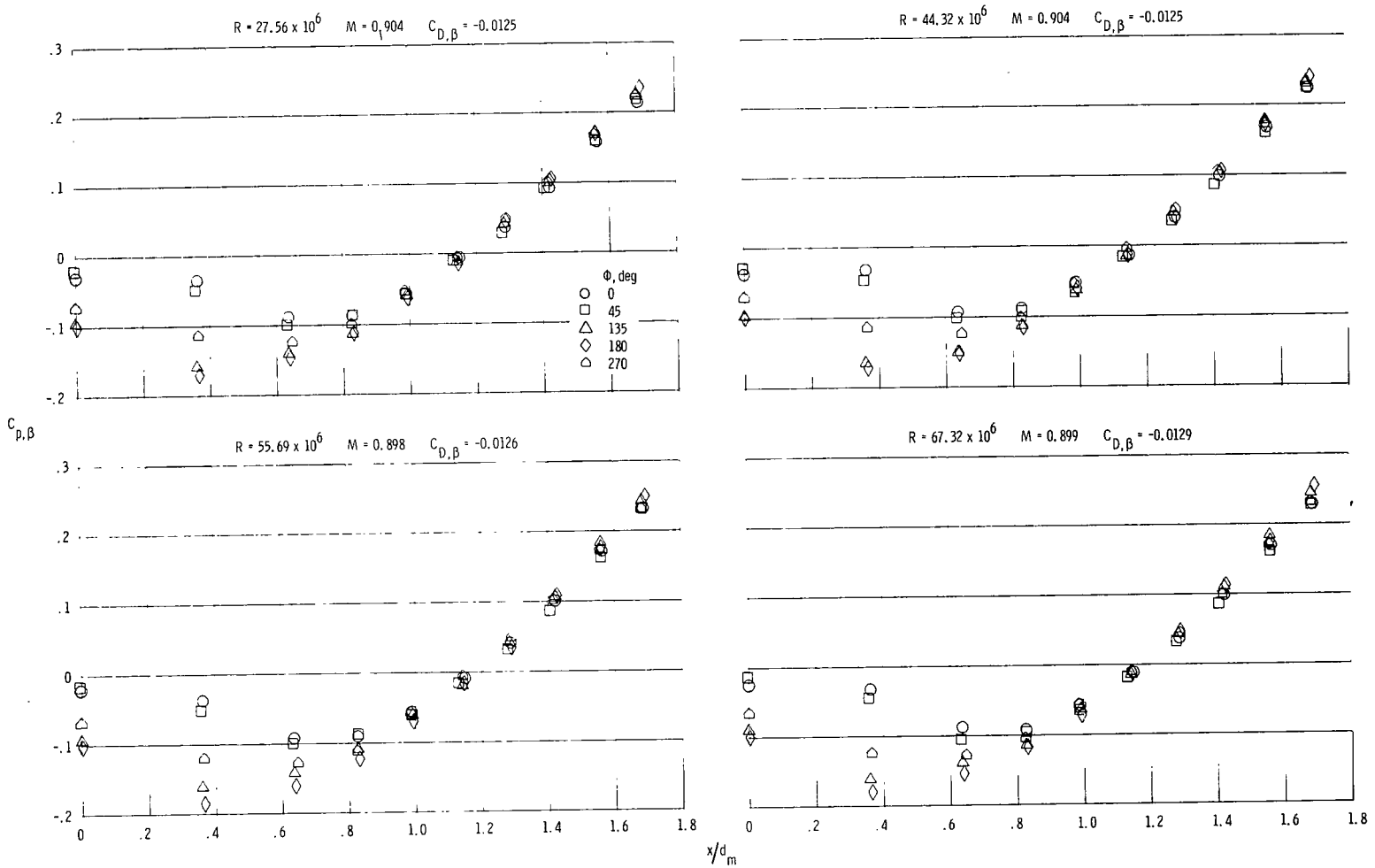


(c) Concluded.

Figure 8.- Concluded.

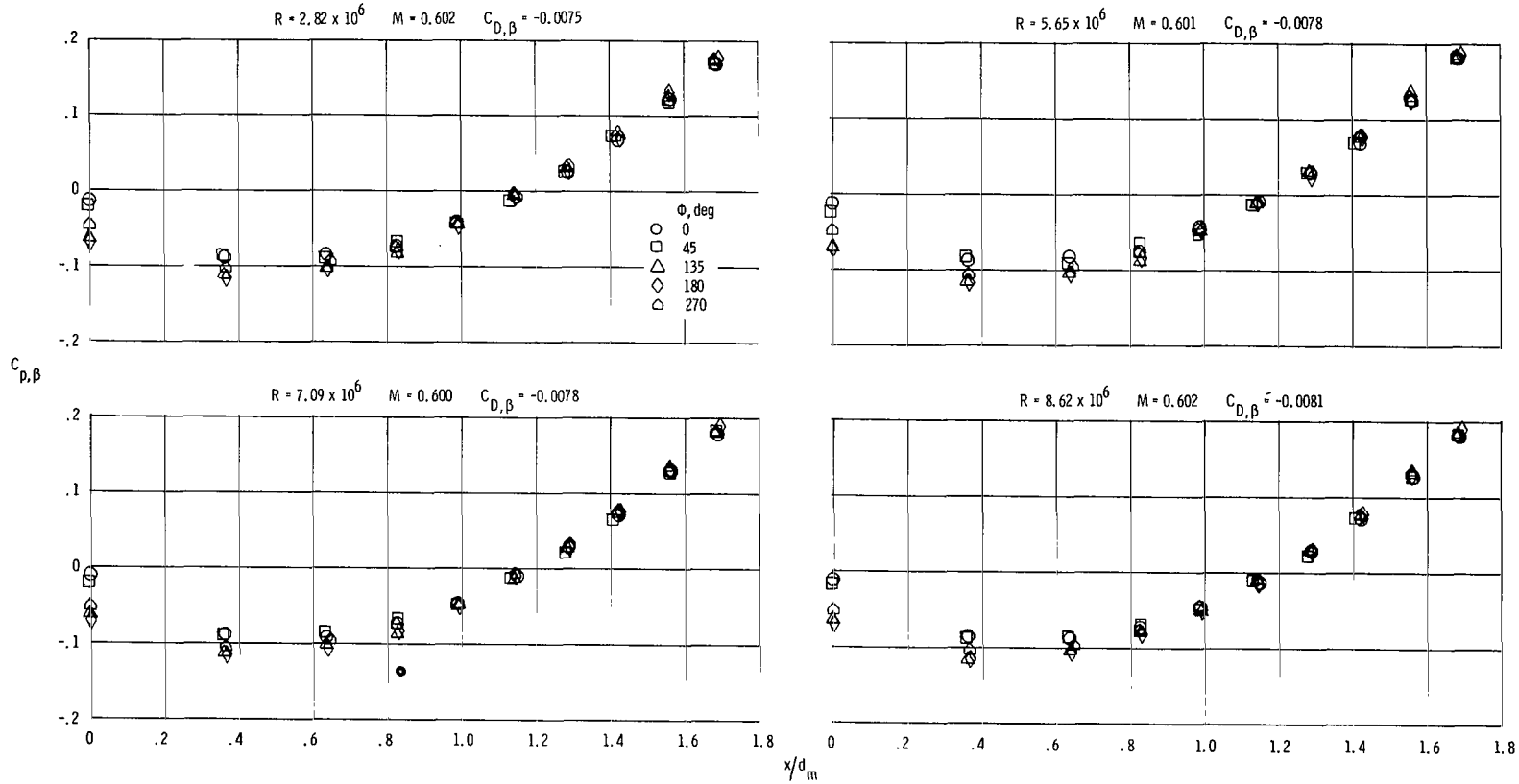


(a) M = 0.6.

Figure 9.- Boattail pressure coefficient distributions at various Reynolds numbers for the circular-arc boattail with wing in middle position.

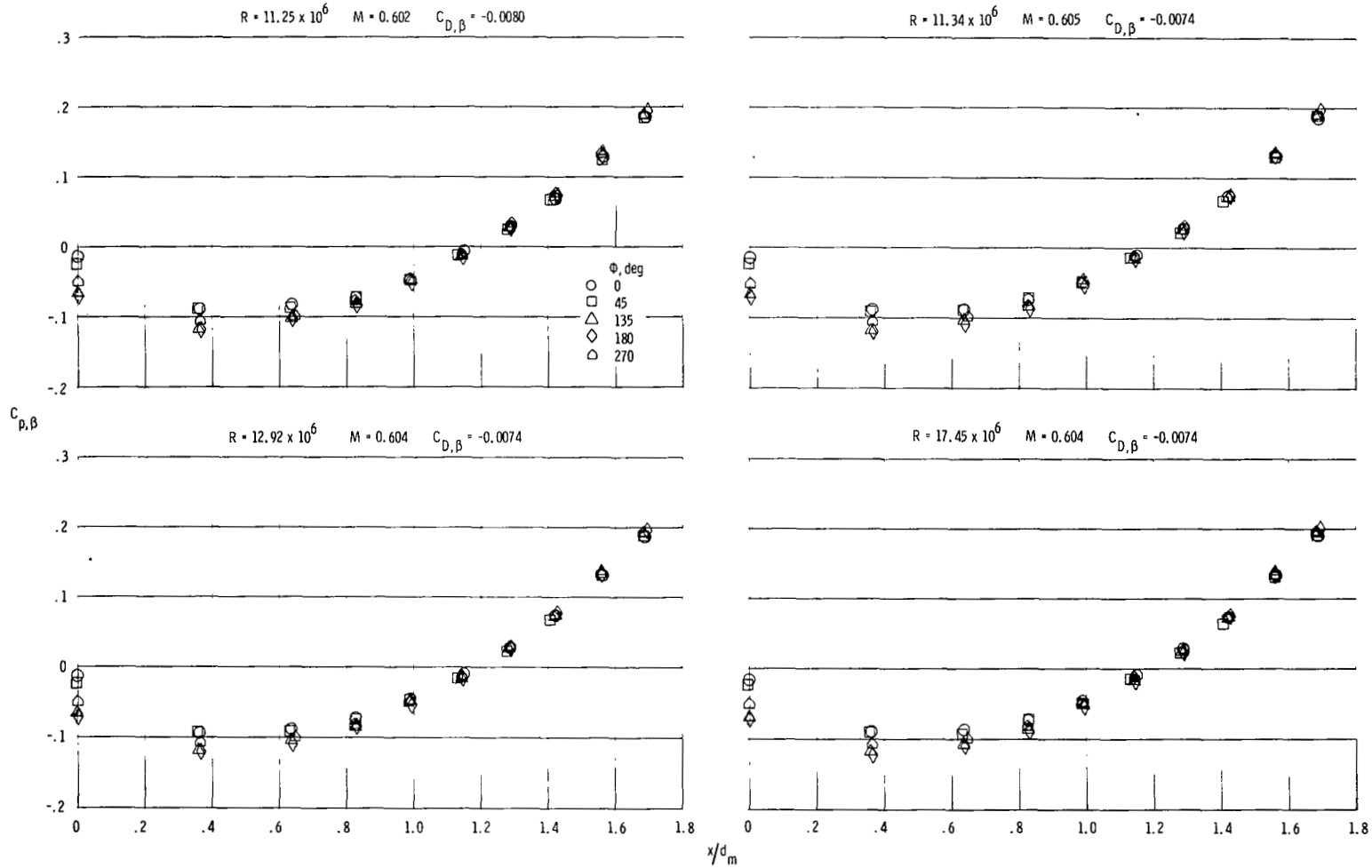


(a) Continued.

Figure 9.- Continued.

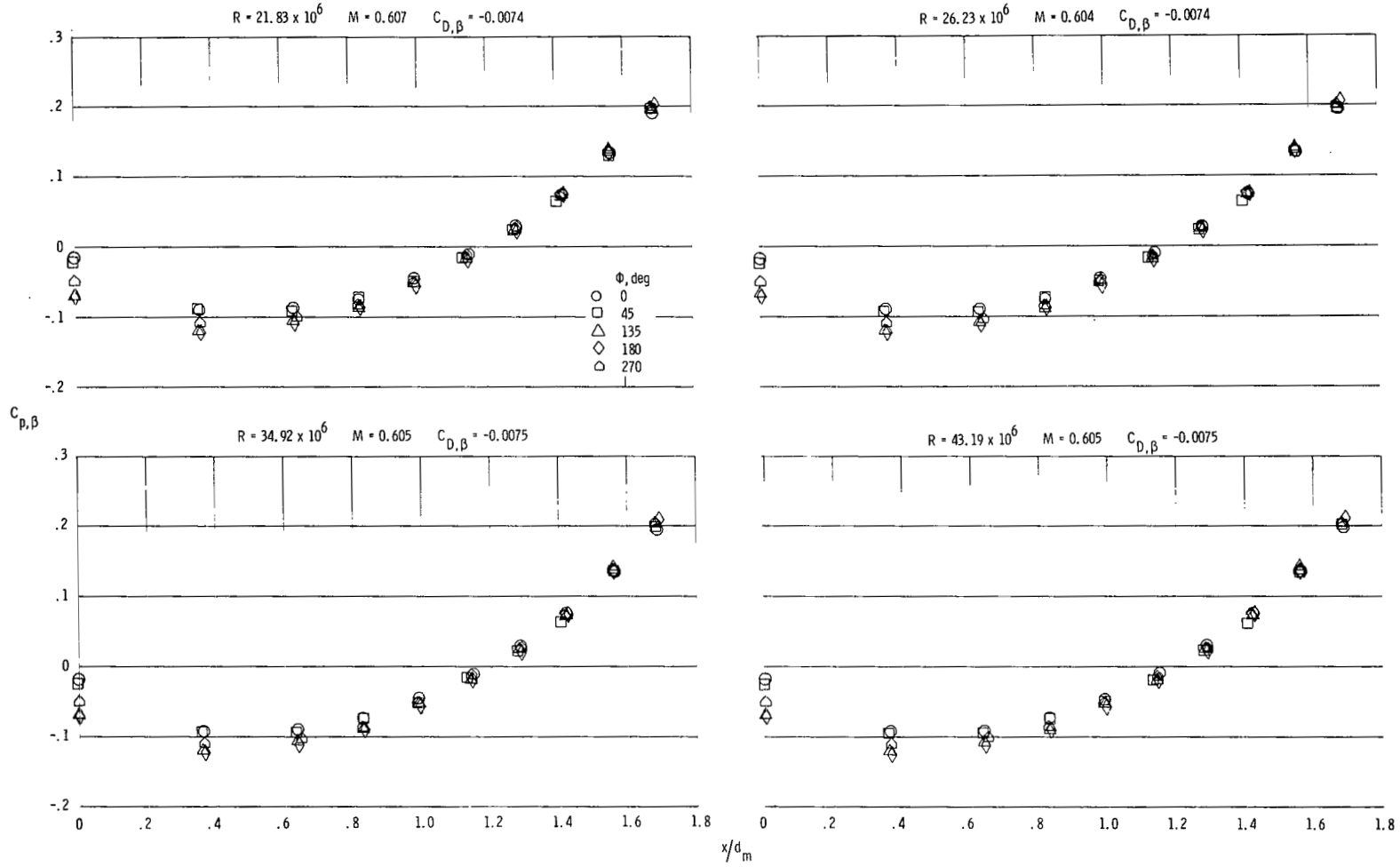


(a) Continued.

Figure 9.- Continued.

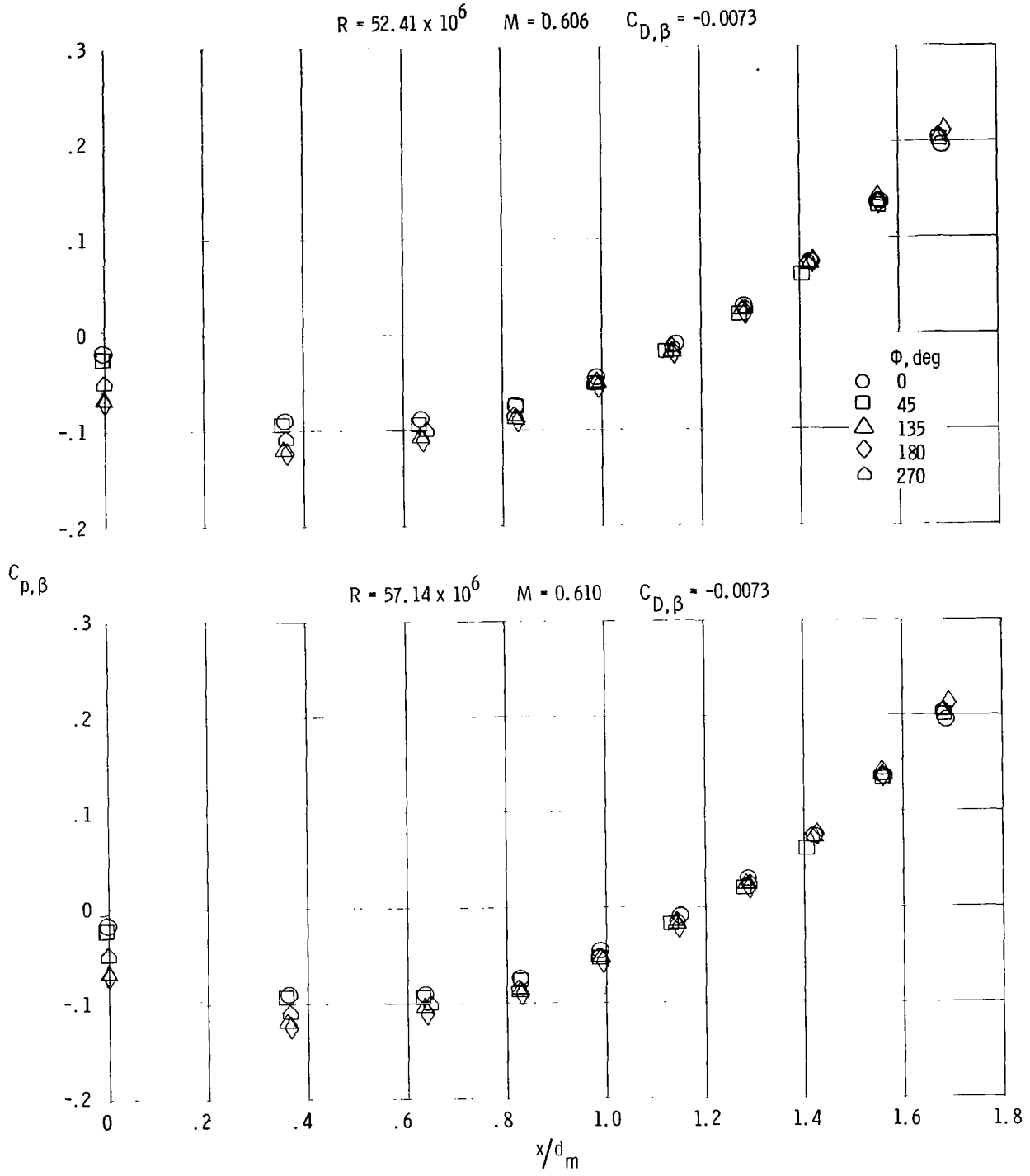


(a) Concluded.

Figure 9.- Continued.

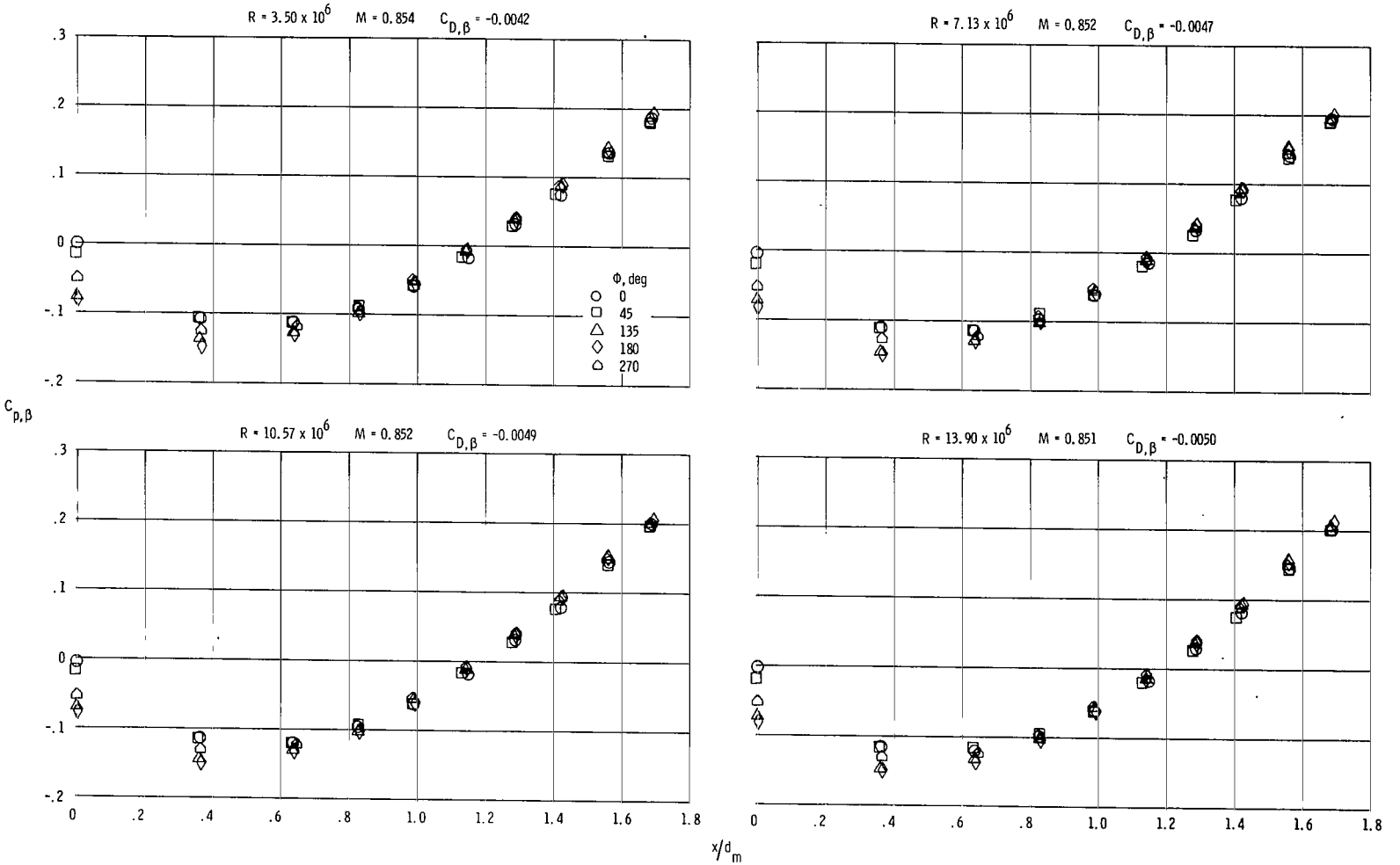


(b) M = 0.85.

Figure 9.- Continued.

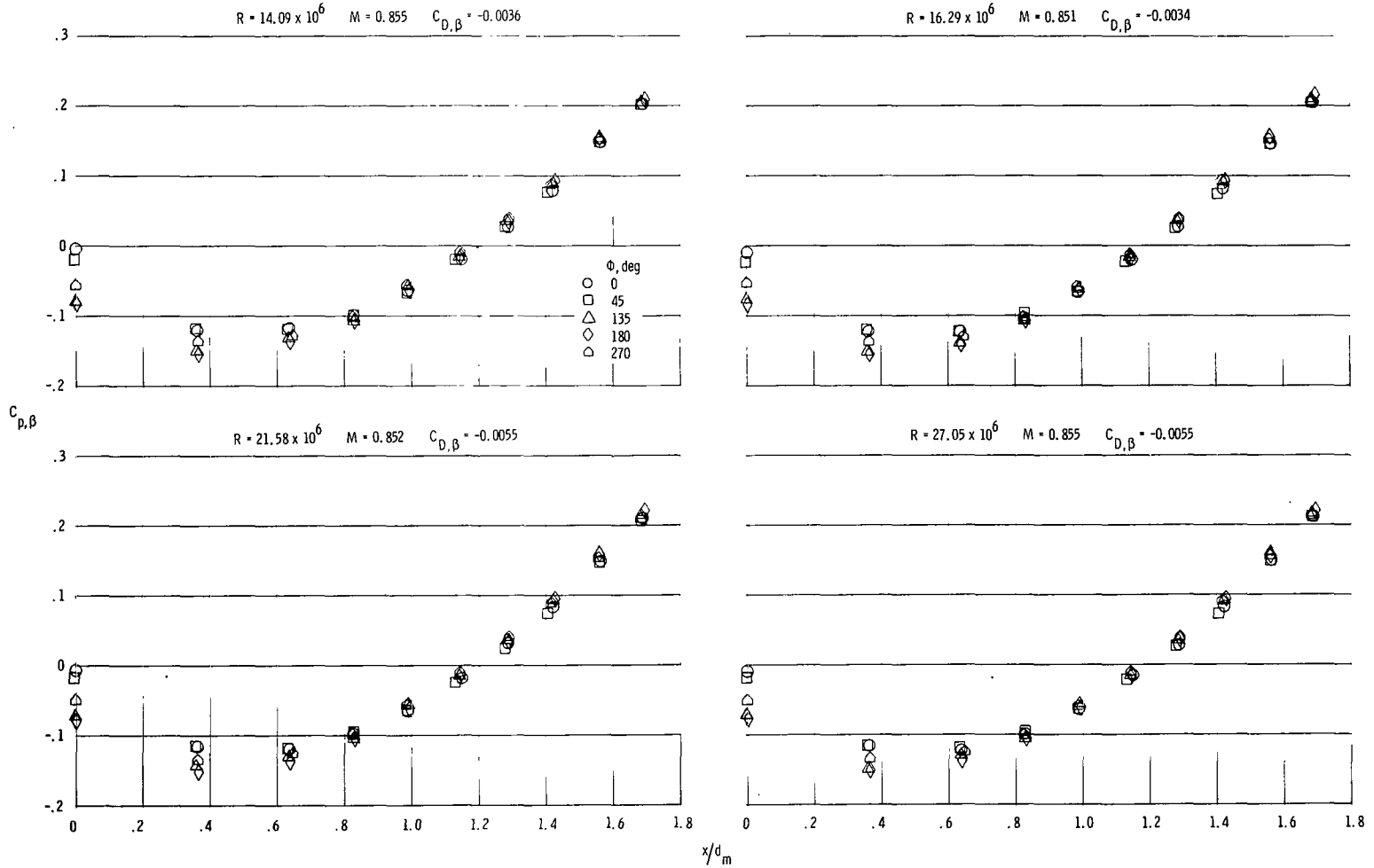


(b) Continued.

Figure 9.- Continued.

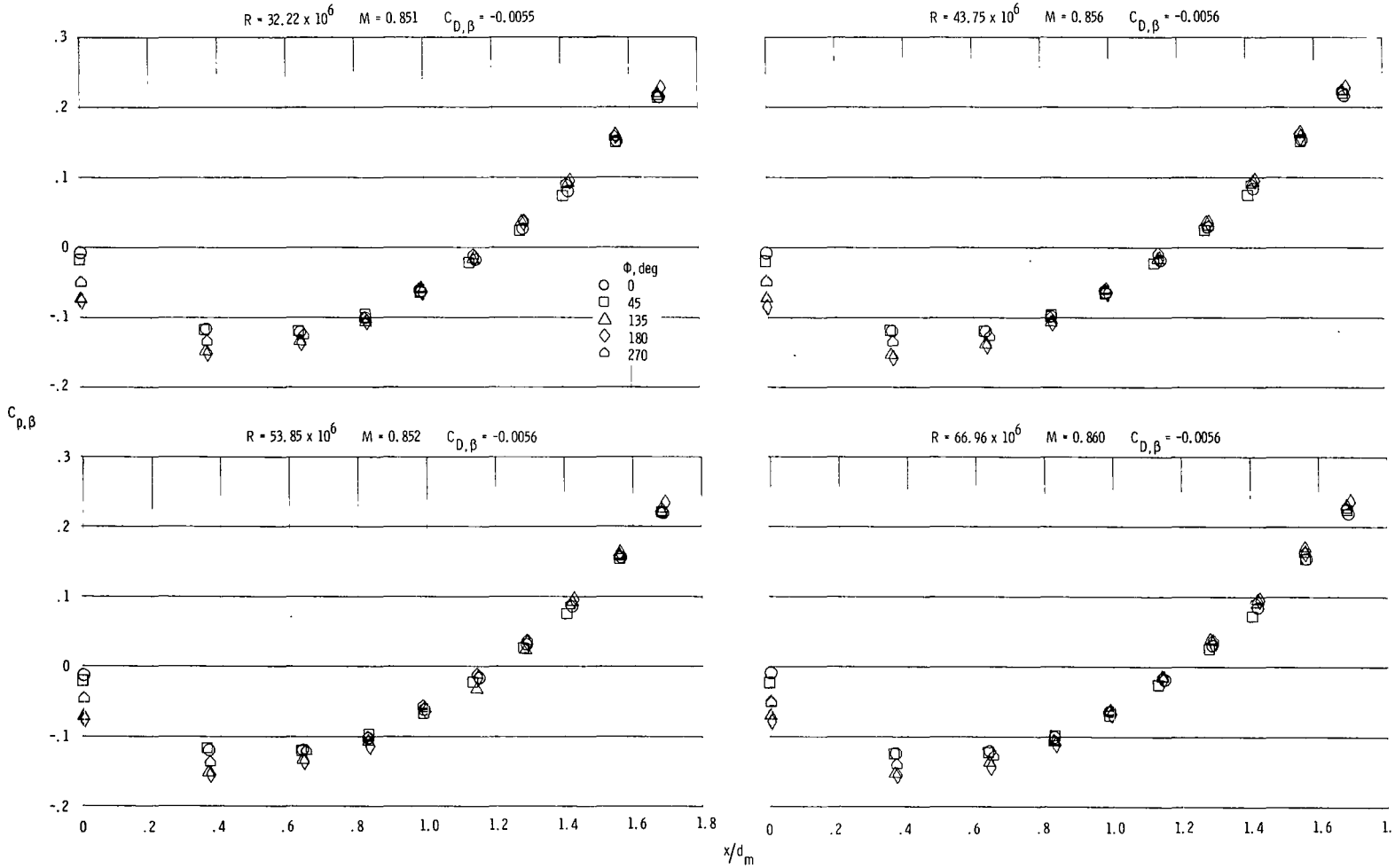


(b) Concluded.

Figure 9.- Concluded.

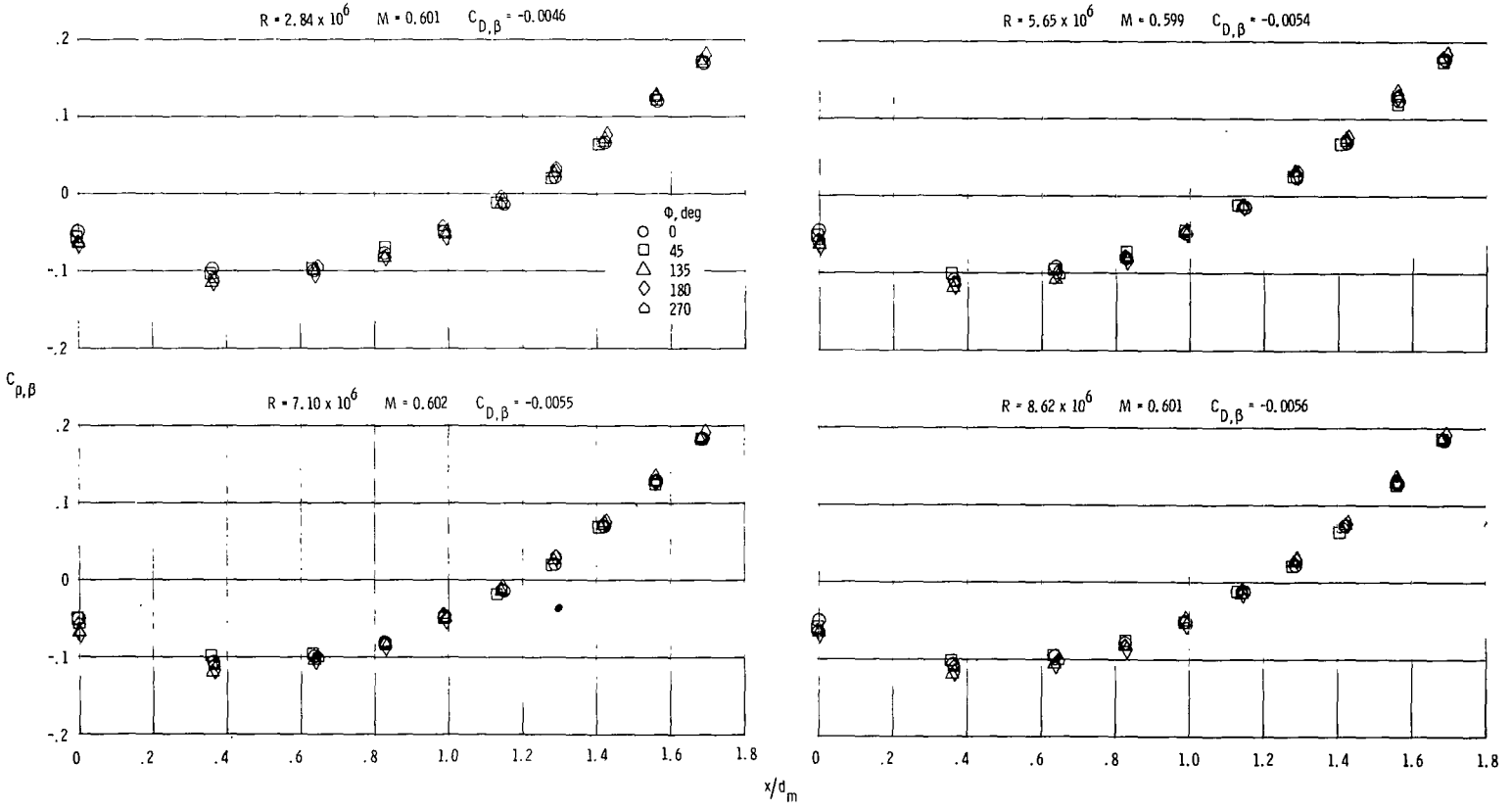


(a) M = 0.6.

Figure 10.- Boattail pressure coefficient distributions at various Reynolds numbers for the circular-arc boattail with wing in forward position.

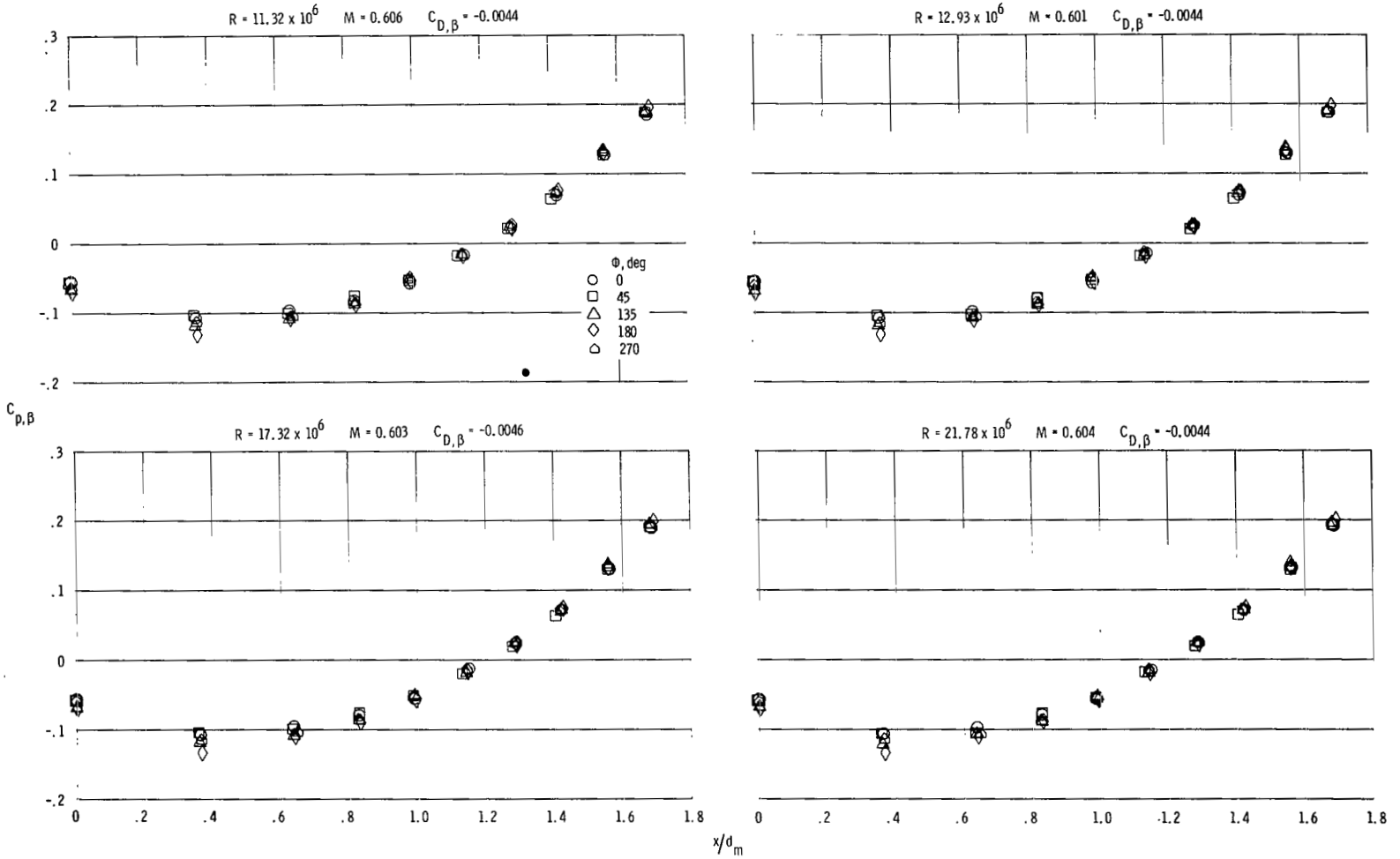


(a) Continued.

Figure 10.- Continued.

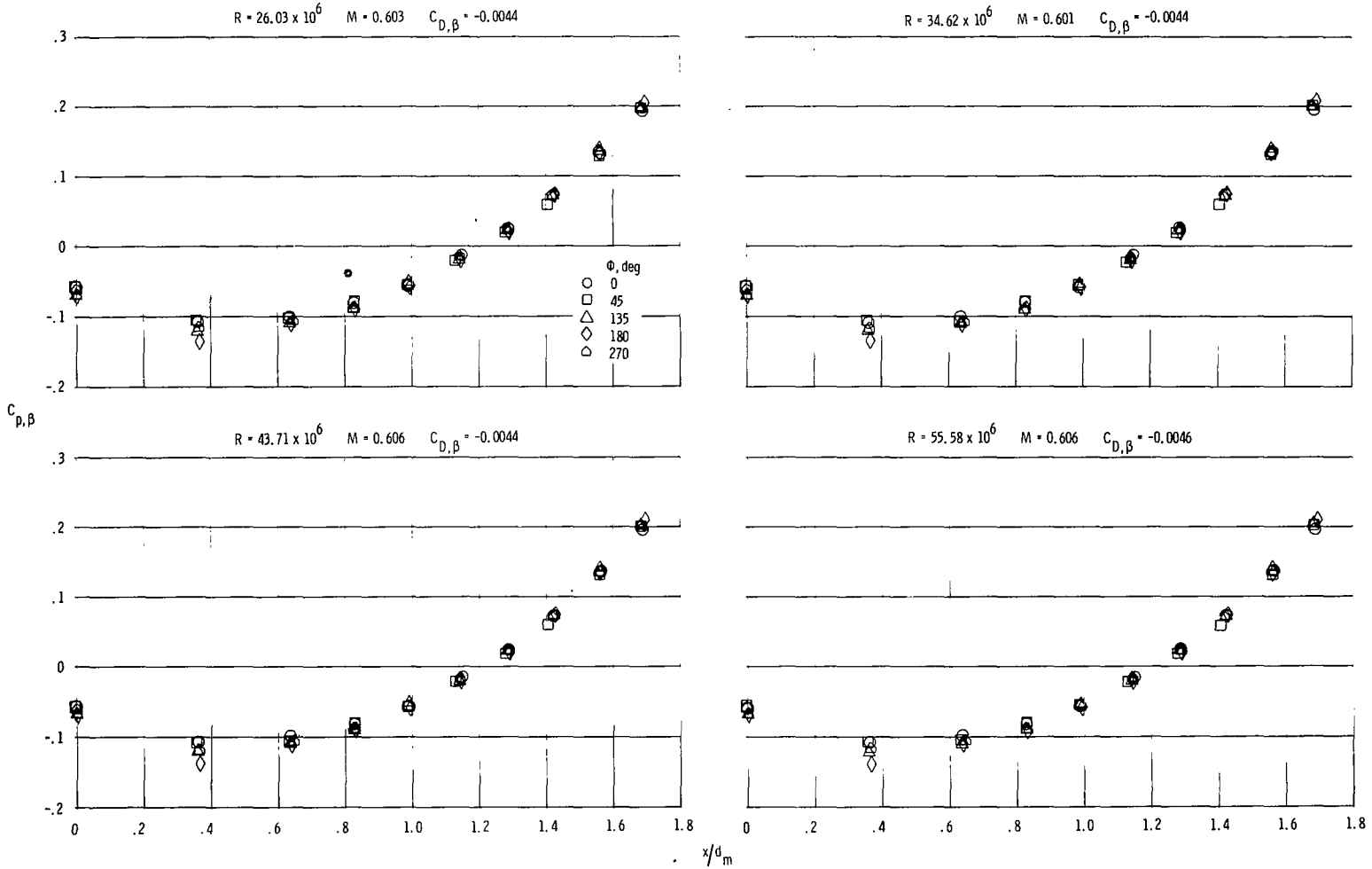


(a) Concluded.

Figure 10. - Continued.

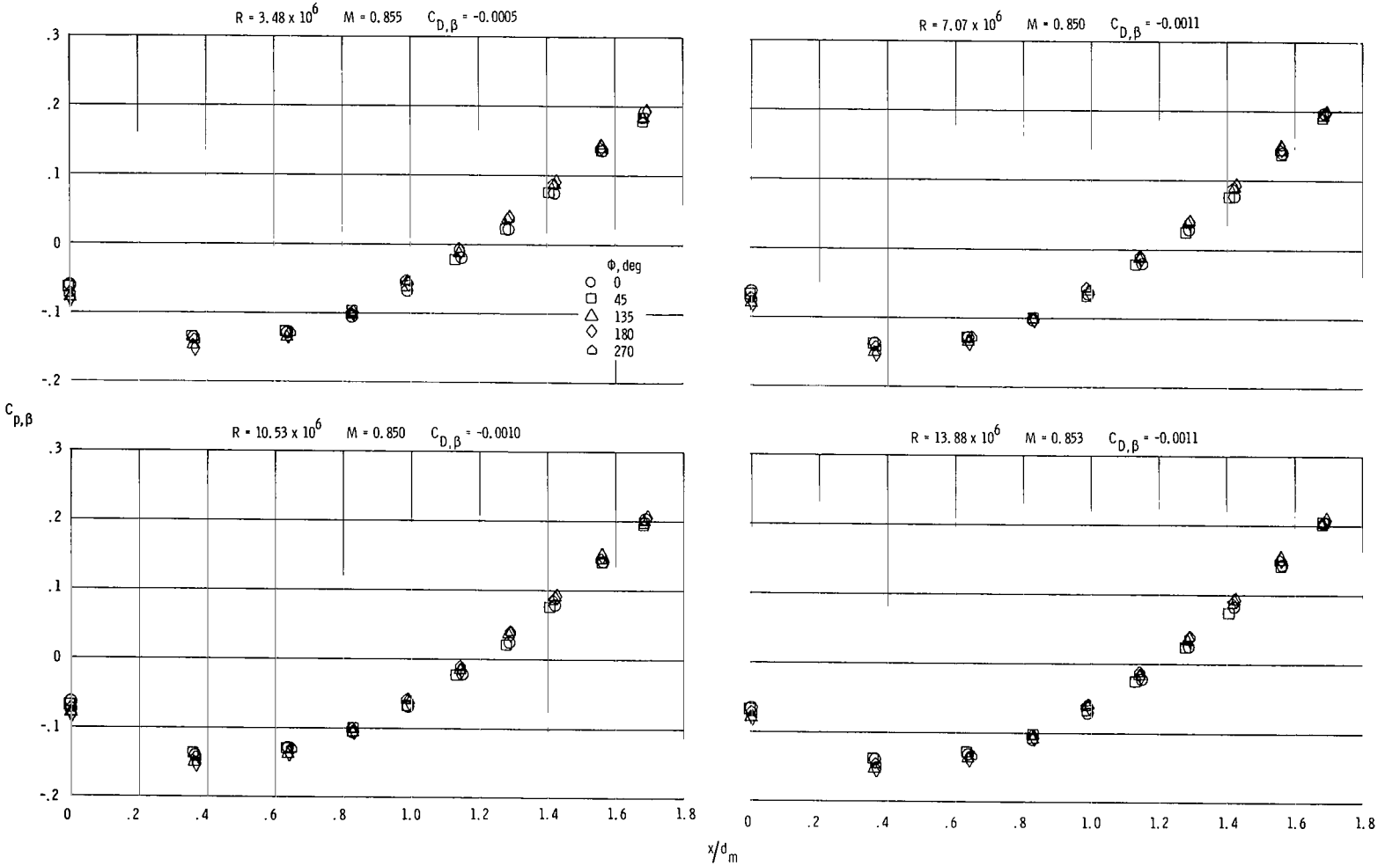


(b) M = 0.85.

Figure 10.- Continued.

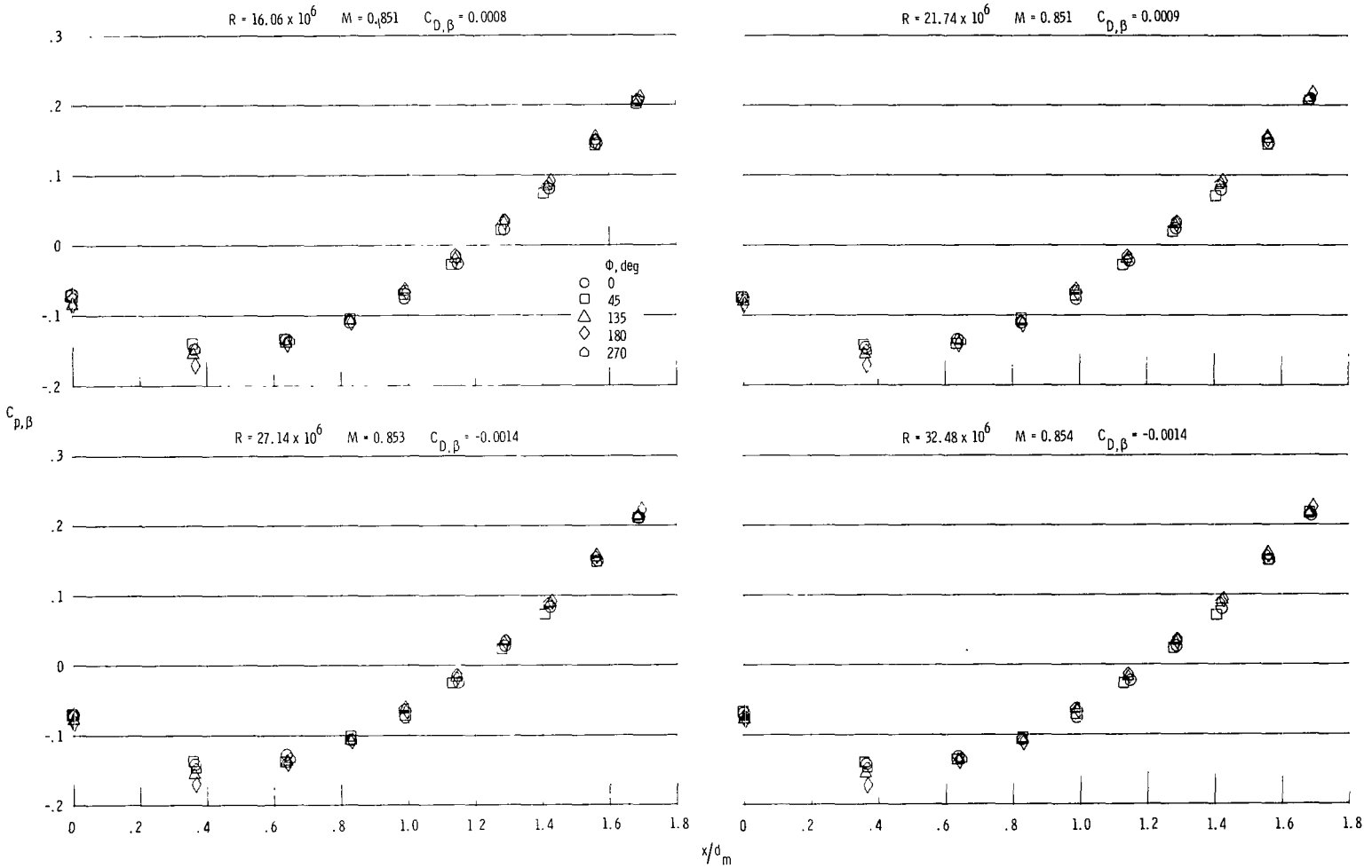


(b) Continued.

Figure 10.- Continued.

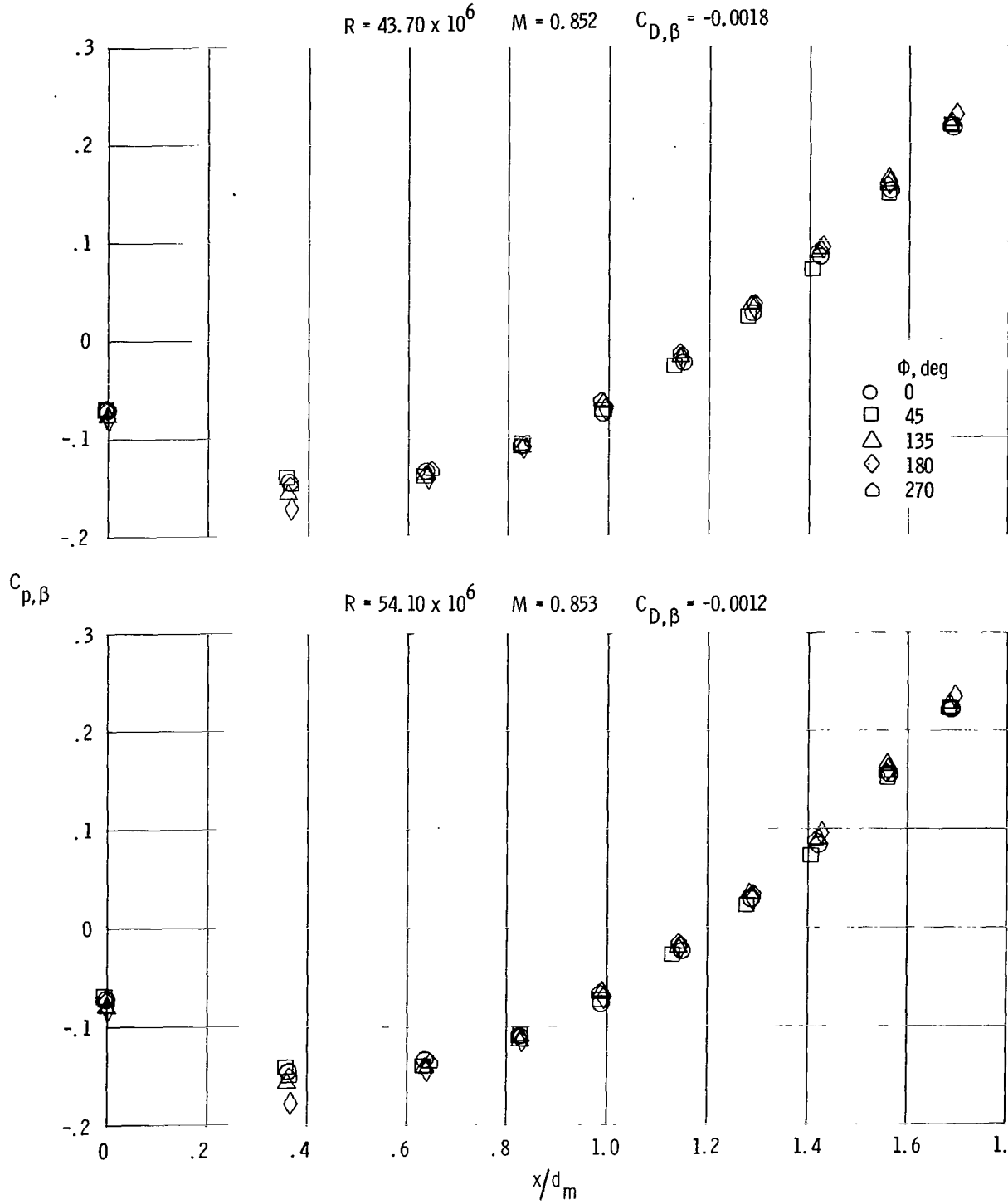


(b) Concluded.

Figure 10.- Continued.

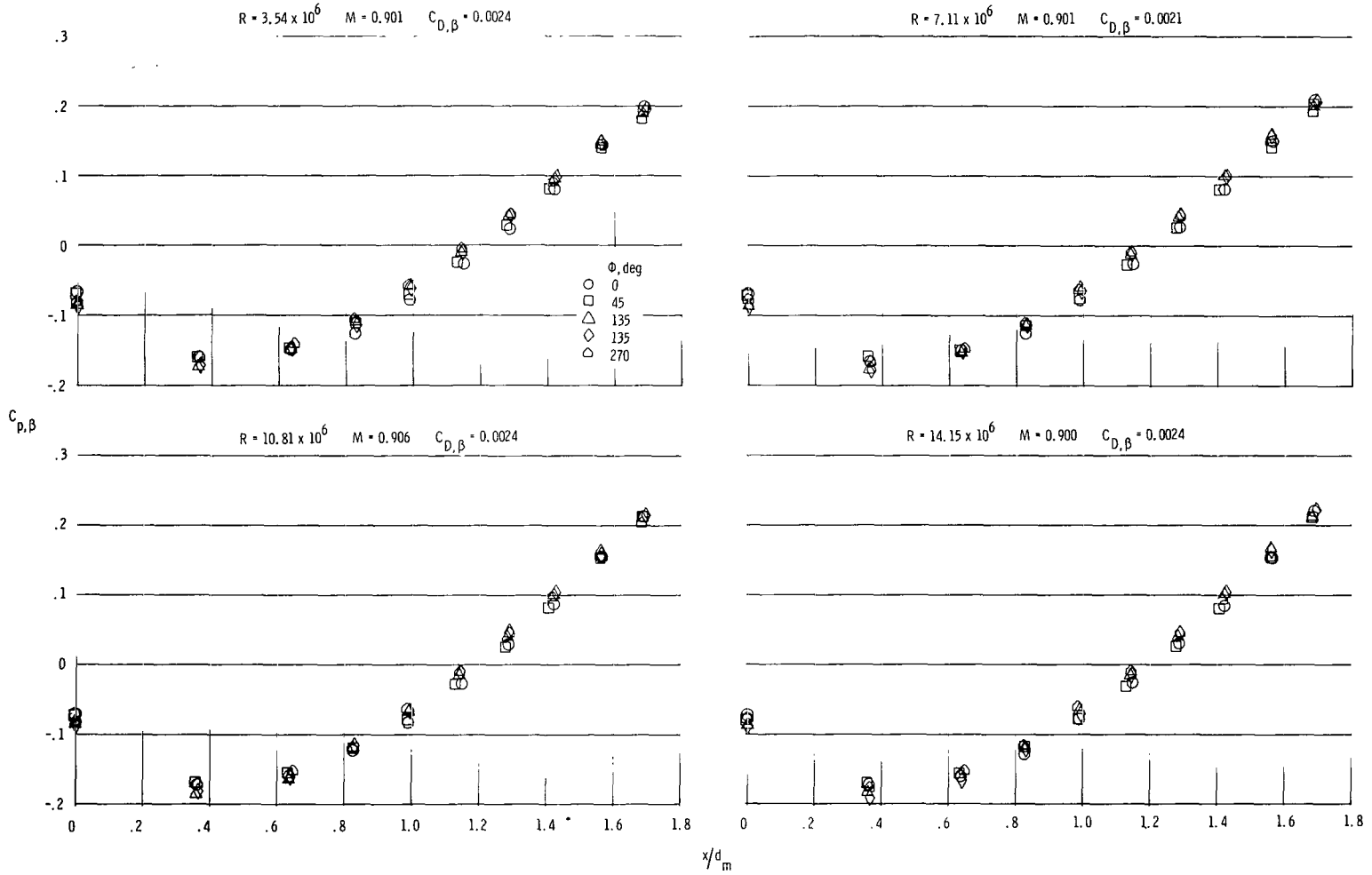


(c) M = 0.9.

Figure 10.- Continued.

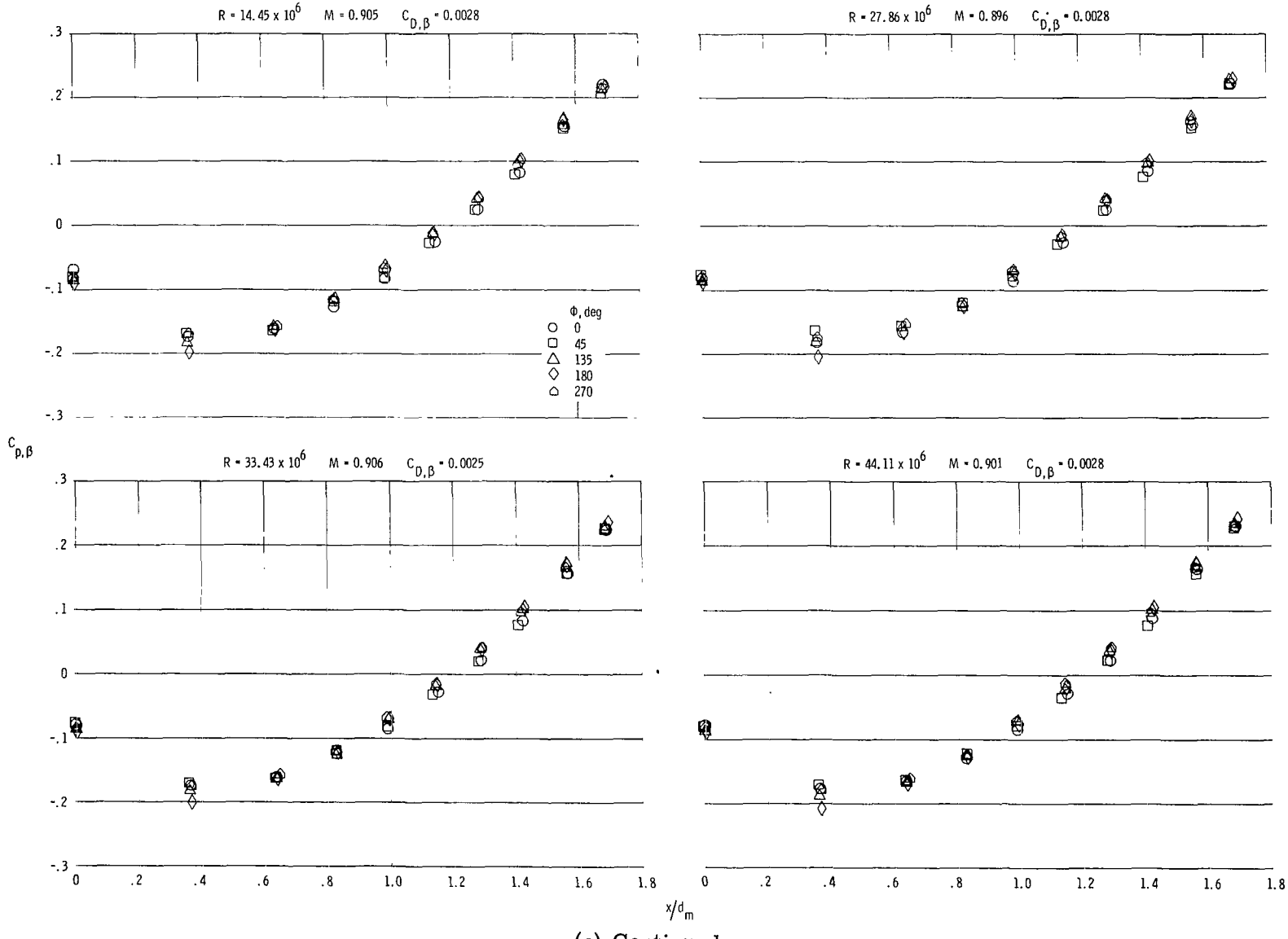


(c) Continued.

Figure 10.- Continued.

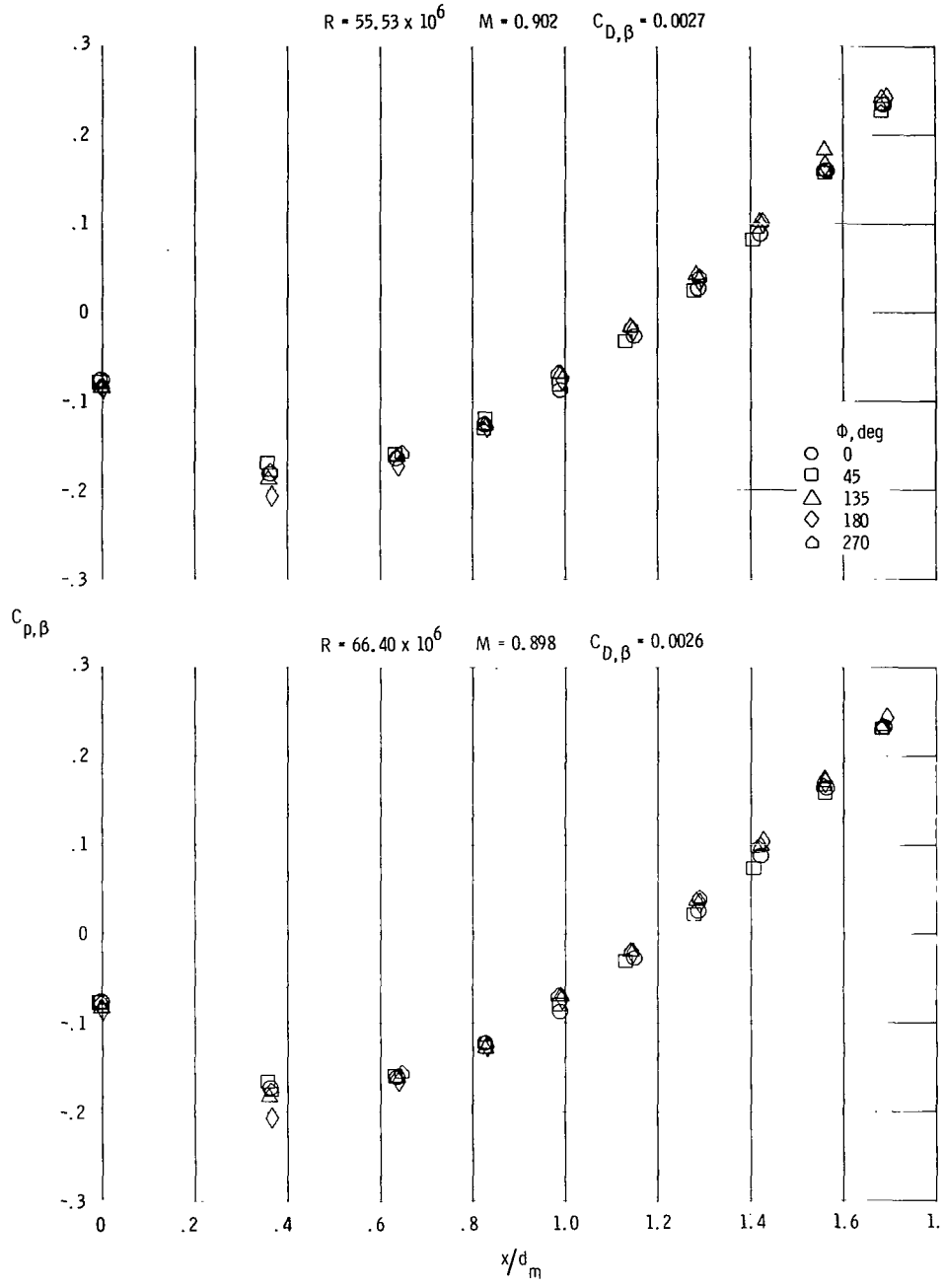


(c) Concluded.

Figure 10.- Concluded.

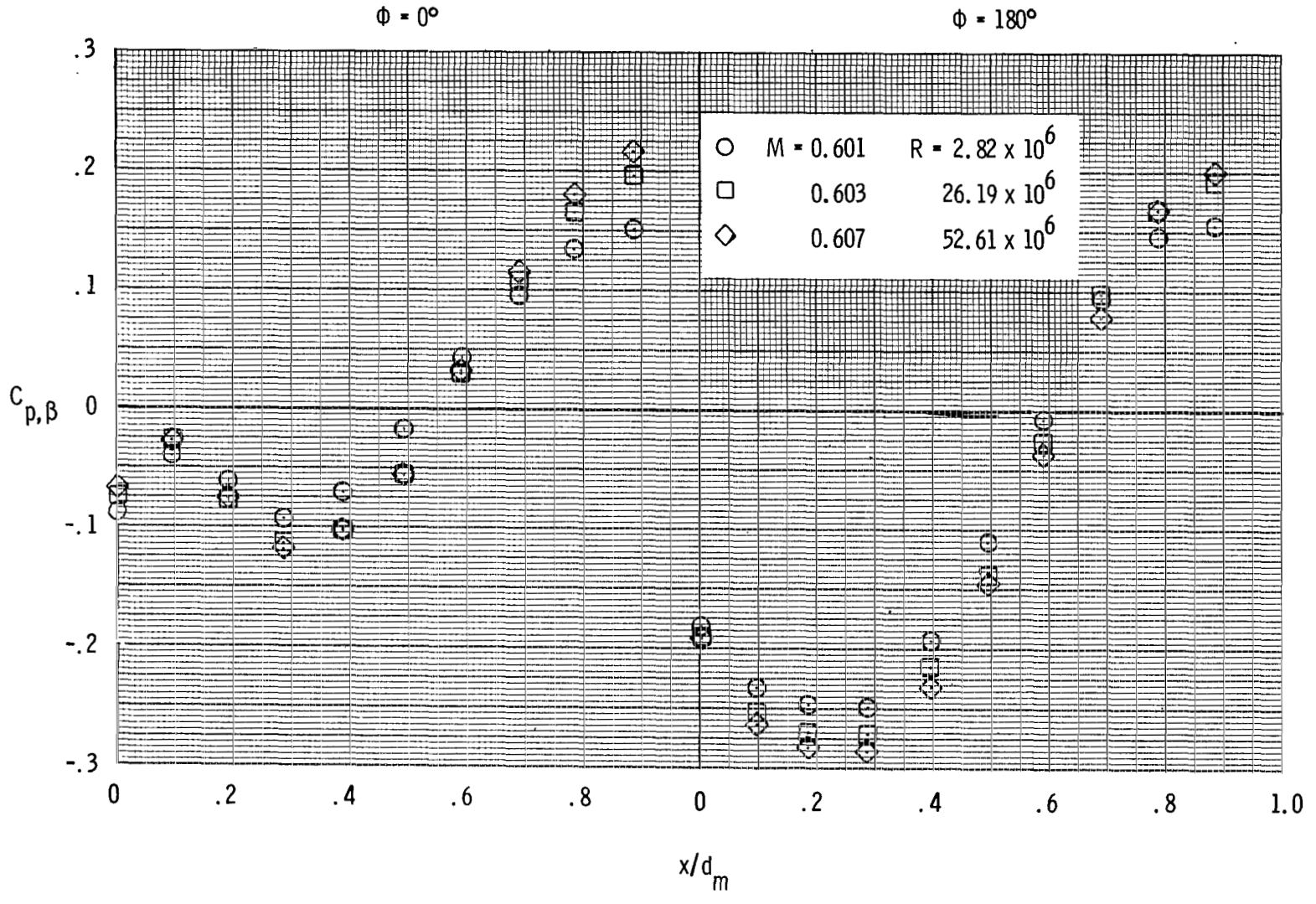


(a) M = 0.6.

Figure 11.- Effect of Reynolds number on boattail pressure coefficient distributions for the circular-arc—conic boattail with wing in the aft position.

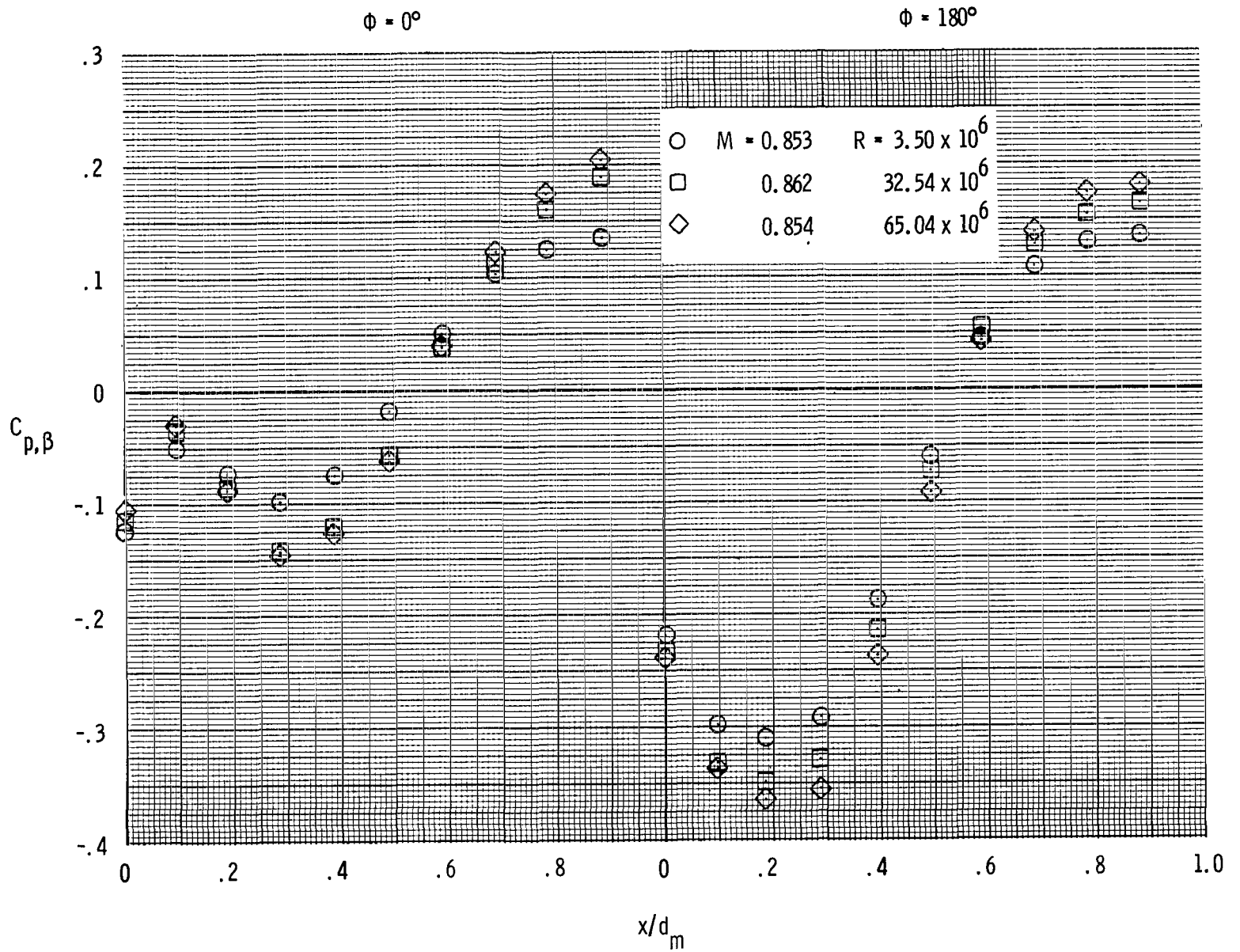


(b) M = 0.85.

Figure 11.- Continued.

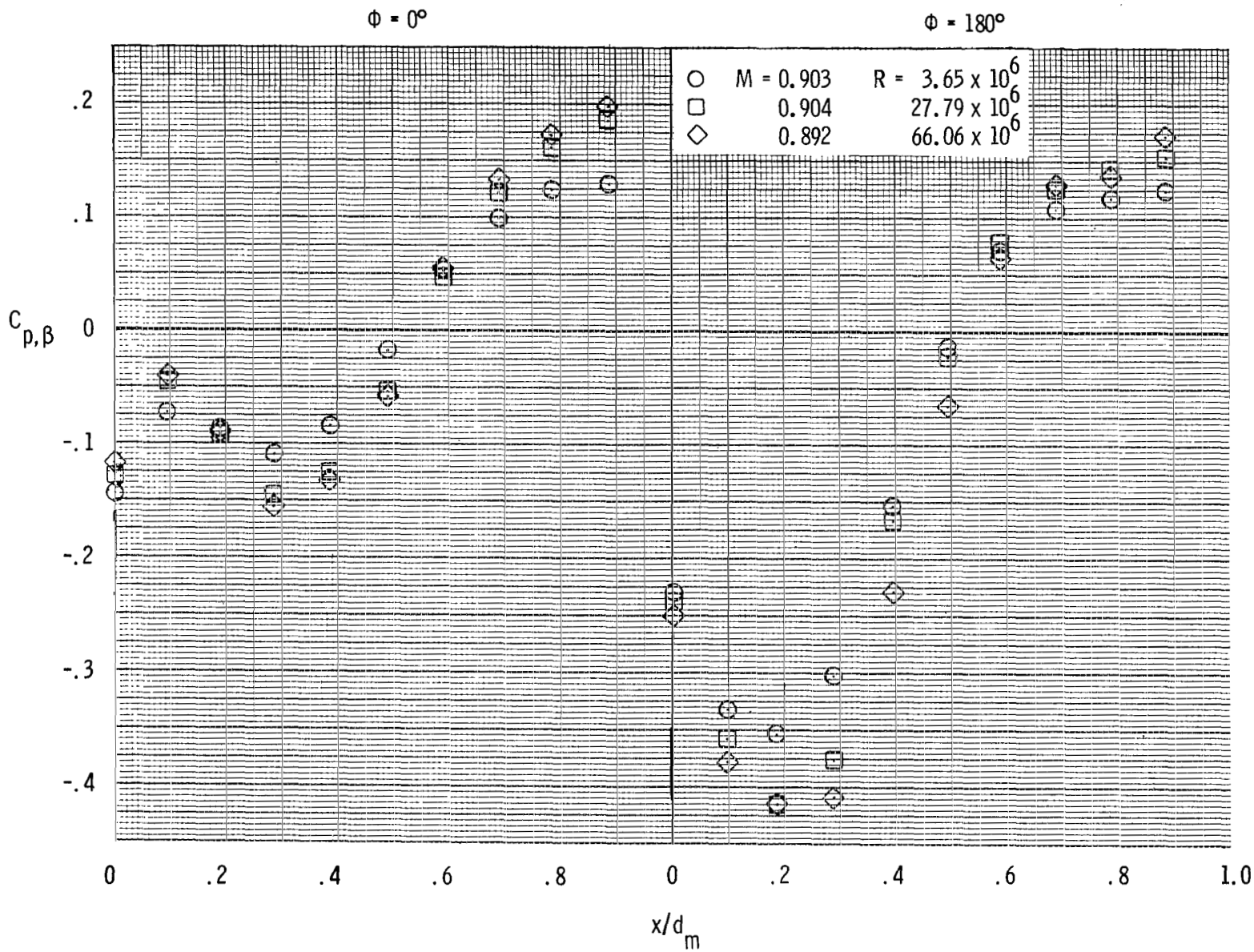


(c) M = 0.9.

Figure 11.- Concluded.

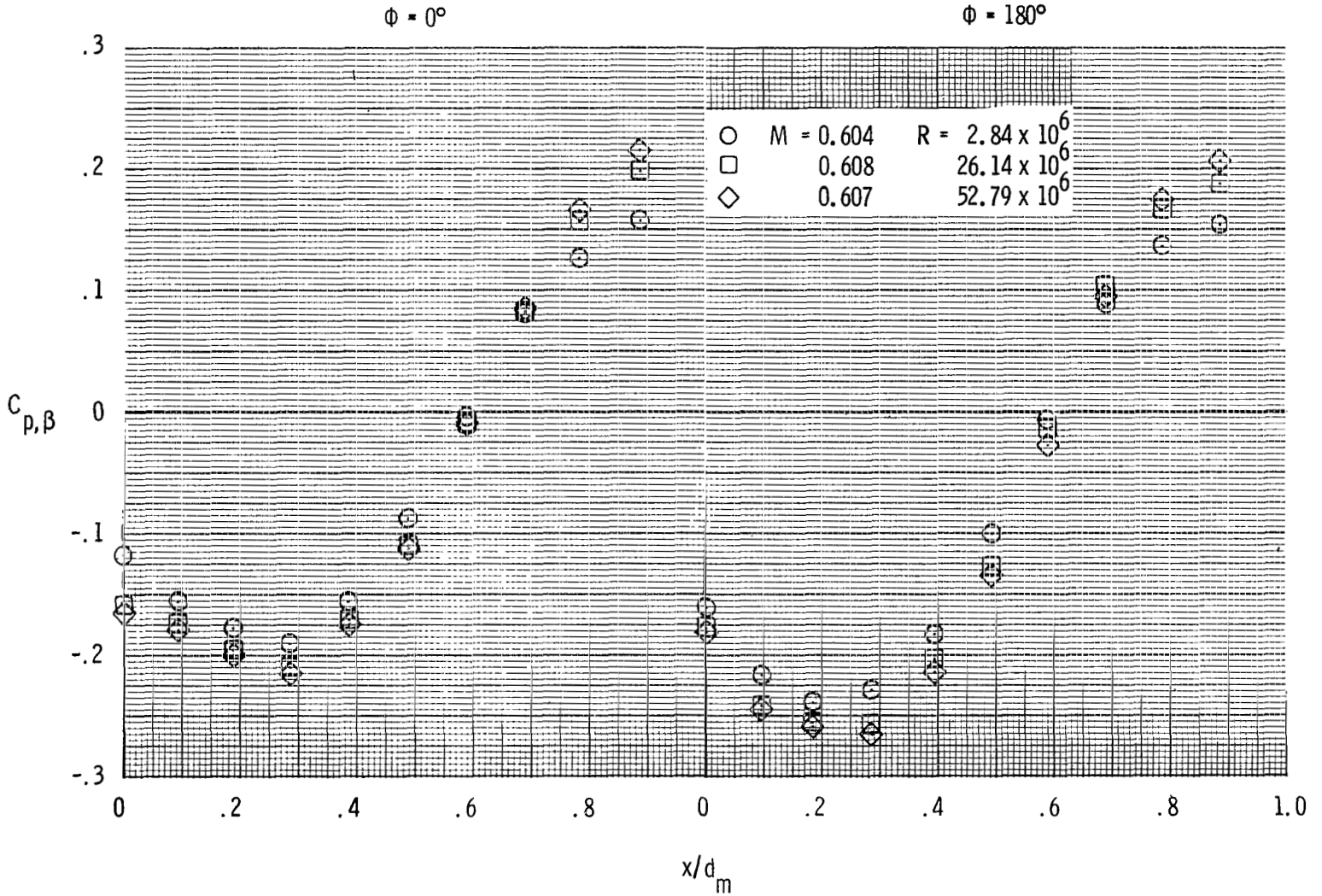


(a) M = 0.6.

Figure 12.- Effect of Reynolds number on boattail pressure coefficient distributions for the circular-arc—conic boattail with wing in middle position.

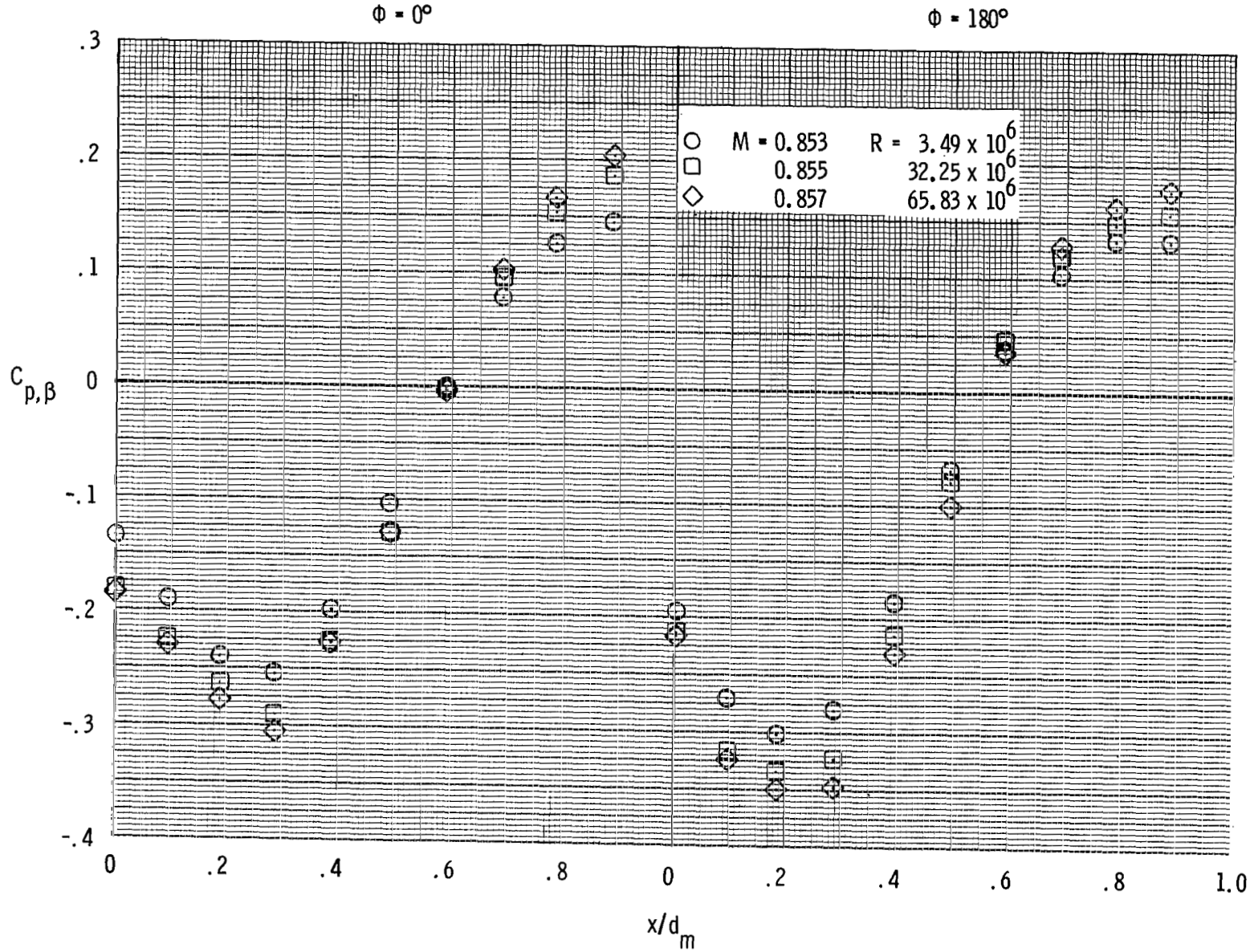


(b) M = 0.85.

Figure 12.- Concluded.

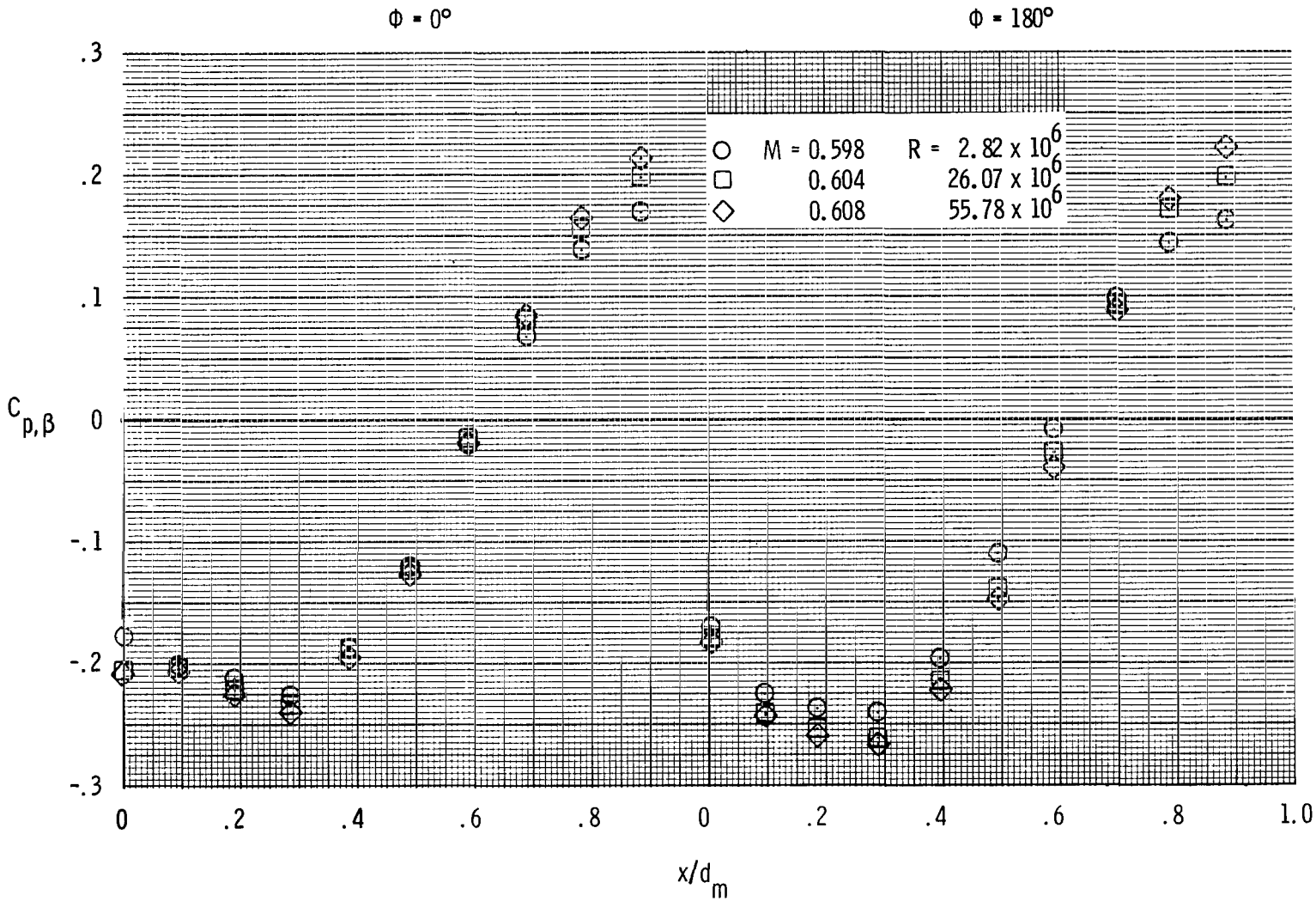


(a) M = 0.6.

Figure 13.- Effect of Reynolds number on boattail pressure coefficient distributions for the circular-arc—conic boattail with wing in forward position.

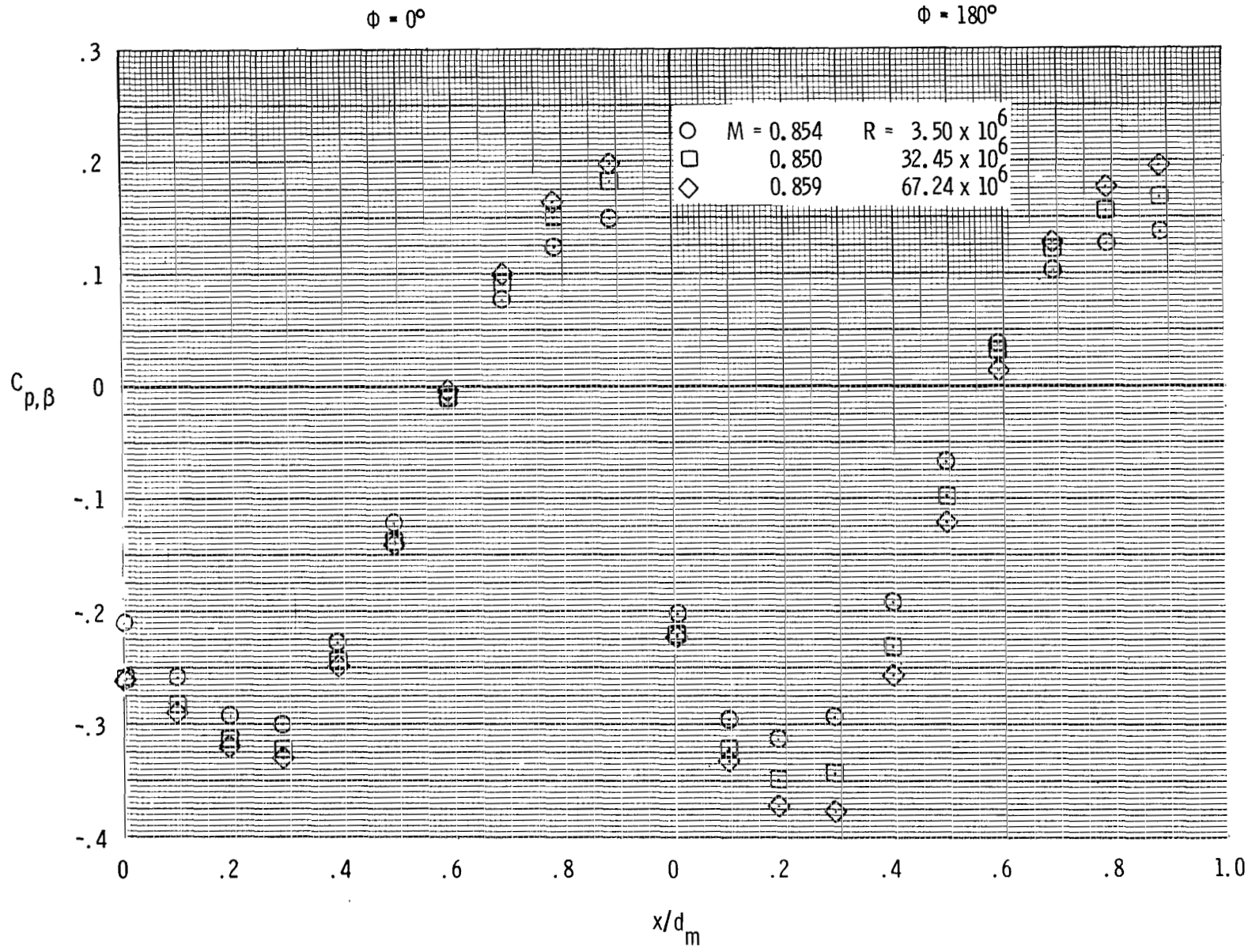


(b) M = 0.85.

Figure 13.- Concluded.

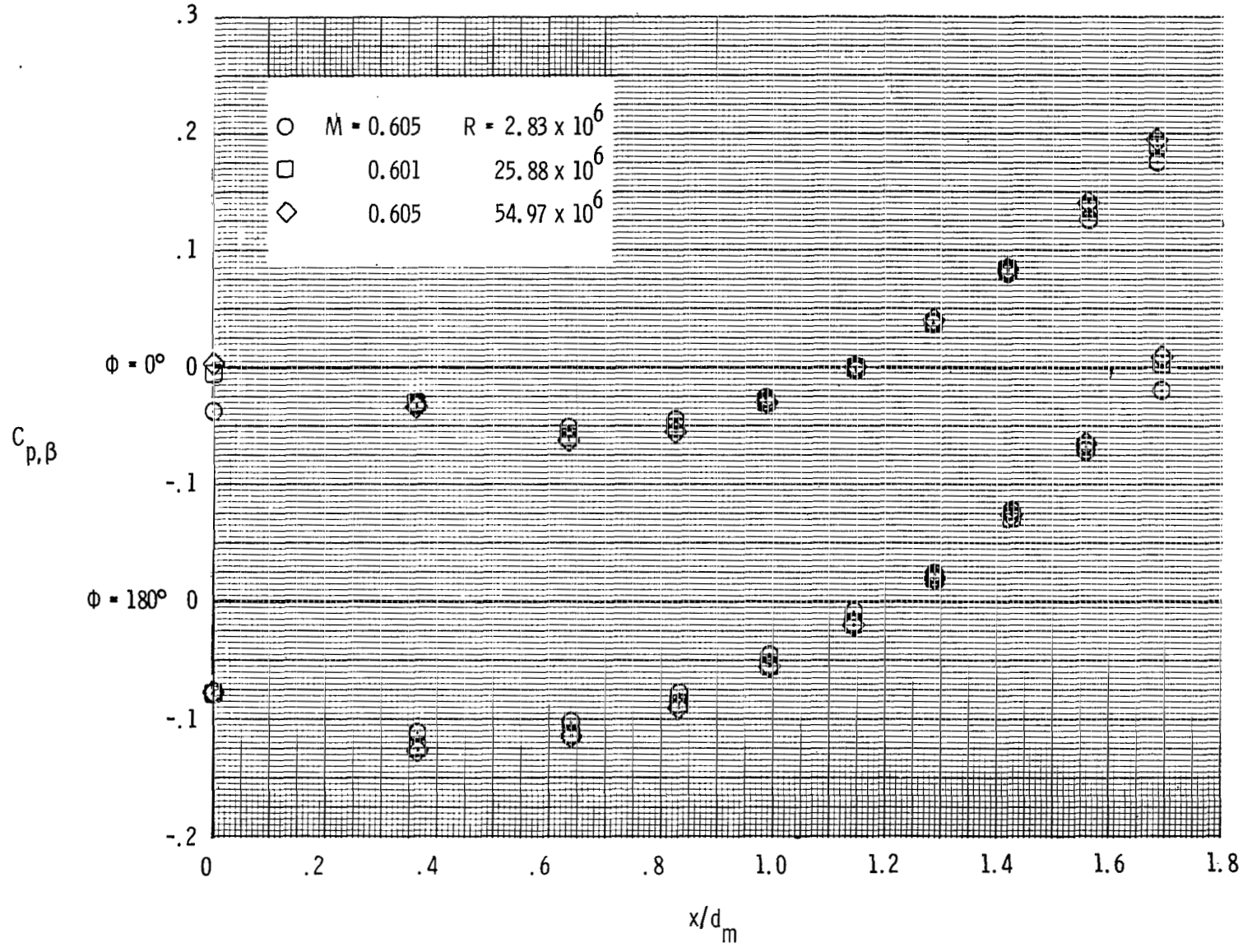


(a) M = 0.6.

Figure 14.- Effect of Reynolds number on boattail pressure coefficient distributions for the circular-arc boattail with wing in the aft position.

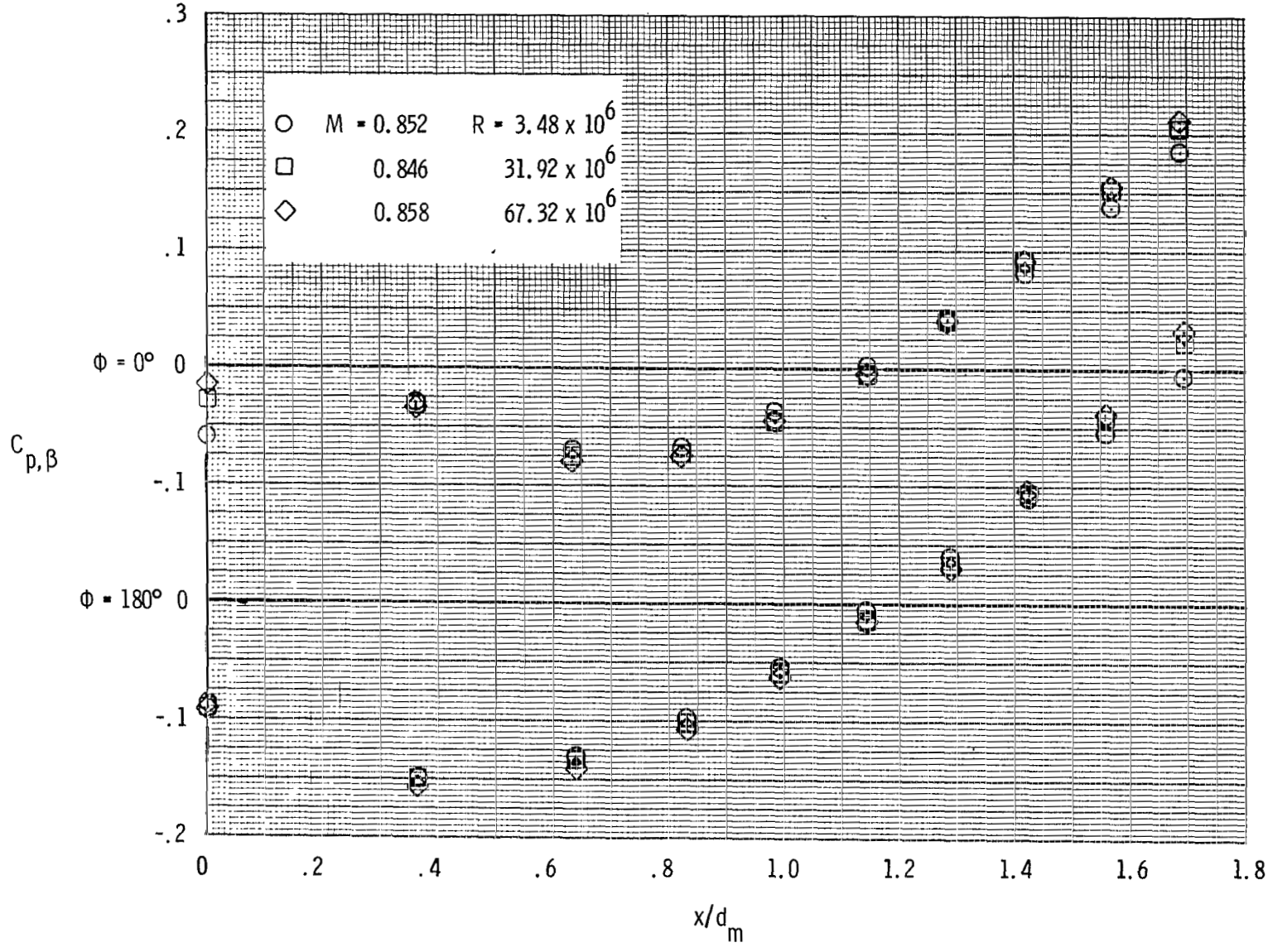


(b) M = 0.85.

Figure 14.- Continued.

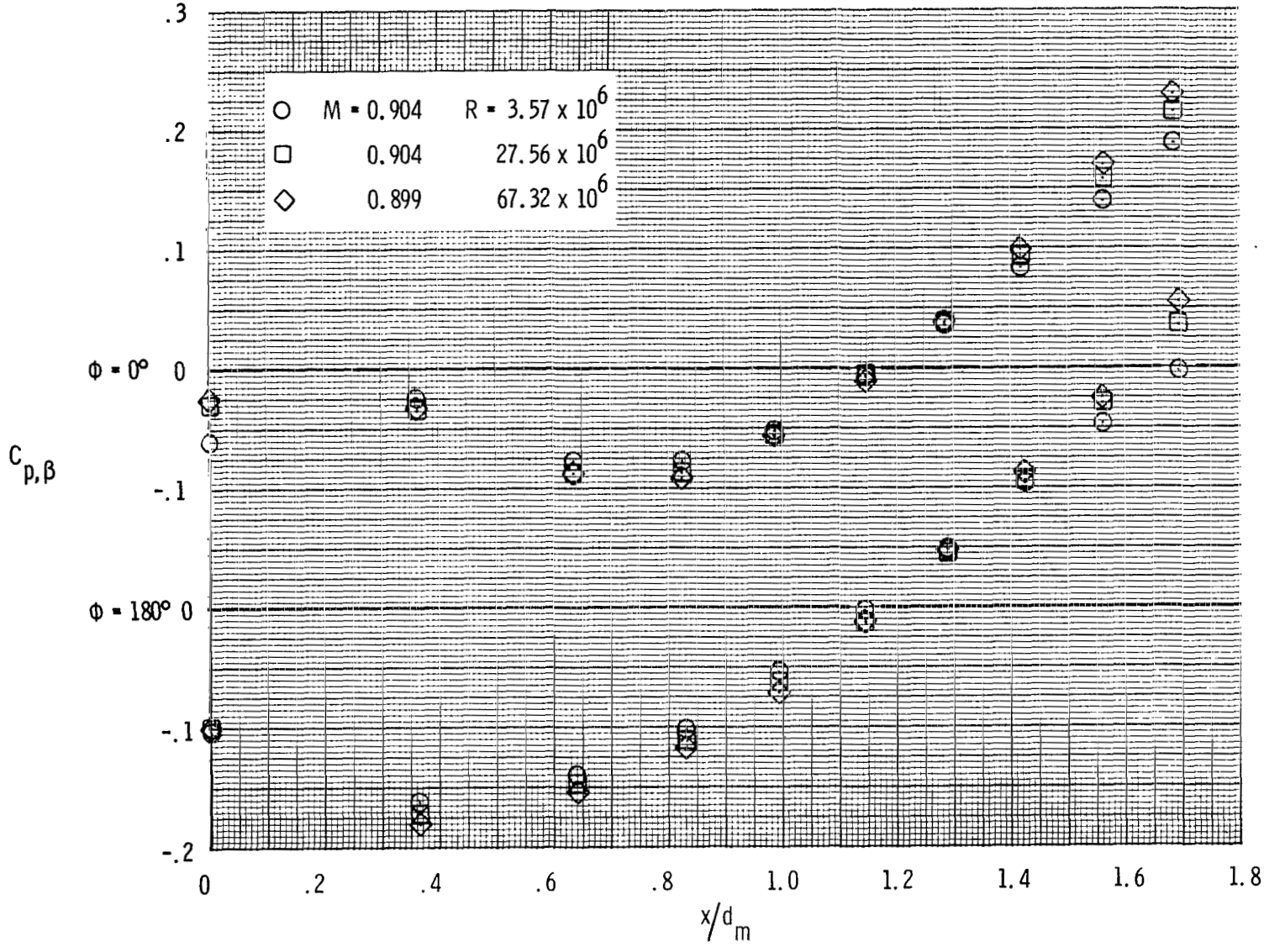


(c) M = 0.9.

Figure 14.- Concluded.

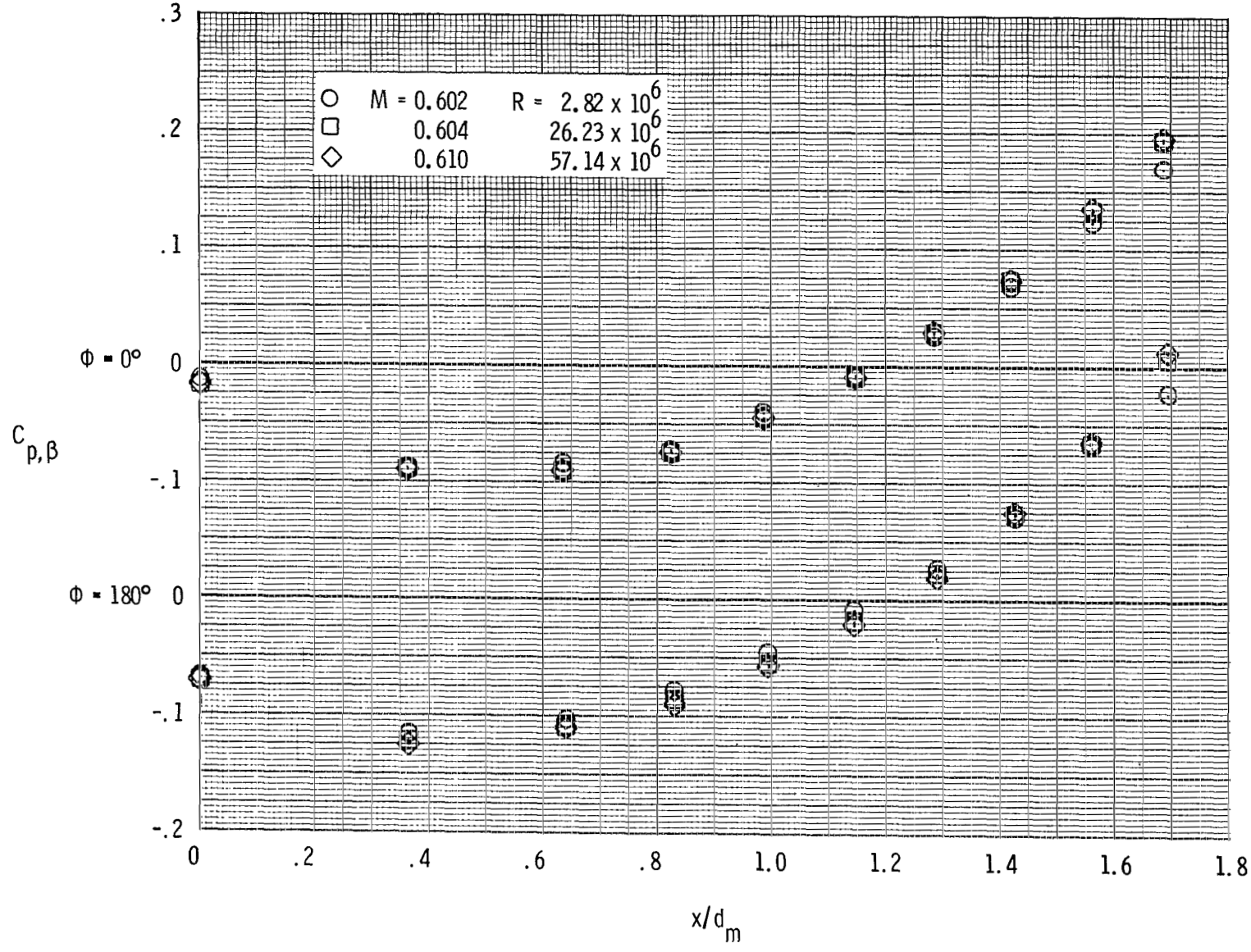


(a) M = 0.6.

Figure 15.- Effect of Reynolds number on boattail pressure coefficient distributions for the circular-arc boattail with wing in middle position.

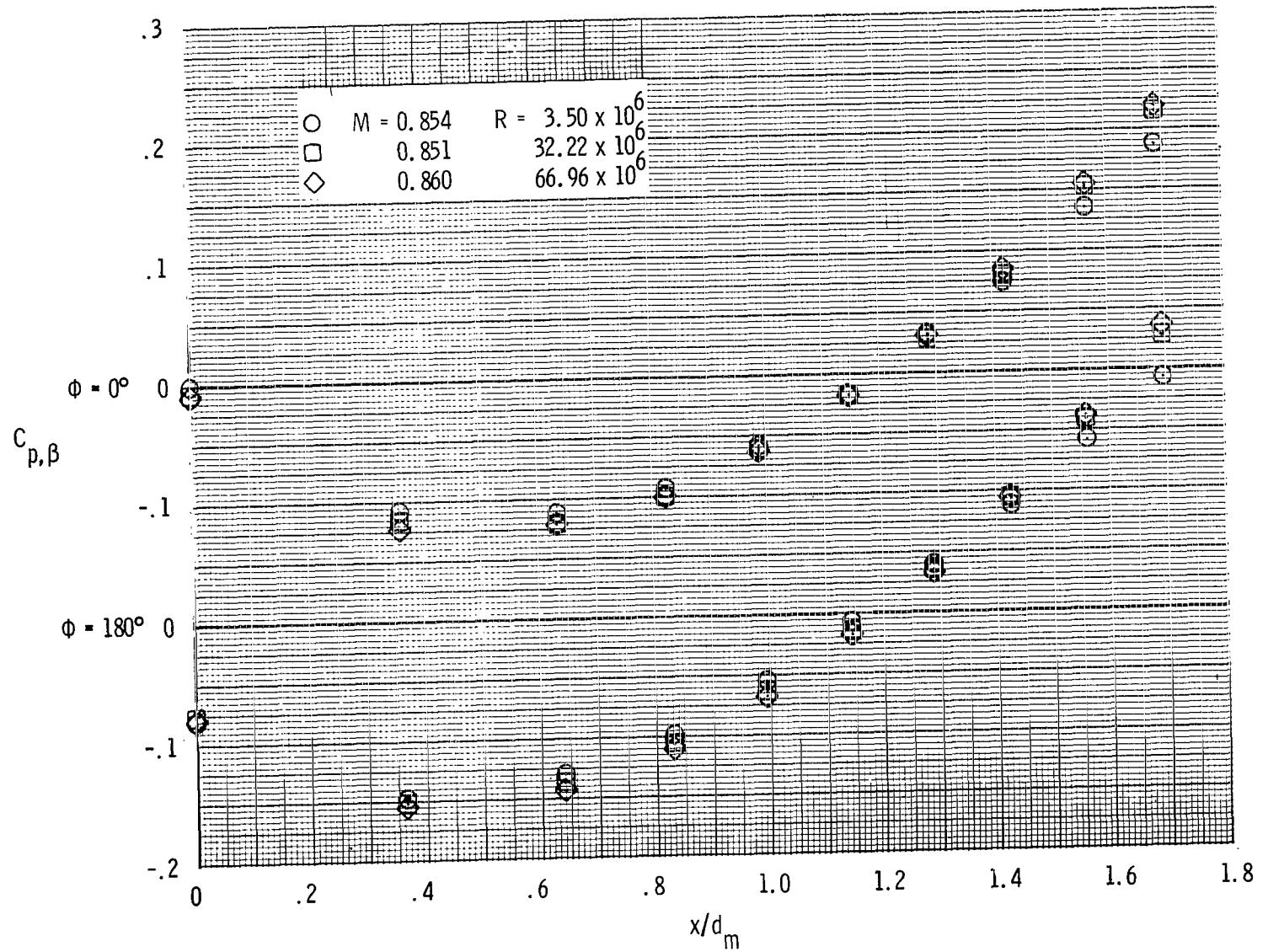


(b) M = 0.85.

Figure 15.- Concluded.

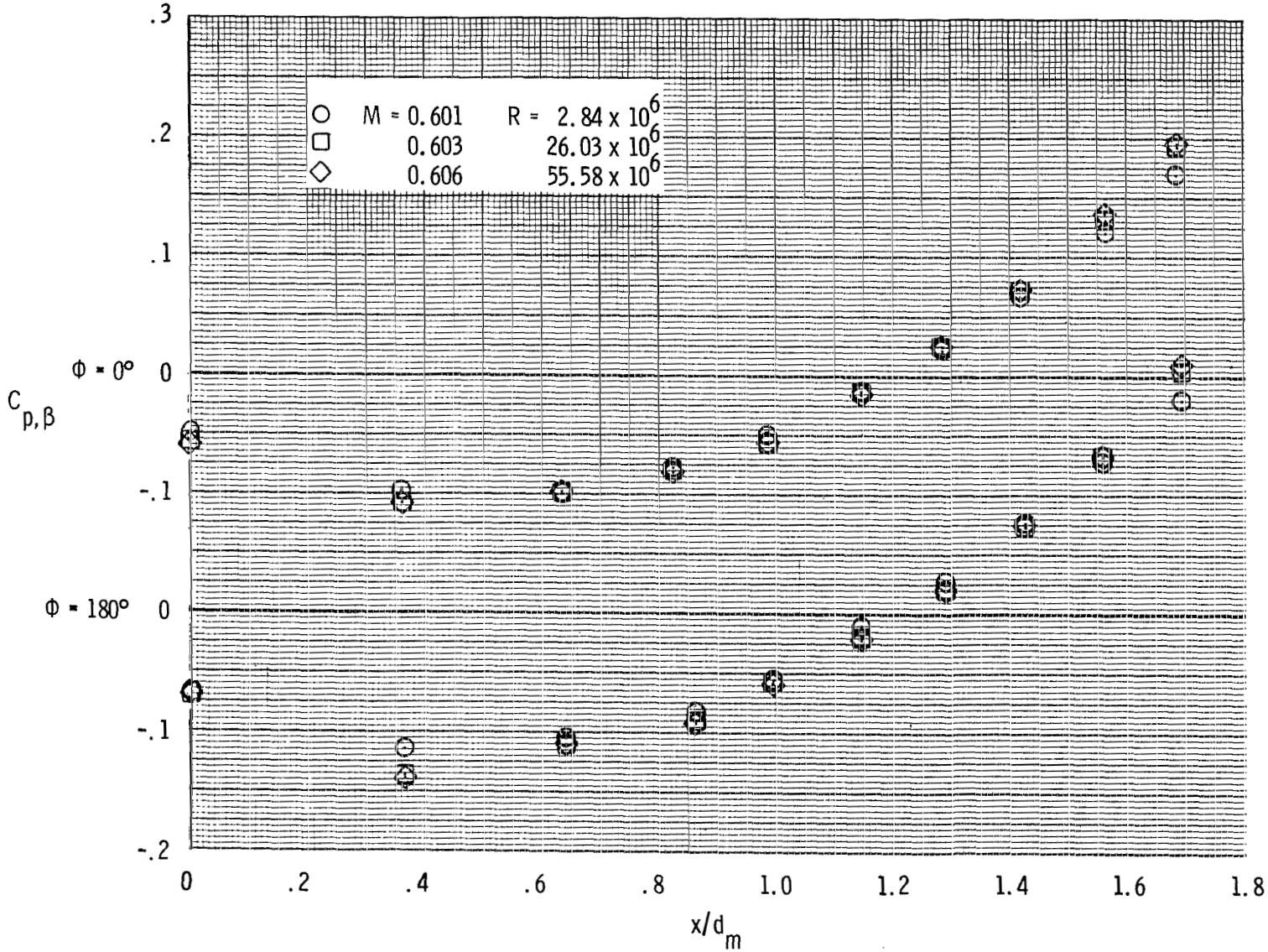


(a) M = 0.6.

Figure 16.- Effect of Reynolds number on boattail pressure coefficient distributions for the circular-arc boattail with wing in forward position.

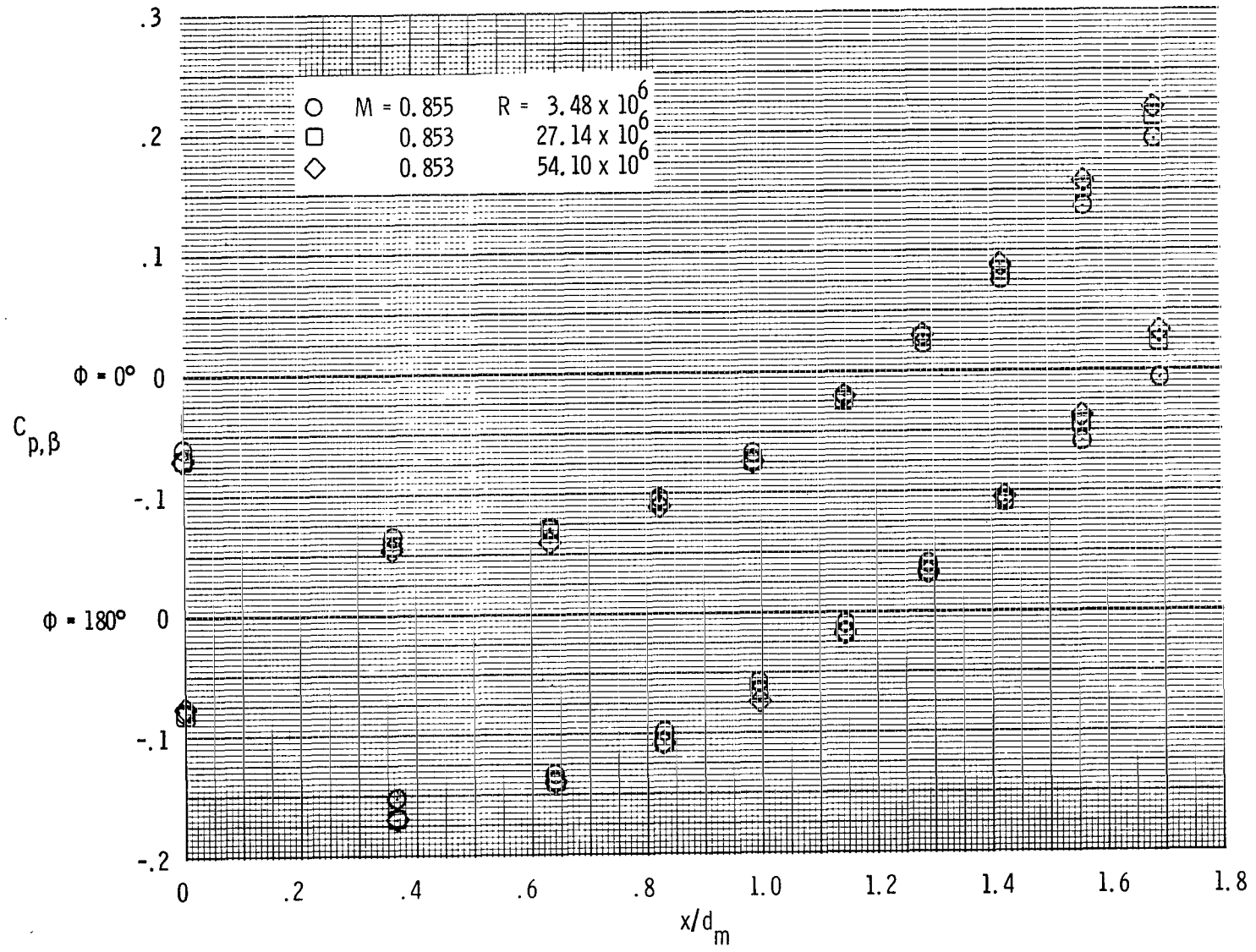


(b) M = 0.85.

Figure 16.- Continued.

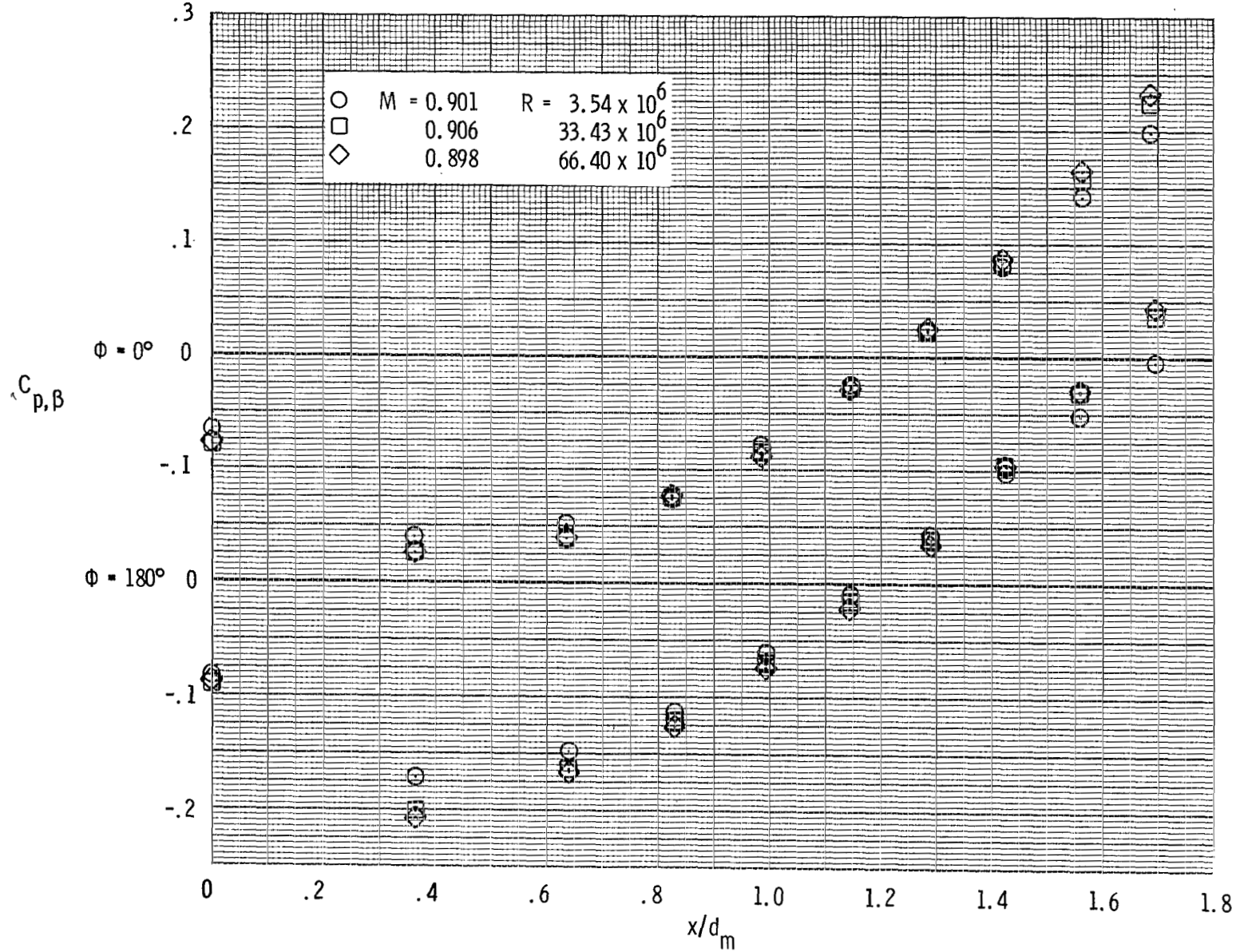


(c) M = 0.9.

Figure 16.- Concluded.

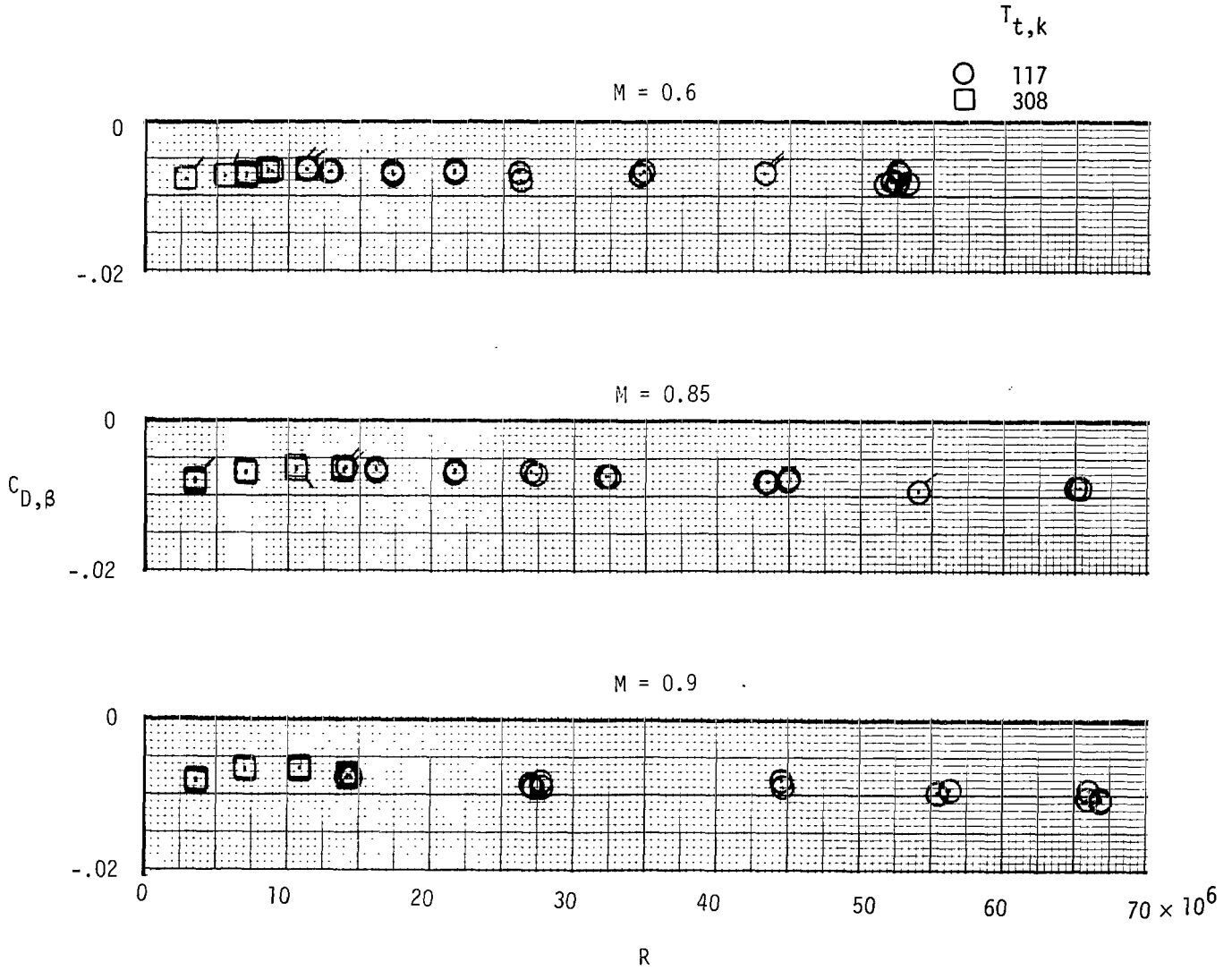


(a) Wing in aft position.

Figure 17.- Effect of Reynolds number on boattail pressure drag for the circular-arc—conic boattail. (Tick marks indicate repeat points.)

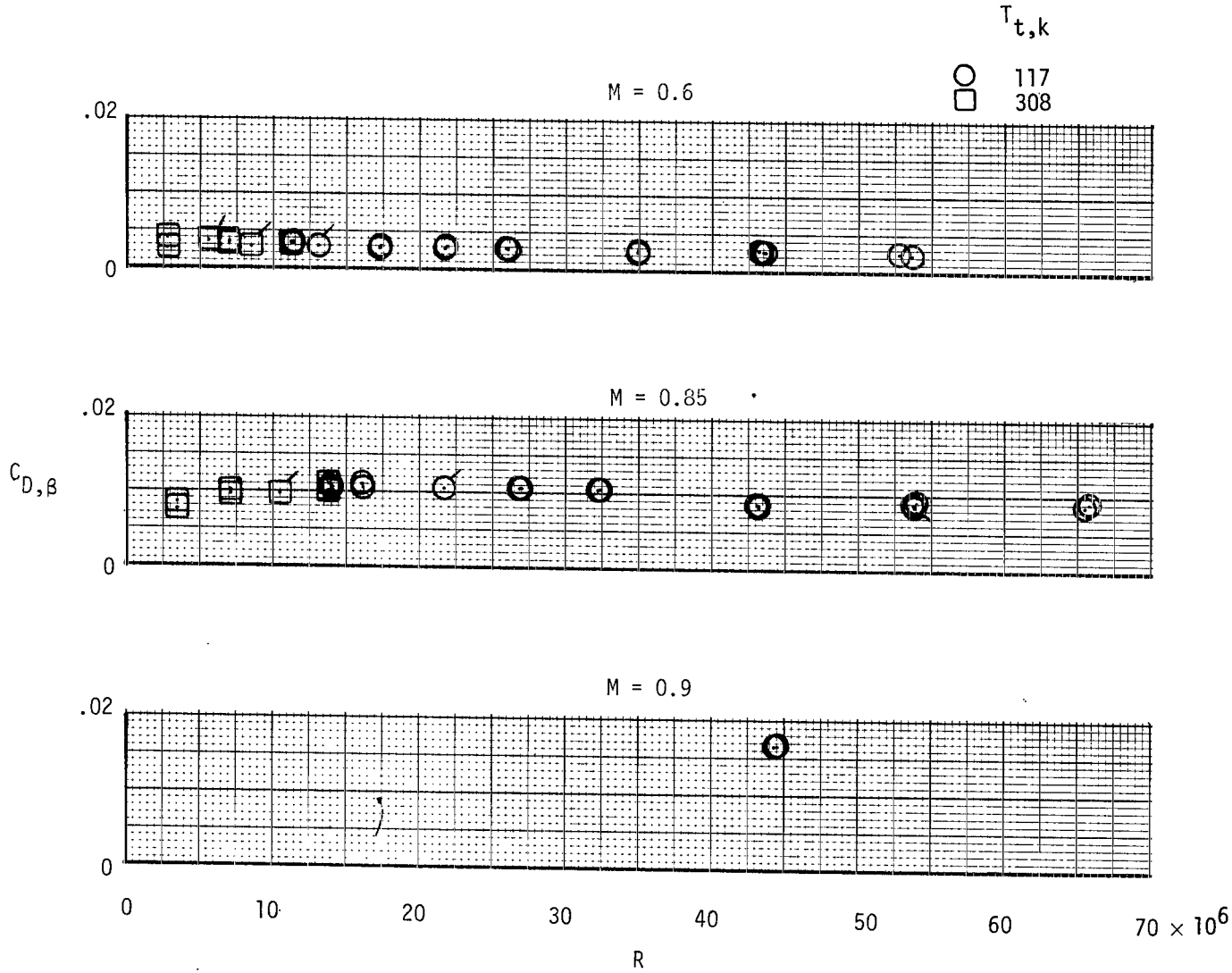


(b) Wing in middle position.

Figure 17.- Continued.

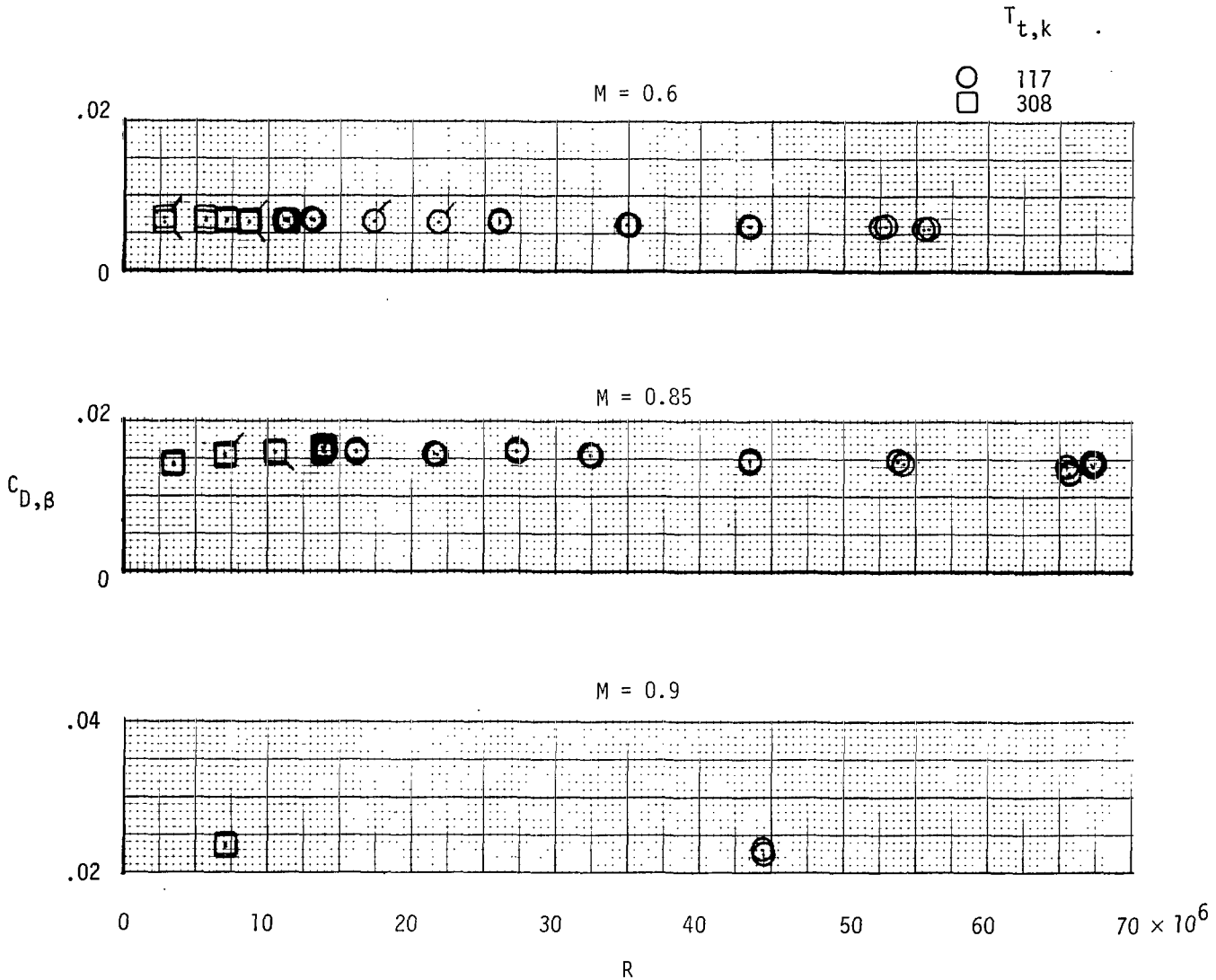


(c) Wing in forward position.

Figure 17.- Concluded.

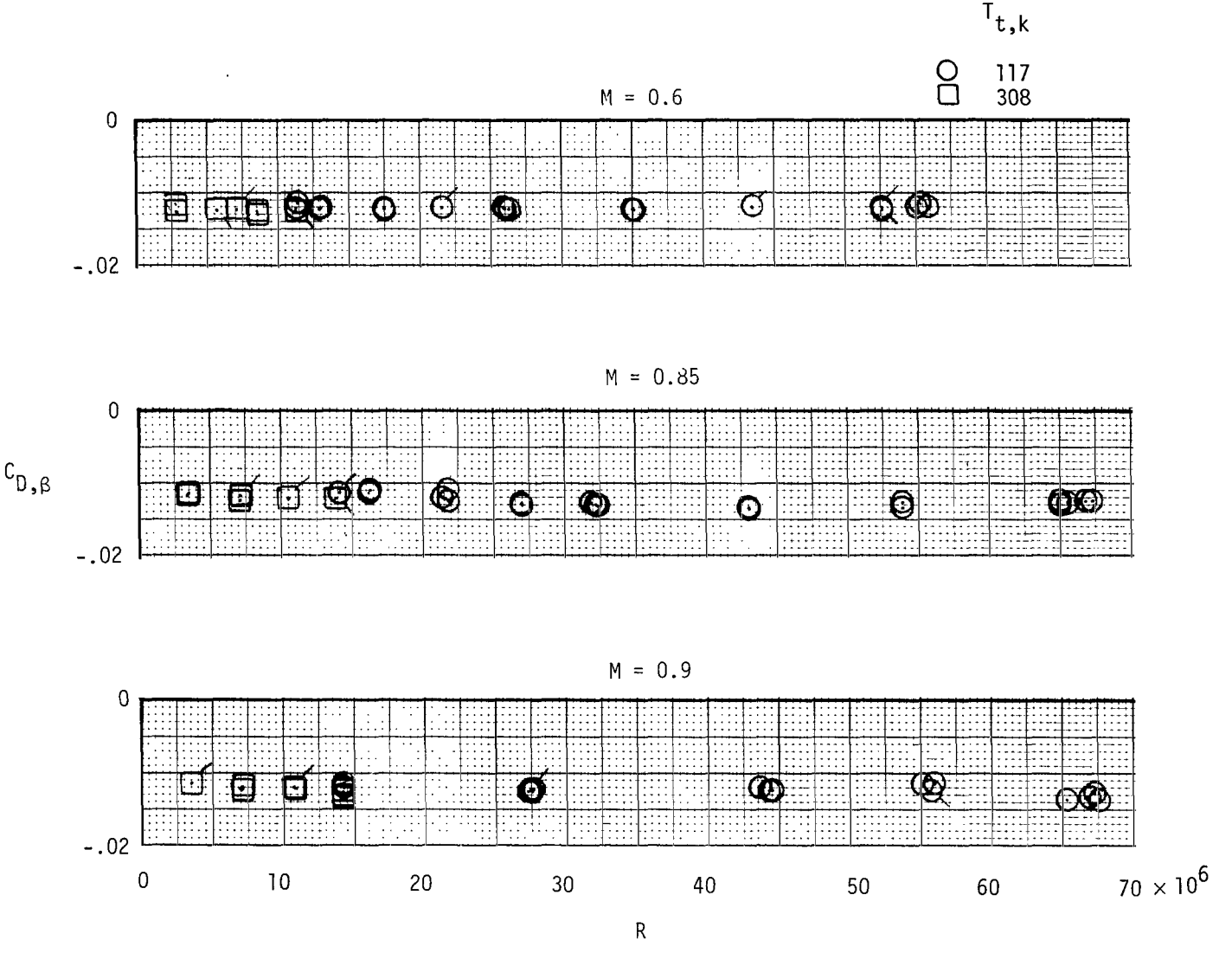


(a) Wing in aft position.

Figure 18.- Effect of Reynolds number on boattail pressure drag for the circular-arc boattail. (Tick marks indicate repeat points.)

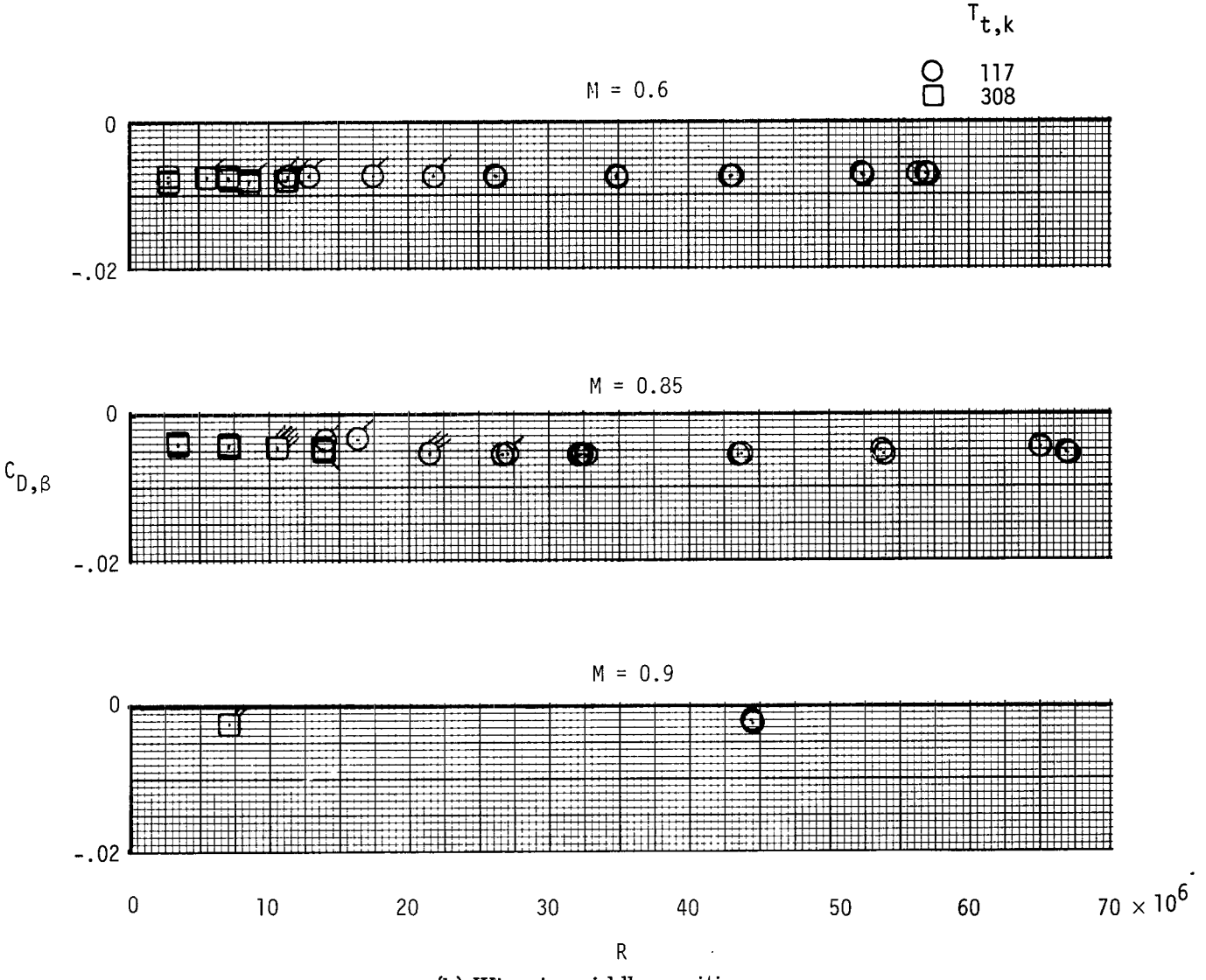


(b) Wing in middle position.

Figure 18.- Continued.

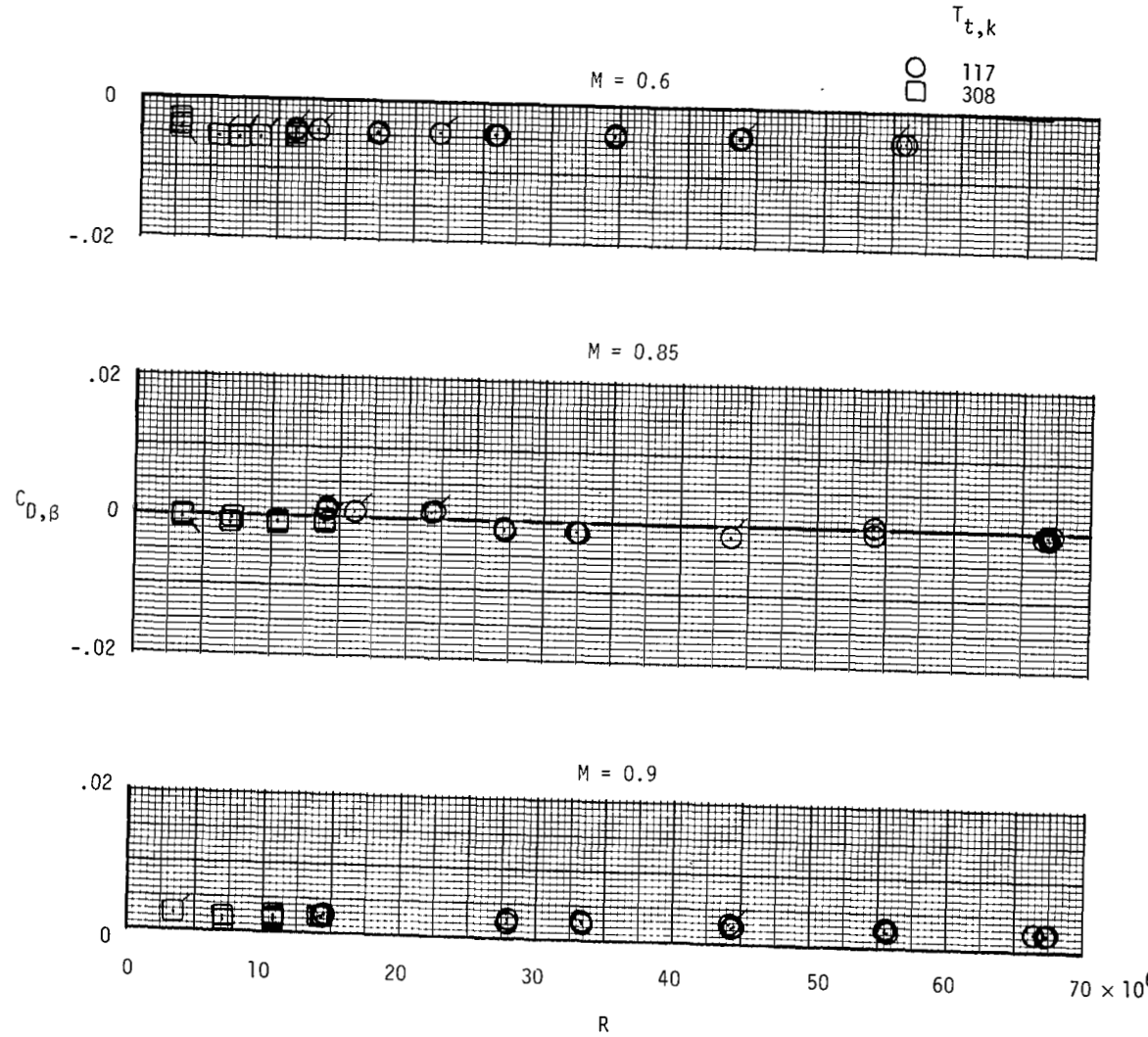


(c) Wing in forward position.

Figure 18.- Concluded.

*"The aeronautical and space activities of the United States shall be conducted so as to contribute . . . to the expansion of human knowledge of phenomena in the atmosphere and space. The Administration shall provide for the widest practicable and appropriate dissemination of information concerning its activities and the results thereof."*

—NATIONAL AERONAUTICS AND SPACE ACT OF 1958

# NASA SCIENTIFIC AND TECHNICAL PUBLICATIONS

TECHNICAL REPORTS: Scientific and technical information considered important, complete, and a lasting contribution to existing knowledge.

TECHNICAL NOTES: Information less broad in scope but nevertheless of importance as a contribution to existing knowledge.

TECHNICAL MEMORANDUMS: Information receiving limited distribution because of preliminary data, security classification, or other reasons. Also includes conference proceedings with either limited or unlimited distribution.

CONTRACTOR REPORTS: Scientific and technical information generated under a NASA contract or grant and considered an important contribution to existing knowledge.

TECHNICAL TRANSLATIONS: Information published in a foreign language considered to merit NASA distribution in English.

SPECIAL PUBLICATIONS: Information derived from or of value to NASA activities. Publications include final reports of major projects, monographs, data compilations, handbooks, sourcebooks, and special bibliographies.

TECHNOLOGY UTILIZATION PUBLICATIONS: Information on technology used by NASA that may be of particular interest in commercial and other non-aerospace applications. Publications include Tech Briefs, Technology Utilization Reports and Technology Surveys.

***Details on the availability of these publications may be obtained from:***

**SCIENTIFIC AND TECHNICAL INFORMATION OFFICE**

**NATIONAL AERONAUTICS AND SPACE ADMINISTRATION**

**Washington, D.C. 20546**